JOURNAL OF MATERIALS SCIENCE 39 (2004) 4729–4797

Review
Adhesively-bonded joints in metallic alloys, polymers and composite materials: Mechanical and environmental durability performance

A. BALDAN
Department of Metallurgical and Materials Engineering, University of Mersin, Ciftlikkoy, Mersin/Turkey
E-mail: abaldan@mersin.edu.tr

The factors affecting the mechanical and environmental durability (or stability), and performance of the adhesively bonded joints in various adherends including metallic alloys, polymers and composite materials are studied in detail. The primary function of a joint is to transfer load from one structural member to another. In most bonded joints the load transfer takes place through interfacial shear. At present, the use of adhesive bonded joints are largely applied to secondary non-critical structures. Whereas the use of adhesive bonding in primary structural applications has been somewhat limited because of the difficulty in defining and predicting joint strength, and designing the joint geometry to optimize strength and reliability. The determination of adhesive joint strength is complicated primarily by the nature of the polymeric material itself. Since these problems are mainly mechanical in nature, stress analysis is required to understand how the force loads are distributed along the adherends and adhesive layer. Most structural engineers consider the durability or stability of a joint to be fatigue related. This is only partly true for adhesive bonds as most durability issues are driven by environmental resistance rather than fatigue loads. The environmental resistance of an adhesive bond is determined by the chemical bonds formed during cure of the adhesive and the resistance of the chemical bonds to environmental degradation. Environmental resistance is fundamental to the durability of a bonded joint or repair. Most in-service failures are caused by environmental degradation of the interface between the bonding surface and the adhesive. Although the use of adhesive bonding is increasing rapidly, there are still important issues which need to be addressed in joint analysis, design, durability, and performance considerations. Therefore, the study of joints usually involves consideration of (a) joint geometries, (b) materials (i.e., adhesives and adherends), (c) loading conditions (i.e., static and dynamic loadings), (d) failure modes (i.e., cohesive, adhesive or mixed failure modes), and (e) temperature and moisture or environmental effects (humidity, solvents, corrosion, temperature extremes, thermal cyling etc.). Therefore, in the present paper the adhesive joints are critically assessed in terms of these factors which affect the durability and performance of them.

There are two basic mathematical approaches for the analysis of adhesively bonded joints: (a) closed-form or analytical model and (b) numerical solutions (i.e., finite element analysis, FEA). In the closed-form approach, a set of differential equations and boundary conditions is formulated. The solutions of these equations are analytical expressions which give values of stresses at any point of joint. The analytical approach for the solution of complex stress distributions in the joints has been progressively refined until recent times. In the second approach, solutions of differential equations are obtained by numerical methods or the continuum is represented by a discrete model at the outset. The solution of these equations gives displacements at the determined points from which strains and stresses can be obtained for any point within the model. Among the numerical methods, finite element analysis (FEA) has been extensively used with success. The two- and three-dimensional finite element analyses approaches have been extensively applied by many workers to analyse the adhesive joints considering the linear and geometric nonlinearities.

1. Introduction

Almost every designed structure requires component members to be connected. The most structurally efficient method of connecting the structures is with shear joints, which are either adhesively bonded or mechanically fastened [1]. In the design of the adhesive joints for engineering structures, strength, stiffness and life are considered to be the most important mechanical properties. Under identical fatigue conditions, adhesively bonded joints are far superior to mechanically fastened joints [2]. Most structural engineers consider the durability or stability of an adhesive joint to be fatigue related. This is only partly true for adhesive bonds as most durability issues are driven by environmental resistance rather than fatigue loads [2].The main disadvantages of mechanical connections are that they do not distribute the load uniformly, thus resulting in large local stresses [3]. In comparison, adhesively bonded joints can achieve in excess of 80% of the tensile strength of the weakest adherend even with a simple single-shear configuration [4]. Therefore, adhesively bonded joint is the most efficient method for joining both metallic and non-metallic (i.e., composite-to-metal bonding) structures where strength, stiffness, and fatigue life must be maximized at a minimum weight [5, 6]. For example, use of tough, moisture resistant, flow controlled, epoxy based adhesives to bond composites to composites, or composites to metals offers a number of advantages [7].

What "successful bonding" implies is consistent strength and long-term reliability [8]. To achieve consistent strength, the bondline thickness must be controlled so that repeatable joints with similar performance characteristics are achieved [9]. Although adhesively bonded joints have many advantages over other structural joining methods, particularly in their efficient load transfer in thin components and structural repairs, the general application of adhesively bonded joints has suffered due to their difficulty to inspect bondline quality following manufacture and in-service life [10]. As pointed out by Hart-Smith [10], the major concern is degradation of the bondline mechanical properties due to either poor surface preparation or inproper curing conditions. Because adhesives bond the entire joint area, good load distribution and fatigue resistance are obtained and stress concentrations (such as those observed with screws, rivets, and spot welds) are avoided. Similarly, because of the large amount of contact area that can usually be obtained, the total joint strength compares favorably with that produced by alternative methods of joining or attachment [11]. Additives can be incorporated to enhance (a) strength, (b) increase flexibility, or (c) provide resistance to various environments.

Adhesives are generally inexpensive and frequently weigh less than the fasteners needed to produce a comparable-strength joint. In addition, the adhesive can also provide [11]: (a) thermal and electrical insulation; (b) act as a damper to noise, shock, and vibration; (c) stop a propagating crack; and (d) provide protection against galvanic corrosion when dissimilar metals are joined. By providing both a joint and a seal against moisture, gases, and fluids, adhesive-bonded assemblies often offer improved corrosion resistance throughout their useful lifetime. When used to bond polymers or polymer-matrix composites, the adhesive can be selected from the same family of materials to assure good compatibility [11].

Adhesives are currently used in many areas such as automobile and aerospace industries. For example, adhesive bonding of metallic structures was welcomed when it was first introduced by de Havillands, in England, on the Hornet and Dove in the middle 1940s (Ref. [10]). Since then, adhesive bonding of aircraft structures has been in use and is still in use on current aircraft projects as a direct alternative to riveting [12]. In the manufacture of automobiles the adhesives are almost always used as basic sealant materials or in non-critical secondary structures. In the manufacture of aircrafts the use of adhesive bonded joints has also largely been limited to secondary non-critical structures such as aerodynamic fairings and wing panels. Therefore, the use of adhesives in truly structural applications has been quite limited. The reasons for these limitations are as follows: (a) a concern about the fatigue and durability behavior of bonded, strutural components over the expected lifetime of the vehicle [13], and (b) secondly, the fracture behavior of adhesive bonded joints, particularly those with dissimilar adherends (i.e., composite-to-metal), is still not well understood [5]. Since the adhesive joints must perform satisfactorily under service conditions, which include static and dynamic loadings and exposure to hostile environments such as water, petrol, other organic solvents, etc and, in many instances, combinations of these conditions, may be experienced. As Jethwa and Kinloch [13] pointed out, it is of prime importance for the adhesives user to be able to develop and recommend "adhesive systems" (i.e., the substrate/surface pretreatment/adhesive) which will possess an adequate service life under the operating conditions which are to be experienced by the bonded structure. This, in turn, leads to the need to understand the mechanisms of failure and to develop test methods (a) for developing and selecting adhesive systems, (b) for quality assurance, and (c) for predicting, quantitatively, the expected service life [13].

The plastic yielding behavior of polymers such as adhesives is well known to be sensitive to the hydrostatic pressure (i.e., Refs. [14, 15]), in contrast to metallic materials. To account for this pressure dependence, various proposals have been made to modify the conventional yield criteria by including a term that accounts for influences of hydrostatic stresses (i.e., Refs. [14–17]). However, due to the fact that the adhesive layer in a bonded joint experiences not only a high stress concentration near the end of the adhesive layer but also triaxial stresses [18] induced by the high constraint imparted by stiff adherends, experimental data of adhesive yielding are scarce. Consequently much of the work to date has been mainly concerned with adhesives in their neat from subjected to simple loading, and it is not clear whether existing yield criteria are applicable in the context of bonded joints. It was recently found [14] that the conventional yield criteria widely employed to model adhesive, such as the modified Tresca criterion

[15, 16], the modified von Mises criterion [15, 16], and the linear Drucker-Prager criterion [16, 19], are unable to characterize the yiels locus. To overcome this difficulty, Wang and Chalkley [14] have used the modified Drucker-Prager/cap plasticity model that is commonly associated with geological materials is adopted in the plasticity of a film adhesive under multiaxial stresses, which provides a good correlation with the experimental data (see Section 8.1 for more detail about this work).

There is a growing trend to optimise the strength, weight and durability of aircraft and spacecraft structures by combining tradational metals with polymeric composites [5]. Composites are more structurally efficient than metals and do not experience galvanic corrosion. Metals, however, have better damage tolerance and failure predictibility than composites and are uneffected by the solvents and temperatures which tend to degrade polymers. In order to optimise the benefits offered by both types of materials, hybrid composite-to-metal structures are increasingly being developed [5]. An example of these structures is an aircraft engine strut containing a light-weight high strength carbon fiber/epoxy fairing joined to damage tolerant aluminum ribs. Although these structures provide an excellent blend of material properties, their success depends upon the integrity of the joints which connect them together [5].

Although the use of adhesive bonding is increasing rapidly, there are still important issues which need to be addressed in joint analysis, design, and durability considerations. The study of joints usually involves consideration [20] of (a) a variety of joint geometries, (b) materials (i.e., adhesives, adherends), (c) loading conditions, (d) failure modes, and (e) temperature and moisture effects (or environmental effects). The analysis of adhesively bonded joints requires a reliable and efficient tool (i.e., such as numerical analysis or finite element analysis, FEA, technique) to obtain stresses, strains, and fracture parameters. Most of the available methods require big investments in computer as well as designer time.

This paper critically assesses the progress in the mechanical and environmental durability and performance of adhesively bonded joints in various technologically important adhesive-adherend systems (i.e., such as metal-metal, metal-composite, metal-polymer, polymer-polymer, composite-composite joint systems).

1.1. Adhesive bond durability

A common type of mechanical loading encountered by structures such as in aerospace industry, especially adhesively-bonded components, is cyclic-fatigue loading. For most materials, the presence of this type of loading is found to lead to a much lower resistance to crack growth than under monotonic loading, and polymeric adhesives are no exception to this observation. Most structural engineers consider the durability of a joint to be fatigue related. However, as pointed out by Davis and Bond [2], this is only partly true for adhesive bonds as most durability issues are driven by environmental resistance rather than fatigue loads. Therefore, the combination of an aqueous environment and mechanical loading such as cyclic-fatigue is a severe test for any adhesive system. Practical tests have shown that properly designed and fabricated adhesive bonded structures do not exhibit fatigue failure [2].

Work by Hart-Smith [21] has shown that bonded joints may be designed such that the adhesive can sustain loads greater than the unloaded strength of the parent material, ensuring that the adhesive will be able to sustain all possible load cases for the original structure. As pointed out by Davis and Bond [2], such adhesive bonds should thus never fail, because the structure would have failed away from the joint before the load necessary to fail the adhesive could be achieved. However, so many adhesive bonds fail in service. The reason is that they do not fail because of deficient design, nor do they fail because of poor materials selection. The deficiencies are usually in the processes themselves, not necessarily in their implementation [2]. Deficient bonding processes have been a significant contributor to the poor performance of adhesively bonded structures.

The past experimental data have shown that the contact thermooxidation can have the considerable effects on the stability performance of the adhesive joints (see for example Refs. [22–25]). The cohesive characteristics of the boundary layers in the adhesive joints are affected by the contact thermooxidation reactions of the polymer catalyzed by iron surface compounds [23, 24]. As pointed out by Kalnins and Ozolins [22], oxygen from several sources can take part in the contact thermooxidation, namely, (a) oxygen which diffuses through the polymer layer, (b) oxygen captured at the interface, and, (c) finally, oxygen which is absorbed or chemisorbed by metal surface oxide. The main features of contact thermooxidation (oxygen uptake, carbon dioxide evolution, change in the carbonyl group content, and change in the layer weight) under conditions of a free access of oxygen through the polymeric layer are kinetically interrelated with the change in peel strength [25]. As shown experimentally by Kalnins and Ozolins [22], the dependence of the rate of change of individual kinetic parameters of contact thermooxidation as well as of peel strength on the thickness of the adhesive layer and on the contact temperature can be described by a simple equation (see Section 9.1 for more detail). The dependence of peel strength on the contact time t can be described by an expression based on the assumption that the magnitude of peel strength is controlled by two main competing processes [22], namely (a) the accumulation of oxygen-containing groups and the oxidation cross-linking which increase the peel strength values, on the one hand, and (b) the reactions of oxidative destruction which decrease peel strength, on the other hand [25].

Water may affect both the chemical and physical properties of the adhesive and also the nature of the interface that exists between it and substrate [26]. Brockmann [27] studied the change in strength and deformability of the adhesive (usually a polymer-based material) layer under hot and humid environmental conditions and concluded that, for aluminum adherends,

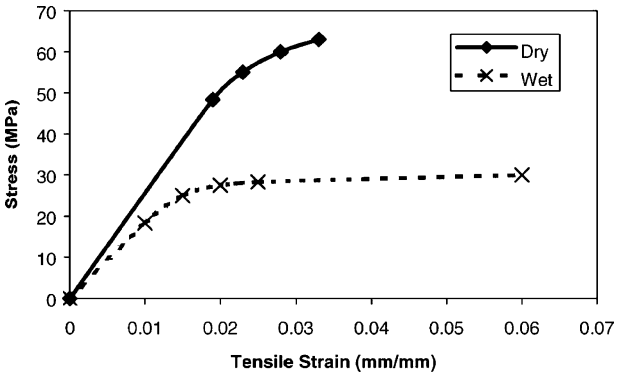

Figure 1 Effect of moisture (i.e., wet and dry) on mechanical properties of adhesive joints [28].

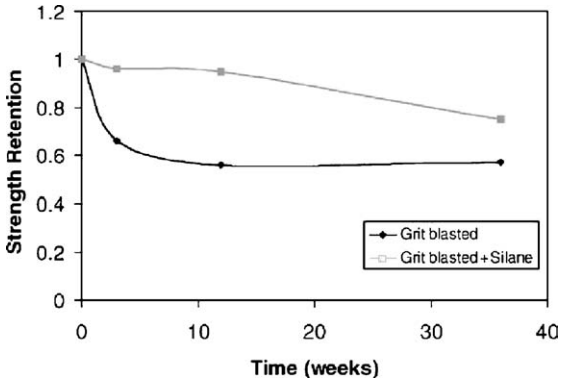

Figure 3 Effect of water uptake on joint strength (i.e., Butt joints) [28].

the water stability is dependent on the adhesive and surface treatment. He pointed out [27] that the two most effective ways to increase stability were: (a) to change the surface condition through special surface pretreatment, and (b) to use corrosion resistant primers.

As is generally known and accepted, adhesively bonded joints will suffer a loss in joint strength when exposed to high humidity, liquid water and/or high temperatures (see for example Fig. 1). It can be seen from Fig. 1 that the E-modulus (the slope of the linear part), yield stress and ultimate stress decrease when the adhesive becomes wet, while the strain to failure increases. In other words, moisture increases the flexibility and ductility of the adhesive. Many studies have demonstrated this for many years (see for example Refs. [28–30]. Abdel Wahab *et al.* [28] have investigated the degradation in the joint strength due to water uptake in terms of the change in mechanical properties and swelling. Fig. 2 shows the effect of water uptake on the swelling strain (i.e., this strain was measured as an increase in disc thickness at different intervals during the aging period). There is an evidence of swelling, which becomes significant as water uptake increases. The maximum swelling strain at saturation reaches 3%. As shown in Fig. 3, the effect of water uptake on the strength of butt joint was determined by testing joints after different intervals of aging in water immersion at 60°C [Note that two surface pretreatments were applied in this investigation: (a) grit blasting, (b) grit blasting + silane]. This figure illustrates the strength retention as a function of immersion time. The rate of degradation in the butt joints is faster than in the single lap joints [28]. The silane improves the durability of both joints. The single lap joints (grit blasted) shows a strength loss of about 30% during the first 3 weeks, then the strength is recovered in the next 3–6 weeks before a further reduction [28]. For the butt joints, the loss in strength is more significant in the first 3 weeks of aging.

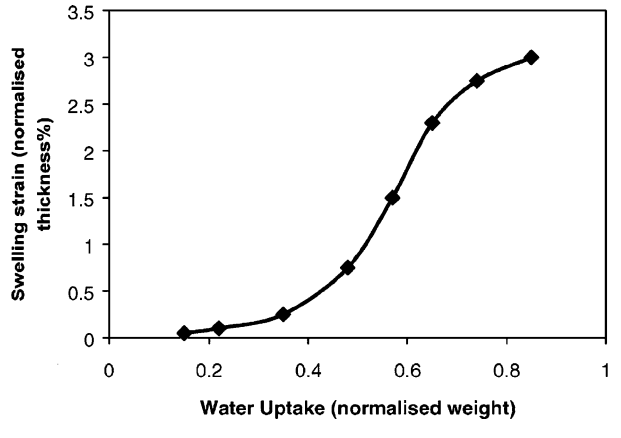

Figure 2 Effect of water uptake on swelling strain [28].

Applications for structural adhesive in a marine environment will generally involve much thicker adherends that used in some other industries. The effect of aging on adhesively bonded joints in a wet environment is particularly important for marine applications [29]. A major concern is the sensitivity of the adhesive to the effects of water. For marine applications [30], an important limitation that has been recognized is the degenerative effect that moisture may have upon the strength of an adhesively bonded joint. Such effects are pronounced when the component is also subject to conditions of high temperature [26, 31] and stress [32]. As pointed out by Knox and Cowling [29], in contrast to the technology used in the aerospace industry, the development of adhesives for bonding steel in marine applications has been governed not only by considerations of the highest possible strength and good durability performance, but more by the consideration of simple and economic process techniques. Accelerated environmental testing is a means of estimating service life or of providing data to rank influencing factors in terms of resistance to degradation [33]. The problem is that such environmental testing does not necessarily reflect the degradation mechanisms in the service environment. The generation of truly representative adhesive bond durability data, with the conventional lap shear joints, requires undesirably long periods of environmental exposure. With developments in adhesives and improvements in bonding technology, even longer periods of exposure will be required, unless durability testing can be modified. More severe environments at higher temperatures and increased loads, whilst reducing test time, may give unrealistic failure modes which would not predominate under service conditions [33]. As an answer to this problem, Arrowsmith and Maddison [34] proposed a smaller bond area than standard and predrilled holes to reduce the diffision path length and therefore the length of environmental exposure time required. However, this was at the expense of the initial strength and sensitivity.

1.2. Basic adhesive joint properties

In a simple system, bonding at an interface is due to adhesion between the adhesive and adherend. One talks of adhesion when a measurable amount of mechanical work is necessary to separate two surfaces of different chemical composion or shape [35]. In order to get good adhesion between adherend and adhesive the first essential work is to ensure good molecular contact.The determination of adhesion strength between compact materials (i.e., such as between adherends and adhesive) is still unsolved problem [36]. Polymeric adhesion may be enhanced by grafting a chemical species at the interface [37, 38]. In various industrial applications, multi-layer polymers are used to give better overall performance than the individual components alone [36]. Typically, one polymer may exhibit high mechanical strength whereas a second polymer may have the properties of impermeability necessary for preventing solvent diffusion. A combination will therefore give both mechanical and chemical resistance, provided the interfacial polymeric adhesion is adequate. Adhesion mechanisms between contacting polymers are various, depending on the type of polymers and contact conditions [39]. Macromolecular chain interdiffusion is important for compatible polymers [40, 41] and chemical bonding can lead to comparable interfacial strength [42]. Overall separation energy, or energy of adhesion, can be very high, considerably greater than expected from considerations of interfacial bonds, and it is since the pioneering work of Gent and Petrich [43] that bulk losses due to polymeric deformation associated with separation have been recognized. An upper limit for the intrinsic energy of adhesion is set at ca. 20 Jm^{-2} when primary bonds dominate [44] (although it is usually much less), yet measured separation energy may often be of the order of kJm^{-2} [45].

The basic adhesive properties are mainly [35] (a) adhesive strength (debonding process), (b) conformobility (bonding process), and (c) cohesive strength. As described by Creton (35), the three specific test methods are used to determine these basic adhesive properties: (a) peel (i.e., tensile transverse) tests (Fig. 4a) to determine adhesive strength (debonding process), (b) quick tack tests (Fig. 4b) to evaluate conformability (bonding process), and (c) a shear test (Fig. 4c) to determine the cohesive strength of the adhesive. From industrial point of view, the main concern is to obtain a value from each test for comparative purposes. Adherend tests (generally consisting of the mechanical seperation of the assembly) are used in order to quantify the adherence level between an adhesive and a substrate. It is now well known that the measured adherence or adhesion energy is a complex function of the adhesion (interfacial energy) and of the energy dissipated in the material during viscoelastic and deformation processes.

The adhesive stresses, peel stress, σ_a, and shear stress, τ_a, are useful basic parameters which can be used in the joint analysis. These expressions are given as [46]

$$\sigma_a = E_a \frac{w_u - w_l}{\eta_a}$$
$$\tau_a = G_a \frac{u_u - u_l}{\eta_a} \quad (1)$$

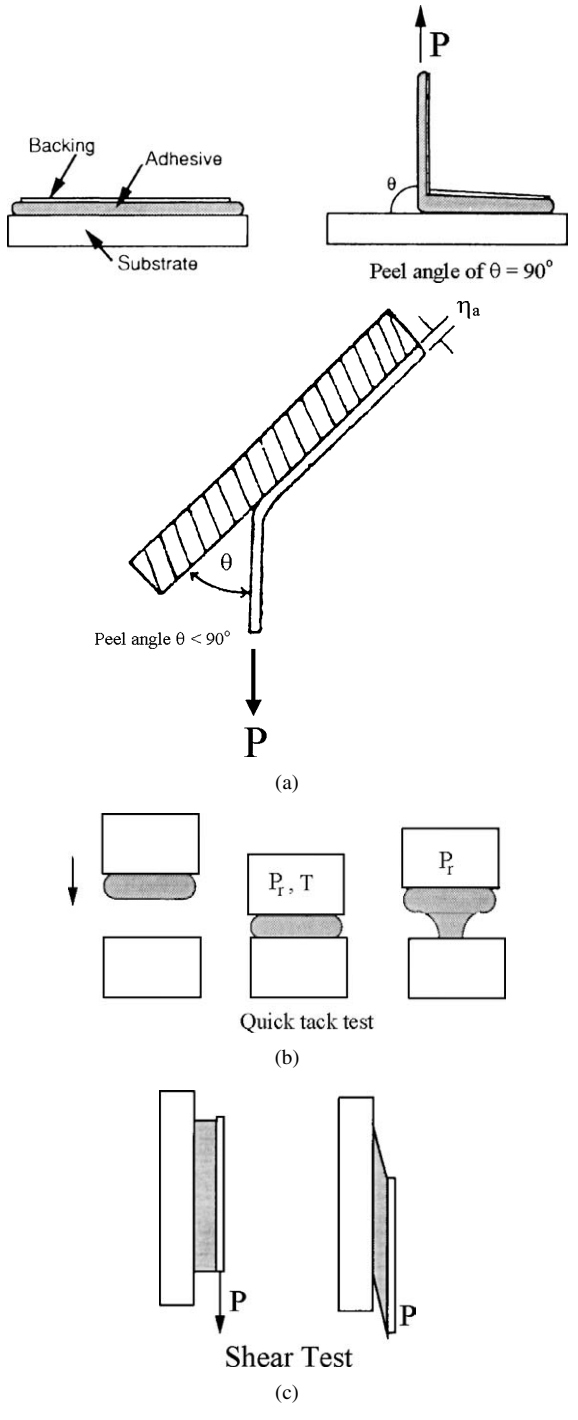

Figure 4 Basic tests for adhesive joints: (a) the peel tests for peel angles of $\theta = 90^\circ$ and $\theta < 90^\circ$, (b) the quick tack test; P_r: pressure; T: temperature, and (c) the shear test.

where w_u and w_l are the joint transfer deflections for upper and lower adherends in overlap, respectively; u_u and u_l are the longitudinal displacements for upper and lower adherends, respectively; η_a is the adhesive layer thickness; E_a and G_a are the Young's modulus and shear modulus of adhesive material, respectively. Due to the very thin adhesive layer, it is assumed that there is minimal variation in the adhesive stresses along the adhesive layer thickness.

As illustrated in Fig. 4a, the peel test, which simulates the removal of an adhesive tape, is the standard indicator of the fracture energy of the adhesive bond (i.e., the debonding process) and is mainly sensitive to

the viscoelastic losses in the adhesive [35]. A thin layer of adhesive is applied to a backing tape which is usually much stronger than the adhesive. The tape is then carefully bonded to an adherend (stainless steel polished to 2-μm roughness) and, finally, it is peeled in a manner shown in Fig. 4a. The peel force per unit width of tape measures directly the energy per unit area to separate the adhesive bond. Unfortunately, peel test results are also sensitive to the peel angle θ at which the tape is removed and to the stiffness of the backing tape, making it difficult to directly compare results from different manufacturers.

The nominal peeling energy or energy release rate, G_p, for a crack propagating at or near to the interface, can be calculated from the peel force, F, using the expression [47]

$$G_p = \frac{P(r - \cos\theta)}{w_a} - W\,\eta_a \qquad (2)$$

where P is the peel force, r is the extension ratio of the peeled leg (i.e., $r = 1 + e$), where e is the maximum strain in the peeled leg), θ is the peel angle, W is the strain energy density in the leg, w_a is the width of the rubber (or adhesive) and η_a is the thickness of the rubber in the unstrained state (see Fig. 4a). When extension in the peeled leg is ignored, $r \rightarrow 1$ and $W \rightarrow 0$, and peeling is carried out at 90°, Equation 2 simplifies [36, 48] to

$$G_p = \frac{P}{w_a} \qquad (3)$$

With this geometry, peel speed, v_p, is equivalent to machine crosshead speed, since it was checked that extension of the peel arm after seperation and under force P was negligible [36]. For example, Ansarifar *et al.* [48] have performed peel tests at an angle of 90° at 23°C on the rubber to nylon 6,6 joint, and the results for the peel force P against the cross-head speed are shown in Fig. 5. In Fig. 5, the first peaks corresponding to the onset of crack growth, where the peeling force was still rising, and the last peak corresponding to when test

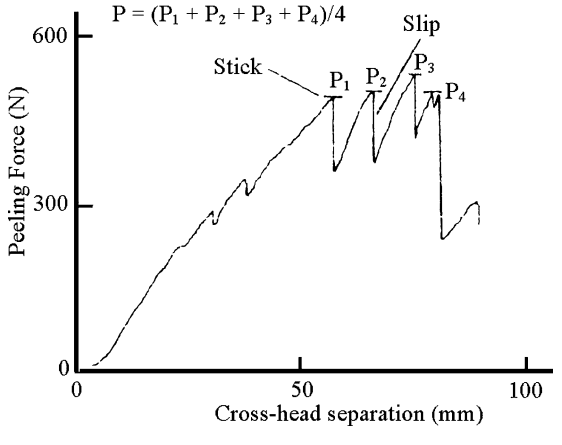

Figure 5 Typical peel force versus cross-head separation trace for a constant rate peel test; trace produced at 60 mm/min cross-head speed after peeling rubber from nylon 6,6 (Ref. [48]). Where P is the peel force, P_3 and P_1 are the maximum and minimum peeling force, respectively.

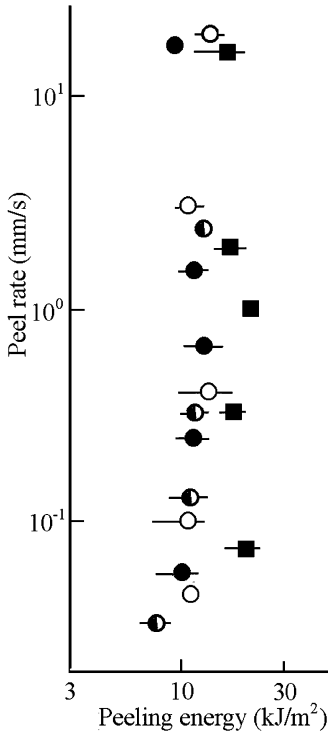

Figure 6 Peel rate versus peeling energy relationship from constant rate peel tests [48]: (■): Nylon, (●): Steel, (○): Aluminum, and (◐): $R_a \sim 1$ μm. Note that the bars indicate the minimum and maximum peeling energies calculated from the minimum and maximum peeling force, respectively, recorded on a typical peeling force versus cross-head separation trace shown in Fig. 5.

stopped or leg break occurred, were ignored (see Fig. 5) . The remaining peaks on the trace were utilized for calculating an average peeling force for the test piece (see Fig. 5). After the peel experiments are completed, force values are placed in Equation 3 to calculate peeling energies G_p for the test pieces. Fig. 6 shows the peeling rate variation as a function of the peeling energy determined using the above method.

The most widely used experimental parameters in peel test are (a) the peeling rate, (b) temperature, and (c) thickness of the adhesive. Fig. 7a shows the peel energy of an SBR adhesive on a Mylar substrate as a function of the peeling rate and at different temperatures [43]. It is clear from the data that, similarly to the viscoelastic properties, the peel energy data can be superimposed on a single master curve using the Williams-Landel-Ferry (WLF) time-temperature superposition [19], as shown in Fig. 7b. Such a result is typical from peel tests of pressure sensitive adhesive tapes and implies that the measured energy of adhesion is quite sensitive to the viscoelastic losses in the polymer used for the adhesive layer. Another important experimental variable in peel test is the thickness of the adhesive layer. Aubrey *et al.* [50] found that for a poly (*n*-butyl acrylate) (PBA) the 90° peel strength (i.e., tensile transverse strength) was independent of the adhesive thickness (in the 15–85 μm range) in the low peel rate regime, but that the rate at which they observed a transition from cohesive to fibrillar fracture to adhesive nonfibrillar fracture increased with thickness.

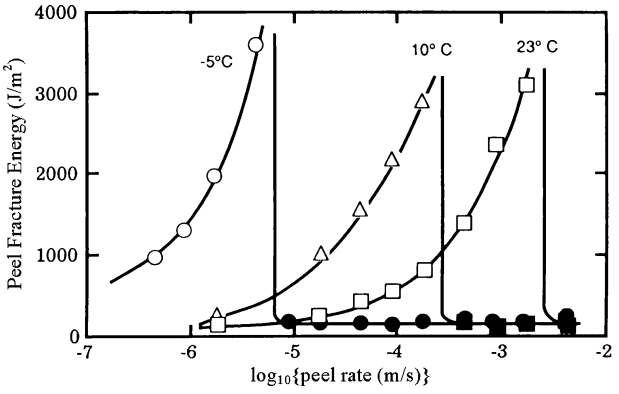

(a)

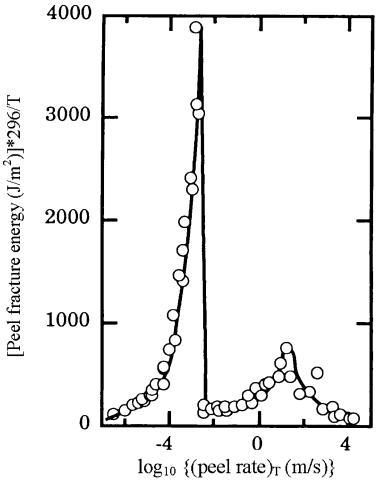

(b)

Figure 7 Peel fracture energy against rate of peel for SBR adhesive on a Mylar [43]. (a) Fracture energy versus the peel rate v_p and (b) Master relation for peel fracture energy against rate of peel v_p reduced 23°C.

Guiu and Shanahan [36] have investigated empirically and theoretically the effects of time, temperature and peel rate on the peel energy using two semi-empirical polymers (i.e., EVOH and PE*) at various peel angles. Fig. 8 summarises peel test results at temperatures in the range of 0–70°C and for peel speeds in

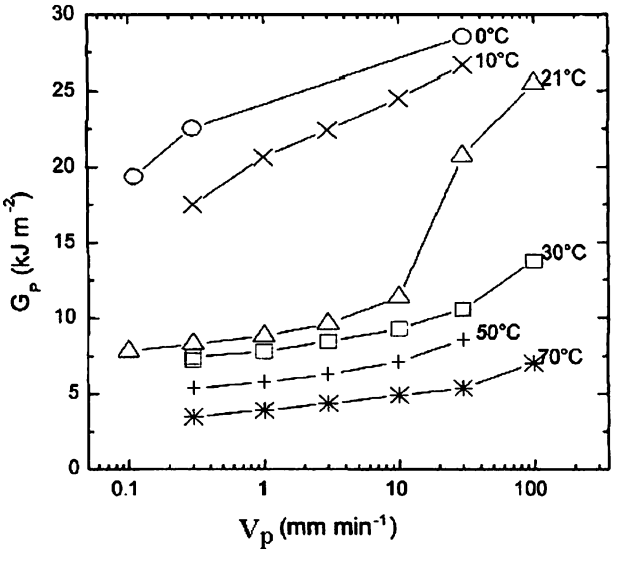

Figure 8 Peel energy, G_p, versus peel rate, v_p, at different temperature. Abscissa being on a logarithmic scale [36].

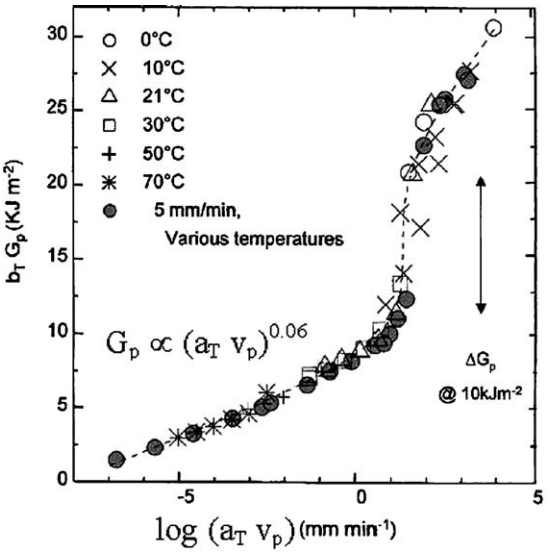

Figure 9 Master curve of (temperature-corrected) peel energy, $b_T\ G_p$ versus (temperature-corrected) peel speed, log ($a_T\ v_p$) (Ref. [36]).

the range of 0.1–100 mm min^{-1}. Note that the peel energy G_p was calculated using the Equation 3. They have constracted a master curve to combine these variables in a single equation , in a manner of the classic Williams-Landel-Ferry (WLF) treatment [19] developed for elastomers above their glass transition. Therefore, they attempted to combine the results of Fig. 8 by empirically using a time-temperature transition factor, a_T:

$$\log a_T = 0.11(T_o - T) \tag{4}$$

where T_o is equal to 21°C, the reference temperature. T is a temperature. A small, vertical shift correction was also applied to take into account effects due to thermal expansion [19, 43, 51]. This thermal expansion correction, b_T, is equal to $(T_o + 273)$ $(T + 273)$ and is, consequently, quite small. Fig. 9 presents the master curve of $b_T G_p$ versus log ($a_T v_p$) obtained for the temperature range of 0–70°C. Here G_p is the overall energy, and v_p the peel speed. With a reference temperature of $T_o = 21$°C, it can be seen that the master curve for $b_T G_p$ versus log ($a_T v_p$) is most acceptable and shows an approximately linear increase in the lower speed range, with a gradient of ca. 0.06, consistent with the bulk behavior of polyethyelene [52, 53].

Guiu and Shanahan [36] have also investigated this problem theoretically. Polymeric relaxation phenomena are associated with molecular motion resulting from thermal agitation. It may be considered that the shift factor a_T represents the difference between the characteristic relaxation time, t, at a given temperature, T, and the equivalent relaxation time, t_o, at a reference temperature T_o, such that $t = a_T t_o$. For semi-crystalline polymers, an Arrhenius type relation may be applied on a dependence of t as a function of temperature for secondary transition (local macromolecular motion) [54, 55], such that

$$t = t_o \exp\left(\frac{Q}{R_g T}\right) \tag{5}$$

where Q is an activation energy, R_g is the ideal gas constant and T is (now) in Kelvin. Consequently, Gui and Shanahan [36] constructed following relation for a_T:

$$\log a_T = \log \frac{t}{t_o} = \frac{Q}{2.3R_g}\left(\frac{1}{T} - \frac{1}{T_o}\right) \quad (6)$$

Provided the temperature difference $(T_o - T)$ is not too great, with respect to T_o, Equation 6 may be simplified to

$$\log a_T \approx \frac{Q}{2.3R_g T_o^2}(T_o - T) \quad (7)$$

which is precisely of the form of Equation 4.

Fig. 10 shows $\log(a_T)$ versus T, both with empirically obtained values and two lines. The dotted line corresponds to the empirical fit, as given by Equation 4 and the full curve represents Equation 6 after application of non-linear regression analysis. It can be seen that, although the empirical fit seems slightly better, application of Equation 6 gives acceptable agreement. A value for Q of 199 ± 5 kJmol^{-1} was obtained, which is close to that given in the literature for polyethelene: 220 kJmol^{-1} [54]. Therefore, Guiu and Shanahan [36] suggested that the time and temperature effects observed during peel are principally governed by (a) process(es) of bulk energy dissipation in the polyethelene.

As shown in Fig. 4b, the quick tack experiments probe the instant adhesion and are an indication of the ability of the material to form a contact very quickly (i.e., conformability) to the substrate. The tests that have been designed to probe this property can be divided into two categories [35]: (a) those measuring the force of separation, and (b) those measuring the energy. The main test probing the force is that of probe tack [56], where a flat cylinder is brought into contact with the adhesive film and subsequently removed at a fixed crosshead speed. In this geometry, the maximum force of separation is taken as the measure of adhesion. Alternatively, a loop tack test has also been used where the adhesive is put on a tape and the force necessary to unstick the loop of tape from the substrate is measured [35].

Among the tests probing the energy, the most widely used are the rolling ball test or the rolling cylinder test where a standardized steel ball is allowed to roll from an inclined plane on a sticky surface and the distance it rolls before stopping, or alternatively the largest ball that will not roll on the inclined plane, is a qualitative indication of the energy involved in bonding and debonding the adhesive from the adherend [35].

Finally, in order to measure the resistance to shear, a shear test method is used (Fig. 4c). This test is particularly crucial for all permenant and semi-structural applications where a large deformation with time under moderate stress is detrimental [35]. The adhesive is tested either in static shear, where a fixed load is applied and the time to failure of the adhesive bond is recorded, or in dynamic shear, where a constant shear rate is imposed and the force is monitored. This is basically a creep test and will give an indication of the cohesive strength of the adhesive after a long time. The important experimental parameters in shear test are the load and the temperature for the static shear, along with the shear rate and the temperature in the dynamic test.

The peel strength of the adhesively bonded joints are affected by the contact thermooxidation [22, 25]. In order to study the effects of contact thermooxidation on the peel strength of adhesive joints, Kaelble [57] developed a model of the peel mechanics for an elastic flexible adherend and a visoelastic adhesive layer bonded to the rigid adherend (see Fig. 11a). It was shown that the peel strength (i.e., tensile transverse strength) A_p is proportional to the adhesive layer thickness η_a. This

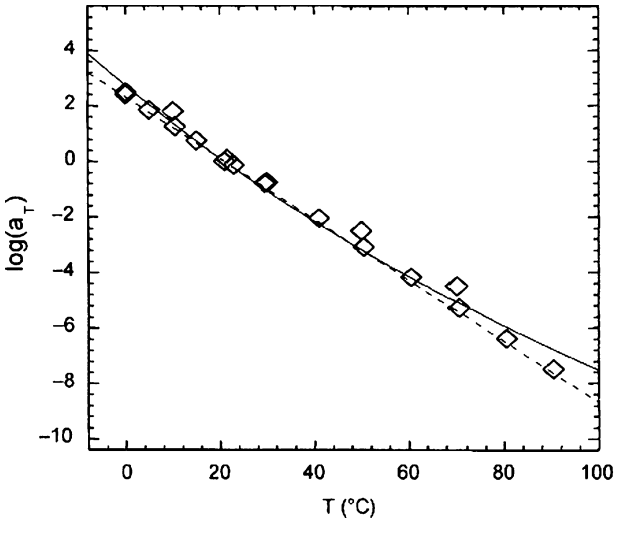

Figure 10 Shift factor a_T used to obtain the master curve at 21°C in Fig. 9 (Ref. [36]): (◇): experimental, (------): 0.11 $(T_o - T)$, and (——): $Q/2.3R_g(1/T - 1/T_o)$.

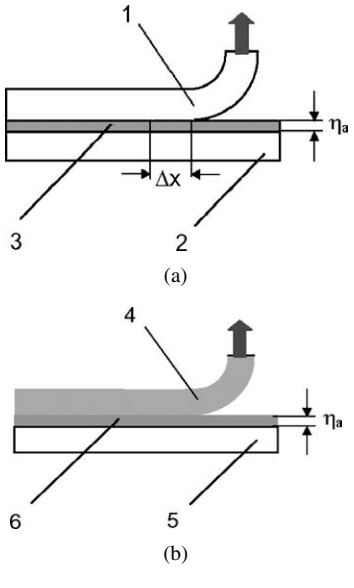

Figure 11 Scheme of an adhesive joint [22, 57]: (a) an elastic flexible adhesive [1] and viscoelastic adhesive layer [3] bonded to the rigid adherend [2] and (b) a flexible adhesive [4] bonded to steel [5] through the boundary layer [6].

proportionality was confirmed experimentally and was established to be valid even for comparatively thick (up to 25 μm) adhesive layers [58]. In accordance with Kaelble's model, the peel strength can be expressed as $A_p = \eta_a Z$, where Z is a complex term which takes into account the strength deformation charcteristics of the system (i.e., tensile and shear moduli of the adhesive, boundary cleavage, and boudary shear stresses) and the peel angle θ. In the case of T-peel tests, cleavage stresses predominates [59] and $Z = \sigma_o^3/2E_a$, where σ_o is the boundry cleavage stress and E_a is the tensile modulus of the adhesive.

Taking into account the origin of the gradient of macromolecules changes in the polymer boundary layer near the interface with metal and, as a result, the existence of the respective gradient of the strength—deformtion characteristics of the polymer, Kalnins and Ozolins [22] have adopted the Kaelble approach in their analysis of contact thermooxidation. They considered the residual boundary layer with thickness η as peculiar "adhesive" which joins the metal with the either part of the polymer layer (see scheme in Fig. 11b):

$$A_p = \frac{\eta \sigma_B^2}{2E_a} \tag{8}$$

where σ_B is the tensile strength and E_a is the tensile modulus of the polymer in the boundry layer. They pointed out [22] that this is rather a foggy speculation. The most serious thing is that the residual layer is not uniform. According to the SEM data they have taken the adhesive thickness η as an average value. In fact, the peel strength A_p (the peel force P versus the width of the peeled off strip w_a) is the energy per unit rea of the debonded interface (see Fig. 11b).

$$A_p = \frac{P\,\Delta x}{w_a\,\Delta x} \tag{9}$$

where Δx is the elementary displacement of a delaminated front line, $P\Delta x$ is the elementary work of fracture, and $w_a \Delta x$ is the elementry delaminated area. To exclude the dependence of the peel strength on the thickness η, Kalnins and Ozolins [22] calculated the peel energy characteristic as $A_V = A_p/\eta$. In accordance with Equations 8 and 9, they developed the following expression:

$$A_V = \frac{P\,\Delta x}{w_a\,\Delta x\;\eta} = \frac{\sigma_B^2}{2E_a} \tag{10}$$

where $w_a\,\Delta x\;\eta$ is the elementary volume of the adhesive. Consequently, A_V is the peel energy per unit volume of a polymer layer involved in the deformation followed by fracture, which depends only on the strength-deformation characteristics of the adhesive (σ_B, E_a). (It should be mentioned that the ratio $\sigma_B^2/2E_a$ is equal to the unit work of fracture of the elastic solid). Kalnins and Ozolins [22] have used Equation 10 in their study of contact thermooxidation, which will be presented in Secion 9.1.

2. Adhesively bonded joints

2.1. Types of adhesive joints

Several simple (and standard) adhesively bonded joints used in industry are shown [46, 60–63] in Fig. 12: (a) single-lap joint, (b) double-lap joint, (c) scarf joint, (d) single-lap joint with spew [61], (e) single-lap joint with chamfer [61], (f) filleted single-lap joint [46, 61], (g) recessed joint [62], and (h) tapered joint [63]. The spew can be considered as the result of the adhesive squeezed out of the lap region at the moment of the joint manufacture. A recessed (or a gap) joint is obtained by removing portions of the adhesive from the interior of the overlap. The single-lap shear specimen is the most convenient one for testing quality of adhesive bond and that application of adhesive on both rough sides of adherends is proper way leading to the highest shear strength [64]. In the development of bonded joints for structures, a simple joint can be fabricated first and tested for its suitability in structures. The size of the joint can be first estimated from a knowledge of the part sizes to be joined, allotted space for the joint, and a general idea of how much overlap is required to carry the load. With such knowledge, preliminary joint designs can be made that can be refined using an iterative analysis procedure.

As pointed out by Maheri and Adams [65], while the tensile lap-shear specimens are commonly used for quality control, it is almost impossible to determine the adhesive properties from such tests owing to the complex stress and strain distributions inside the joints. Therefore, it is necessary to know the the mechanical properties, particularly the stress-strain curve and moduli in order to determine the stresses and strains in adhesive joints in variety of configurations [66–70].

As stated above, the simplest and most popular solution for adhesively bonding two sheets is the single-lap joint. However, from the structural view point, the single-lap joint has two harmful features [61]: (a) the offset of the two sheets causes a bending action in the joint, adding additional stress components; (b) the stress distribution in the lap is not constant and displays peaks at its ends. After the simplified solution of Volkersen [71] (developed for riveted joints but applicable also to adhesive bonds)and the more complete study of Goland and Reissner [72] (which accounted for the peel stress) much effort has been spent over six decades to determine the stress field of the single-lap joint and to obtain the "optimal" design of the joint.

In structural adhesive joints, the T-joint is one of typical joint geometry which is used to bond two plates at a right angle (i.e., 90°) (see Fig. 4a) or some other angle (see Fig. 4a). The design and analysis of such joints depend on the joint geometry, and also on the relative stiffness of adherends and the adhesive [73]. Generally, the joints are subjected to load in the plane of the adherend or transverse to it. In general, poor results are obtained when the joint is stressed such that tensile transverse (peel) stresses occur, as in the case of side loading [74]. Compressive transverse stresses do not generally cause failure. Compressive forces in the direction of the sheet will only cause problems when the sheet buckles [70]. T-joints have not been extensively analyzed although they are used in many applications

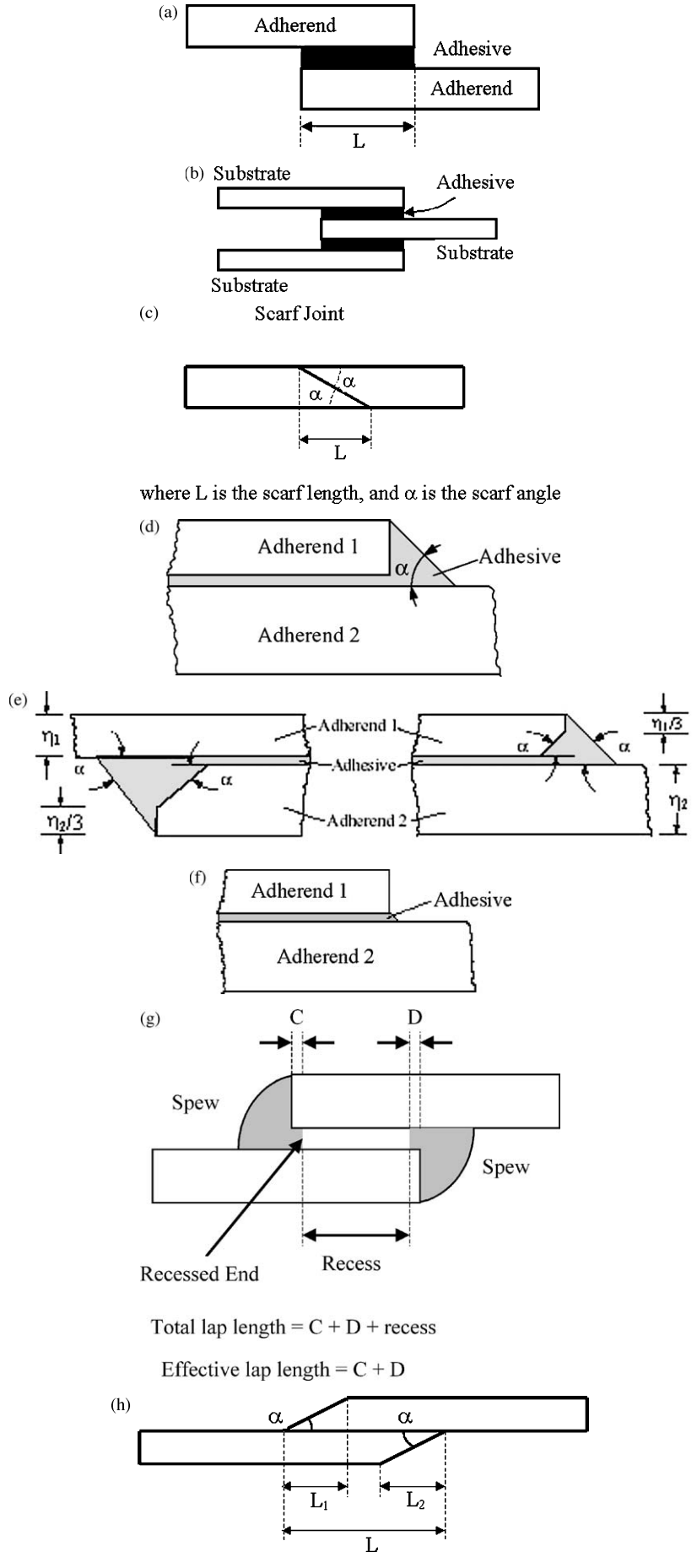

Figure 12 Types of adhesive joints used in industry: (a) single-lap joint, (where L is the joint overlap length), (b) double-lap joint, (c) scarf joint (where L is the scarf length, and α is the scarf angle); (d) single-lap joint with spew (where α is ther spew angle), [61], (e) single-lap joint with chamfer, (where α is the chamfer angle, η_1 and η_2 are the thicknesses of the adherends) [61], (f) filleted single-lap joint [46, 61], (g) recessed joint (where total lap length $= C + D+$ recess; efeective lap length $= C + D$) [62], and (h) tapered lap joint, (α is the tapered angle, L_1 and L_2 are tapered lengths) [63].

such as in the automotive industry [75]. Adams *et al.* [70] showed variations of T-joints which may be encountered in practice. Shenoi and Violette [76] used adhesively bonded composite T-joints in small boats and investigated the influence of T-joint geometry on the ability to transfer out-of-plane loads.

The adhesive joints are very complex in nature since they have different geometrical shapes. Therefore, there are still problems to be solved using the different methods such as shape optimisation, numerical solutions and finite element analysis methods.

2.2. Mechanical durability design principles

In spite of the increased usage of adhesive bonding in structural applications, the determination of adhesion strength and durability remains largely empirical in nature. This can result in over conservative design leading to structural redundancy or, conversely, to failure of adhesively bonded joints, typically due to the combined effects of complex modes of loading and environmental degradation.

Many early bonded joint designs were based on the joint strengths and optimal overlap lengths determined from lap-shear tests. The incorrect assumption inherent in that approach is that the shear stresses in a bonded joint are uniform, so that twice the overlap length provides the joint with twice the load capacity [2]. However, early work by Goland and Reissner [72] showed that the adhesive shear stresses are non-uniform, with high shear stresses at the ends of the joint and a low shear stress in the center of the joint. As Davis and Bond [2] have underlined, the consequence of this is that, for moderate to long overlap lengths, doubling the overlap length of a joint simply adds to the low stress area in the joint and contributes nothing to the load capacity of the joint.

In many circumstances, the adhesive layer is designed to carry a high level of stress, for example, in bonded composite repairs to thick-section primary aircraft structure [77] and hence is prone to yielding under in-service loads. One recent development in bonded composite repair technology has been in the area of repairs to curved surfaces, with a view to reducing the critical stress levels. Bonded composite repairs to curverd surfaces induce through-thickness stresses as well as shear stresses in the adhesive [14]. Consequently, a valid yield criterion is of considerable importance to the design and analysis of bonded reinforcements. Due to the constraint imparted by the stiff adherends, the adhesive layer in the bonded joint experiences a high degree of constraint [78]. On the one hand, the resulting triaxial constraint induces hydrostatic stresses that promote crazing and void growth, leading to brittle failure. On the other, the high degree of constraint implies that the adhesive layer is more resilient to shear deformation than in the neat form [79].

Hart-Smith [21] extended the Goland and Reissner analysis [72] of bonded joints to allow for plastic behavior in the adhesive. Hart-Smith approach assumes that the adhesive behaves ideally elastic-perfectly plastic (see Fig. 13b). The data for design were obtained from thick adherend tests (i.e., specified by ASTM D3983-93) (see for example Fig. 13a). This analysis indicates that, within certain limit of overlap length and adherend thickness, bonded joints can be designed such that the load capacity of the bond is greater than the unnotched strength of the parent material. This specification simplifies joint design procedures in great extent [6]. As summarized in their recent paper by Davis and Bond [2], an adhesively bonded joint may be designed by predicting (a) the load capacity P, and (b) the joint overlap length using the Hart-Smith approach [21]. Assuming that peel effects and thermal stresses are ignored [2], the load capacity P (the load which the adhesive can sustain) of an elastic-plastic adhesive in a single overlap bonded joint is given by Hart-Smith [21] the lesser value of:

$$P = \sqrt{2\eta_{\mathrm{a}}\tau_{\mathrm{a(p)}}\left(\frac{1}{2}\gamma_{\mathrm{a(e)}} + \gamma_{\mathrm{a(p)}}\right)E_{\mathrm{s(l)}}\ \eta_{\mathrm{s(u)}}\left(1 + \frac{E_{\mathrm{s(l)}}\,\eta_{\mathrm{s(u)}}}{E_{\mathrm{s(u)}}\,\eta_{\mathrm{a}}}\right)}$$

or

$$P = \sqrt{2\eta\tau_{\mathrm{a(p)}}\left(\frac{1}{2}\gamma_{\mathrm{a(e)}} + \gamma_{\mathrm{a(p)}}\right)E_{\mathrm{s(u)}}\eta_{\mathrm{a}}\left(1 + \frac{E_{\mathrm{s(u)}}\,\eta_{\mathrm{a}}}{E_{\mathrm{s(l)}}\,\eta_{\mathrm{s(u)}}}\right)} \tag{11}$$

where $E_{\mathrm{s(u)}}$ and $E_{\mathrm{s(l)}}$ are the elastic modulus of the upper and lower adherends, $\gamma_{\mathrm{a(e)}}$, $\gamma_{\mathrm{a(p)}}$ are the elastic and plastic shear strains of the adhesive, $\eta_{\mathrm{s(u)}}$ and $\eta_{\mathrm{s(l)}}$ are the thicknesses of the upper and lover adherends, $\tau_{\mathrm{a(p)}}$ is the plastic shear strength of the adhesive, η_{a} is the adhesive thickness. Note that variables in Equation 11 are defined in Fig. 13a and b as well. Similarly above equations describe the load capacity for a double overlap joint. If the load capacity calculated in Equation 11 is greater than the strength of the parent material, the adhesive will never fail, provided an adequate joint overlap is designed.

The joint overlap requirements can be determined simply by designing the overlap length (see Fig. 13c) such that the adhesive could sustain the parent material unnotched ultimate strength by plastic behavior within the adhesive. This is achieved by determining the required plastic zone overlap length l_{p} from:

$$l_{\mathrm{p}} = \frac{\sigma_{\mathrm{su}}\,\eta_{\mathrm{s(u)}}}{2\tau_{\mathrm{a(p)}}} \quad \text{for a single overlap joint} \tag{12}$$

where σ_{su} is the ultimate tensile strength of the adherend. Additionally, generous allowance must be made for an elastic through to provide the joint with some measure of creep resistance [2]. In a bonded joint, the elastic transfer length L/Ω is the distance necessary for the elastic shear stresses to decay to near zero. A factor of three is applied to that elastic zone length to provide the necessary allowance for creep resistance:

$$l_{\mathrm{e}} = \frac{3}{\Omega} \tag{13}$$

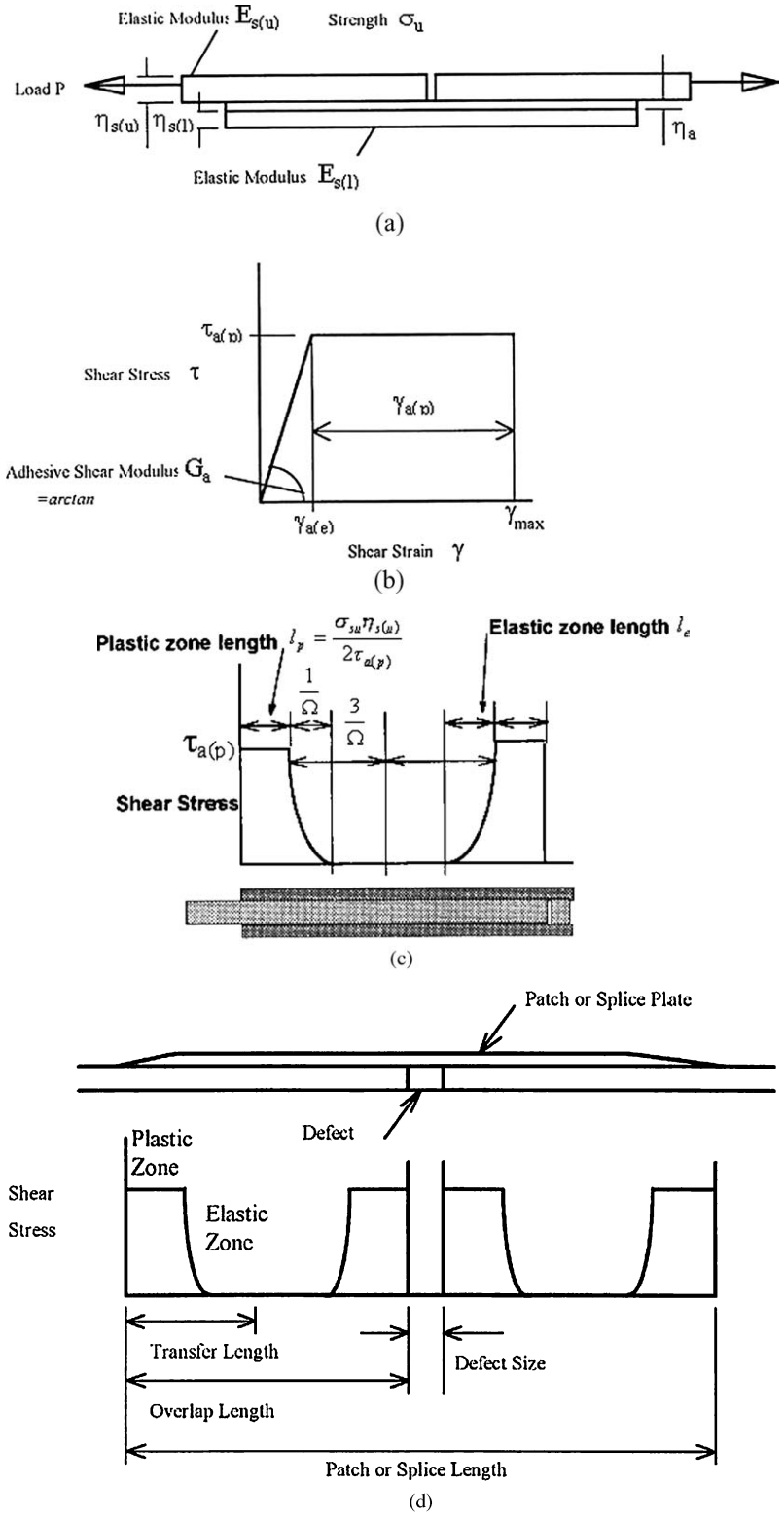

Figure 13 Mechanical design for an adhesive joint [2, 21]: (a) A thick adherend single-overlap joint (i.e., specified by ASTM D3983-93). (b) Shear stress-shear strain curve for an ideally elastic-perfectly plastic adhesive. (c) Methodolgy for determination of overlap length for a bonded joint such that the load capacity will be greater than the unnotched strength of the parent material. (d) Methodology for determination of overlap length for a bonded joint such that the load capacity will be greater than the unnotched strength of the parent material.

where

$$\Omega^2 = \frac{G_a}{\eta_a}\left(\frac{1}{E_{s(l)}\,\eta_{s(u)}} + \frac{1}{E_{s(u)}\eta_a}\right)$$

where G_a is the adhesive shear modulus. As shown in Fig. 13d, the required transfer length (the length necessary to allow complete load transfer from one adherend to the other) is the total of the elastic and plastic zone sizes ($l_e + l_p$). The overlap length (the required minimum distance between the edge of the joint to any discontinuity) is twice the transfer length. For a patch or splice for a butt joint, the minimum patch or splice length must be twice the overlap length.

Joints designed using this approach will always be stronger than the parent material [2]. The ability to

design bonded joints such that the adhesive is never the weakest part of the joint has significant design implications. If the adhesive will not fail due to loading, then there is no requirement to perform detailed design of the joint for the various structural load cases usually required to demonstrate structural integrity, because there is no load case greater than material ultimate for the parent material. All of the above design principles rely implicitly on the integrity of the bond being sustained in service, i.e., the bond is durable.

2.3. Advantages and disadvantages of adhesive bonded joints

Adhesive bonding offers many advantages over the classical fastening techniques such as welding, riveting and mechanical fastening. It has a high resistance to fatigue and as a concequence the life-cycle maintenance costs are significantly reduced [28]. The substantial reduction in weight that can be achieved by the use of adhesive bonding is an important advantage, especially for lightweight structures. In joining lightweight composites, adhesive bonding is the most appropriate joining technique. Almost any material or combination of materials can be joined in a wide variety of sizes, shapes, and thicknesses [11]. For most adhesives, the curing temperatures are quite low, seldom exceeding 180°C. A substantial number cure at room temperature, or slightly above and can provide adequate strength for many applications. As a result, very thin or delicate materials such as foils can be joined to each other or to heavier sections. Heat-sensitive materials can be joined without damage and heat-affected zones are not present in the product. When joining dissimilar materials, the adhesive provides a bond that can tolerate the stresses of differential expansion and contraction [11].

Therefore, the advantages of using adhesively bonded joining methods over conventional mechanically fastened joints can be summarized as [11, 28, 80, 81]: (a) few parts in the joint. Adhesive bonding assembly can simplify the assembly process, increase production and quality and reduce production cost.(b) full load transfer can readily be achieved, (c) the joint is fatigue resilient, (d) the method of construction also seals the joint, (e) a stiffer connection is produced, (f) the connection is light weight, (g) a smooth contour results, (h) the action of the adhesive provides corrosion resistance between the adherends, and (i) no open hole stress concentrations are created.

Despite these advantages, the use of adhesive bonding is not yet widespread. As pointed out by Abdel Wahab *et al.* [28], this is mainly due to its low durability when the structure is exposed to hostile environmental conditions. The effect of moisture on the strength of adhesively bonded joints is significant due to the deterioration of the adhesive layer and the interface. The strength of a joint is decreased dramatically when aged in hot/wet environments. This has been demonstrated in metal/epoxy joints [82, 83] and composite bonded joints [10, 84, 85]. In a metallic joint, moisture diffuses into the joint through the adhesive layer and wicking through the interface. It was reported [86] that in general the moisture diffusion through adhesive is predominant if there was no pre-existing micro-cracks and debonded areas at the interface although this is still an area of some debate. Although some studies have shown that water diffusion in polymers is non-Fickian [87, 88], most researchers assume Fickian diffusion model, for simplicity, in order to evaluate the rate of diffusion in adhesives [82, 89].

The major disadvantages of adhesive bonding [11, 28, 29, 48, 80, 81, 90] are: (a) There is no universal adhesive. Selection of the proper adhesive is often complicated by the wide variety of available options; (b) Most industrial adhesives are not stable above 180°C. Oxidation reactions are accelerated, thermoplastics can soften and melt, and thermosets decompose. While some adhesives can be used up to 260°C, elevated temperatures are usually a cause for concern; (c) High-strength adhesives are often brittle (poor impact properties). The toughness of an adhesive joint may decrease considerably under impact loading conditions. Resilient ones often creep. Some become brittle when exposed to low temperatures; (d) Long-term durability and life expectancy are difficult to predict; (e) Surface preparation and cleanliness, adhesive preparation, and curing can be critical if good and consistent results are to be obtained. Some adhesives are quite sensitive to the presence of grease, oil, or moisture on the adherend surfaces to be joined. Surface roughness and wetting characteristics must be controlled; (f) The joint can not be disassembled readily. Assembly times may be greater than for alternative methods, depending on the curing mechanism. Elevated temperatures may be required, as well as specialized fixtures; (g) The joint design is thickness-limited; (h) Only shear loading is acceptable; (i) It is difficult to determine the quality of an adhesive-bonded joint by tradational nondestructive techniques, although some inspection methods have been developed that give good results for certain types of joints; (j) Many structural adhesives deteriorate under certain operating conditions. The adhesive can be subjected to environmental effects. Environments that may be particularly hostile include ultraviolet light, ozone, acid rain (low pH), moisture, and salt. Thus durability and reliability of a joint over an extended service lifetime may be questioned. The determination of adhesion strength and durability remains largely empirical in nature; (k) Some adhesives contain objectionable chemicals or solvents, or produce them upon curing; and (l) The thermal residual stresses can be induced.

2.4. Stress analysis of adhesive joints

The use of adhesive bonding is increasing rapidly, but there are still important issues which need to be addressed in joint analysis, design, and durability consideration. The durability study of joints involves considerations [91] of (a) a variety of joint geometries, (b) materials (i.e., adherends and adhesives, primers), (c) loading conditions [i.e., static loadings (pure loadings such as shear, tension, and compression or complex loading such as bending) or dynamic (or impact) loadings], (d) failure modes (i.e., adhesive failure,

cohesive failure, mixed failure), and (e) environmental effects (i.e., temperature and moisture effects). The analysis of adhesively bonded joints requires a reliable and efficient tool to obtain stresses, strains, and fracture parameters. Most of the available methods require big investments in computer as well as designer time.

The increased application of adhesive joints was accompanied by the development of mathematical models to analyze the behavior of those joints. There are two basic approaches for the analysis of adhesively bonded joints [i.e., 91, 92]: (a) closed-form or analytical model, and (b) numerical solutions (i.e. finite element analysis, FEA). Analytical models such as the classical work by Goland and Reissner [72] usually involve some simplifying assumptions. However, some of these techniques yield closed-form solutions which generally involve some simplifying assumptions. All are limited to a certain range of geometrical or loading conditions. In the closed-form approach, a set of differential equations and boundary conditions is formulated. The solutions of these equations are analytical expressions which give values of stresses at any point of joint. Several analytical models have been developed for analysis of adhesively bonded joints. The analytical approach for the solution of complex stress distribtions in the joints has been progressively refined until recent times [i.e., 61, 93–97]. In general terms it makes use of the plate theory to model the sheets while some simplified assumption is made for the adhesive layer behavior. The analysis is bidimensional, since it involves a strip of unit width in transverse direction, assuming plane strain conditions. Volkersen [93] improved his previous work by including the peeling stress and assuming a relationship between shearing strain and displacement more correct than that of Goland and Reissner [72]. Segerlind [94] pointed out that as the lap length increases the stresses are in general reduced, but the stress peaks at the lap ends are more marked. Conversely, in the case of lap length the stresses are everywhere higher but more uniform. Renton and Vinson [95] developed an analytical solution for the case of an adhesive joint of orthotropc plates. Ojalvo and Eidinoff [96] accounted for the variation of the stresses through the adhesive thickness and investigated on the adhesive layer thickness effect. Bigwood and Crocombe [97] developed an analytical solution capable to describe not only simple lap joints but also more complicated geometries.

In the second approach, solutions of differential equations are obtained by numerical methods or the continuum is represented by a discrete model (i.e., finite element analysis model) at the outset. A system of algebraic equations is derived, commonly from energy functions. The solution of these equations gives displacements at the determined points from which strains and stresses can be obtained for any point within the model. Numerical methods provide a general tool for anaysis of arbitrary geometries and loading conditions. Among the numerical methods, finite element analysis (FEA) has been extensively used with success; however, this kind of analysis requires the generation of a large set of data in order to obtain reasonably accurate results. Although the convenience of modern finite element programs has significantly improved analysis efficiency, a large investment in engineering time and computer resources is still required for many practical problems. Finite element modelling can be a useful tool in the understanding of the behavior of adhesive joints, especially when it is combined with an extensive experimental programme.

As mentioned previously, the single-lap joint has been used extensively in many studies due to its simplicity and practical application. One of the first finite element analyses of a single-lap joint was published by Wooley and Carver [98]. They used plane stress elements, performed linear analysis, and modeled the adhesive layer with two rows of elements, thus obtaining the stress variation across the adhesive thickness. Many other two-dimensional (2-D) models of single-lap joints followed this work. Similar linear analyses were done by Guess *et al.* [99]. They used a more refined mesh, which allowed them to identify significant stress gradients across the adhesive thickness. Harrison and Harrison [100] did a simplified analysis in which they considered rigid adherends and studied the adhesive deformations. Adams and Peppiatt [101] used the plane strain triangular elements to model a single-lap joint and considered the adhesive layer to have either a square edge or a spew fillet.

The stress analysis of adhesively bonded joints is complex because the joints rarely see simple or pure loading of any type (e.g., shear, tension or compression) but, rather, are usually subjected to some bending. Details stress analysis of balanced joints (for example, such joint given in Fig. 12a) can be found in studies such as by Goland and Reissner [72] and Oplinger [102]. It is therefore useful to give some mathematical expressions in order to better understand the effects of bending loading on the adhesive joint behavior, as this subject was recently reviewed by Li and Lee-Sullivan [46] in their joint stress analysis for an idealized geometry of the unfilleted single lap joint using the analytical solution approach.

In general, the bending moment at the end of the overlap, M_o, can be related [46] to the applied in-plane loading, P, and the adherend thickness, η_s, by the bending moment factor, k, where

$$M_o = P\left(\frac{\eta_s}{2}\right)k \tag{14}$$

It is noted that P is the applied tensile force per unit adherend width. The physical significance of Equation 14 may be explained as follows: The two opposing forces, P, applied to the joint are not co-linear, so there will be some bending applied to the joint in addition to the in-plane tension. As the applied tensile force increases, the overlap correspondingly rotates to reduce the bending moment, i.e., k decreases with increasing η_s (Ref. [46]).

In order to improve the accuracy of the FEM simulation in the numerical analysis the following longitudinal stress values at the top/bottom surface points for

the bending moment M_o and its factor k at the overlap end may be used [46]:

$$M_o = \frac{\sigma_{bending} I}{t/2} = \frac{\eta_s^3 \sigma_{bending}}{6\eta_s} = \frac{\eta_s^2 \sigma_{bending}}{6} \quad (15a)$$

$$k = \frac{M_o}{\frac{1}{2} P \eta_s} = \frac{\eta_s \sigma_{bending}}{3P} \quad (15b)$$

where $I = \eta_s^3/12$ is the centroidal moment of inertia per unit adherend width, $\sigma_{bending}$ is the bending stress at the ovelap end.

Li and Lee-Sullivan [46] have also reviewed the analytical solutions for an idealized geometry of the unfilleted single-lap joint since most analytical solutions in the literature are derived on the assumption of an idelized geometry of the unfilleted single-lap joint. The available expressions for the bending moment factor k at the overlap end are supplied in Refs. [102–104]. Tsai and Morton [105] discussed the discrepancies and controversies in these theoretical solutions. According to Li and Lee-Sullivan [46], among the models reviewed, the k model offered by Oplinger [102] seems to be, by far, the most complete and therefore, they have applied this model to their recent work [46]. Oplinger's [46, 102] expression for the bending moment factor k_{op} is

$$k_{op} = \frac{\tanh(\xi l_s)\left\{R_3 R_o\left(1 + \frac{\eta_a}{\eta_s} + C_2\right) - 8R_4 \frac{\tanh\frac{\mu_1 c}{\eta_s}}{\tanh\frac{\mu_2 c}{\eta_s}}\left[C_1\left(1 + \frac{\eta_a}{\eta_s}\right) + C_2\right]\right\}}{\tanh(\xi l_s)\left[R_3 R_o - 8R_4 C_1 \frac{\tanh\left(\frac{\mu_1 c}{\eta_s}\right)}{\tanh\left(\frac{\mu_2 c}{\eta_s}\right)}\right] + \sqrt{8} R_o (1 - C_1)\tanh\left(\frac{\mu_1 c}{\eta_s}\right)} \quad (16)$$

where l_s is the outer adherend length, η_a the adhesive thickness, η_s the adherend thickness, c the half-overlap section length.

Where

$$R_o = \sqrt{\frac{12 P_B}{G_a \eta_s}}, \quad R_3 = \frac{2}{\sqrt{4\left(1 + \frac{3\eta_a}{4\eta_s}\right) + \frac{R_o^2}{4}}},$$

$$R_4 = \frac{1}{R_3}$$

where P_B is the applied tensile force per unit adherend width for the bottom surcace points, G_a the shear modulus adhesive material.

$$C_1 = -\frac{9P\eta_a}{4\left(1 + \frac{3\eta_a}{4\eta_s}\right) G_a \eta_s^2}\left[\frac{1 + \frac{\eta_a}{\eta_s} + \frac{P\eta_a}{G_a \eta_s^2}}{4\left(1 + \frac{3\eta_a}{4\eta_s}\right) + \frac{3P\eta_a}{G_a \eta_s^2}}\right]$$

$$C_2 = \frac{3P\eta_a}{G_a \eta_s^2}\left[\frac{1 + \frac{\eta_a}{\eta_s} + \frac{P\eta_s}{G_a \eta_s^2}}{4\left(1 + \frac{3\eta_a}{4\eta_s}\right) + \frac{3P\eta_a}{G_a \eta_s^2}}\right],$$

$$\mu_1 = \frac{\sqrt{\frac{6P}{E'\eta_s}}}{\sqrt{4\left(1 + \frac{3\eta_a}{4\eta_s}\right) + \frac{3P\eta_a}{G_a \eta_s^2}}}$$

$$\mu_2 = \sqrt{\frac{8 G_a \eta_s\left(1 + \frac{3\eta_a}{4\eta_s}\right)}{E'\eta_a} + \frac{6P}{E'\eta_s}}$$

$$\xi = \sqrt{\frac{P}{D}}$$

($D = \frac{E'\eta_s^2}{12}$, individual adherend bending stiffness), and

$$E' = \frac{E_s}{1 - \nu_s^2}$$

(E_s is the adherend Young's modulus under plane strain conditions, and ν_s is the adherend Poisson's ratio). The adhesive stress expressions for Oplinger model can be found in Ref. [104].

3. Defects in adhesively bonded joints: Modes of failure

The determination of adhesive joint strength is complicated primarily by the nature of the polymeric material itself, in that the mechanical behavior of the adhesive is sensitive [106] to (a) moisture condition, (b) strain rate (i.e., loading conditions; simple loadings such as shear and peel stresses and complex loading such as bending), (c) temperature, and (d) other environmental conditions. The second major complication with regard to adhesive joint strength prediction is the failure process, and therefore by implication, the failure criterion to use. Identifying and interpreting the locus of failure and crack propagation behavior are significant aspects in evaluating the mechanical properties of adhesively bonded joints, and have been interests for many years. While it is believed that materials always fail at the weakest location, the locus of failure, while closely related to material properties (such as tensile strength), quality of adhesion at the interface, and fracture toughness of the bonds, depends also on the stress state at the crack tip. The locus of failure is closely related to the direction of cracking. The allowable loads on a joint are the loads at which micromechanical damage (or defects) first occurs that will eventually lead to macromechanical damage. Thus the micromechanical damage can be the basis for the selection of ultimate-load-prediction techniques and the prediction of failure modes of the joints. Defects in adhesively bonded joints can be characterized in various ways such as (a) bondline defects [i.e., 10, 80, 107, 108], and (b) the modes of micromechanical damage at the joint (i.e., the failure characters) [i.e., 2, 10, 60, 64, 106, 109]. The prediction of failure in adhesive joints is of great importance in the use of bonding for structural applications. The certification process requires calculations to be made regarding the strength of critical bonds in the structure,

as well as experimental tests to prove these calculations.The mode of failure is recognized as the vital issue, regardless of the amount of any crack (disbond) growth. A poor bonding surface would be denoted by even small areas of adhesion (interfacial) failures, although it usually results in complete interfacial failures. For example, failures confined within the matrix, between the adhesive layer and adjacent fibers in composites, would normally be regarded as indicative of acceptable bond strength and durability, assuming that the bond also passed its short-term static strength requirements [10] (which is one way of verifying that the adhesive was exposed to acceptable thermal profile during cure).

Ansarifar *et al.* [48] have studied the bonding failure of rubber to steel, aluminum and nylon 6,6 substrates by means of peel tests. They observed that under constant load bond failure occurred in a time-dependent manner at or near the interface, and is cohesive within the rubber and very close to the covercoat. This is caused by a time-dependent cavitation of the rubber in the highly stressed region of the peel front. Slow time-dependent bond failure observed in the rubber by Ansarifer *et al.* [48] attributed entirely to ozone attack has been reported in the past [47]. Constant load peel tests covering a range of peeling energy were carried out at different ozone concentrations ranging from 0.25 (atmospheric) to about 20 parts per hundred millions [47]. This study showed that below a certain energy level, there was very little growth along the bond and the peel rate was essentially independent of peeling energy, but increased significantly as a function of ozone concentration. However, from the time-dependent rate of crack growth against the peeling energy (see Fig. 6) Ansarifar *et al.* [48] suggested that failure was mainly due to the physical rupture of the rubber at the peel front and was not caused by ozone attack.

Ansarifar *et al.* [49] have also studied the bonding rubber to nylon 6,6 substrates with commercial organic solvent-based or water-based bonding agents and tested by means of peel tests to evaluate the bonding failure. Peel tests were performed under constant load at an angle of 90° and at ambient temperature (∼23°C). Using the newly developed constant load peel test-method [48, 110] (see Section 4.2 for more detail about this test method), bond failure produced over the wide range of peel rate. There were two distinct stages of failure during peeling, irrespective of the rate of peel. They were: (a) stick stage and (b) slip stage. In the stick stage [48], no crack-growth occurred as the rubber adherend was extended, and the peel angle θ remained at about 90° .Whereas in the slip state [48], the cleavage front advanced at or near the interface, and at a rate faster than the cross-head speed. Moreover, in the slip stage the angle of peel was much smaller [48], e.g., 45°, and the force applied to rubber adherend varied considerably and continuously as the rubber was peeled. This test showed that there were two possible failure mechanisms: (a) cohesive, and (b) mixed modes. The primer had reacted with the surface of the nylon creating a third phase, which in peel tests had been the weakest layer and failed cohesively, or the failure was mixed mode, i.e., some cohesive in the primer layer and some interfacial between nylon and primer. In each case, the primer layer had been cohesively the weakest aspect of the joint. Under constant load, bond failed in a time-dependent manner at or near the interface. The time-dependent failure of the bond during the peeling test was caused by a time dependent cavitation of the rubber in the highly stressed region of the peel front, where strands of rubber were observed to form in tension perpendicular to the bond plate. In fact, the eventual rupture of these strands caused the time-depended failure of the bond.

A common contributor to premature interfacial failures is some form of pre-bond moisture [10]. For example, moisture can be present in an undried composite laminate cured long before it was bonded, as condensation on the surface of adhesive film not stored or thawed out properly, or absorbed within adhesive film which had been left out for too long in the lay-up room. Water absorbed by the nylon filaments before the original laminates are cured with the peel ply in place is also identified as a contributing problem [10]. Adverse effects of moisture are alleviated, or sometimes totally eliminated, by such good venting that all water is sucked off during the cure instead of being trapped at the interface between the adhesive and the composite components.

Xu *et al.* [111] have recently investigated the effects of hot/humid environment on the failure mechanisms of galvanized steel to polypropylene (PP) composite lap shear joint specimens under the Cataplasma aging tests and cyclic moisture/temperature tests, with and without primer. After the lap shear testing, they observed that without primer, the locus of failure of the aged joints shifted close to the galvanized steel/adhesive interface at the edges of the joints. With primer, the joints primarily failed at the primer/galvanized steel interface. Using the Environmental Scanning Electron Microscope (ESEM), the locus of failure was observed to be partially within the adhesive close to the adhesive/galvanized steel interface and partially at the galvanized steel interface in the edges of the joints. Corrosion of zinc layer on the galvanized steel was found in the interfacial failure region. In the central region of the adhesive joints, the failure was still at the adhesive/PP composite interface. Clearly, the adhesion at the adhesive/PP composite interface degrades more slowly than at the adhesive/galvanized steel interface under Cataplasma environment. The loss of adhesion in a high moisture environment was mainly due to corrosion of the galvanized steel.

Xu *et al.* [111] have also investigated the effect of primer on the failure mechanisms. In the moisture environment, adhesion at both the adhesive/PP composite interface and adhesive/primer interface degrades more slowly than at the primer/galvanized steel interface. Therefore, the durability of their joints is mainly dependent on the retention of adhesion at the interface between the primer and the galvanized steel adherend. They observed defects such as cavities and pinholes in the primer layers. The primer layer on the galvanized steel was blistered as a result of Cataplasma aging. The

blisters were intitiated at internal cavities and at the edges. The centers of the blisters were corroded first and the disbondment of the zinc/primer interface occurred around the corroded area. Intergranular corrosion took place on the surface of the galvanized steel. It was found that oxygen significantly accelerated the process of blistering. In contrast, there were many blisters on the primer coating of the galvanized steel soaked in an open bottle under same conditions. The increase in the number of blisters was attributed to easier access of oxygen. Xu *et al.* [111] concluded that the connection between the presence of oxygen and blistering indicates that the debonding is dependent on a cathodic reaction leading to reduction of oxygen. Therefore, they suggested that the blistering is essentially a result of cathodic debonding of the primer/galvanized steel surface. A schematic of the blistering process is shown in Fig. 14.

3.1. Bondline defects

As a result of discussion presented above, bondline defects in adhesively bonded joints can be generalized [80, 107, 108] as either a (a) debond or (b) a weak bond, as seen in Fig. 15 . In the structural integrity of an adhesively bonded joint there are two main problems. These are the effect of debonds and weak bondlines on the load transfer and durability of the joints. Therefore, the integrity of the bondline in the adhesively bonded joint is quite an important phenomenon. The bondline is schematically defined in Fig. 16. In adhesively bonded joints a debond is simply characterized and identified as a separation between the two adherends. As a result two traction-free surfaces are created. The gross form of a debond is illustrated in Fig. 15a, however, other traction-free microscopic forms of separation include voids, porosity and micr-cracking in the adhesive. During in-service operations, debonds are generally

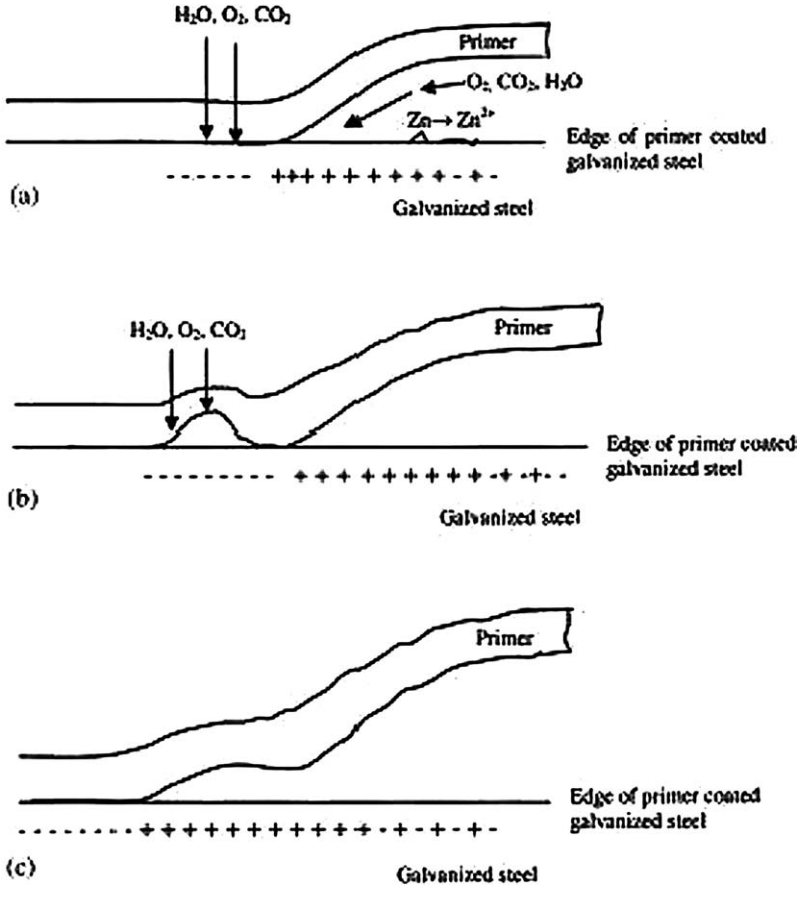

Figure 14 A schematic of blistering process from the edge of a specimen of primer-coated Galvanized steel [111, 112]: (a) corrosion of galvanized steel at its edge, (b) blistering of the primer, and (c) delamination of the primer.

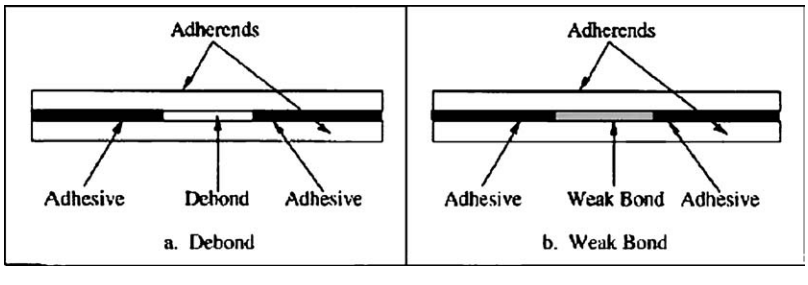

Figure 15 Generalized bondline defects in adhesively bonded joints [80, 108]: (a) debond and (b) weak bond.

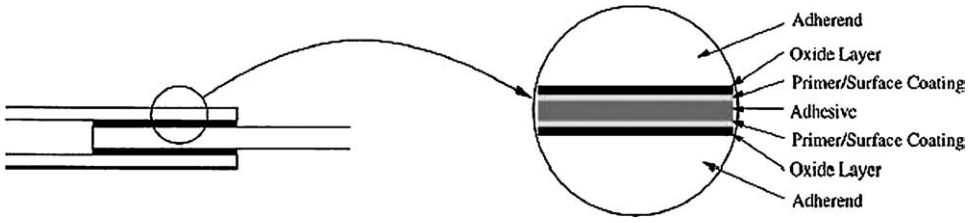

Figure 16 Adhesively bonded joint bondline [80].

associated with moisture penetration at panel edges and bolt holes, bolt inserts in honeycomb panels, poor surface preparation, impact and/or local over-heating. Debonds are typically identified using common NDI methods, such as ultrasonic inspection and acoustic emission.

Although the composites are manufactured correctly according to the short-term quality control coupons tested, they separate in service. The issue is not one of structural overloading. As indicated by Knox and Cowling [29], the interface between the adhesive and the composite surfaces simply debonds without the slightest trace of either material ever having adherend to the other. In some cases, the details have been known to separate before manufacturing had been completed. What appears to be a common element in many of these problems is contamination introduced by the use of "release" peel ply without subsequent through abrasion of the bonding surfaces [29].

In contrast to a debond, weakly bonded joints show no sign of separation in the bondline. A weakly bonded joint is still effectively bonding the two adherends together. This is shown in Fig. 15b where there is a weakening of either the adhesive or the bondline interface. Currently available NDI methods can not reliably identify weak bonds due to the absence of traction-free surfaces [80]. The identification of weak bonds in joint production as a quality assurance measure is conducted through witness coupon destructive testing [113]. In comparison with the bulk, the structure of the boundary layer is less organized [114]. This agrees with the conception of a weak boundary layer offered long ago by Bikerman [115]. As pointed out by Hart-Smith [10], the cause of weak bonds should be acknowledged as processing errors- and they usually would be, except for one further problem. As noted above, such weakness are invariably undetected by conventional (or even exotic) ultrosonic inspections, suggesting to some that the parts might not be defective after all. Only when there is zero tolerance of interfacial failures in acceptance criteria, regardless of any measured strength, can standard lap-shear testing of coupons be relied upon to distinguish between durable and suspect bonds. Again, the fact that most of these coupons (and parts) do not simply fall apart as soon as they have been made has created the illusion that there is nothing wrong with any of the bonds. And, even when the majority of such bonds separate in service, the fact that some of them do not is often sufficient to convince some people that those which did must have been overloaded and that the failures had nothing to do with the processes used to make the bonds or the laminates [10].

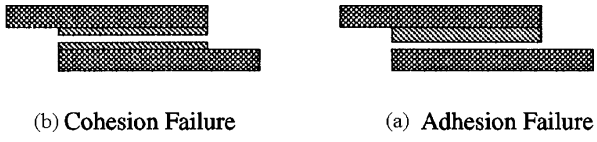

Figure 17 Types of failure in adhesively bonded joints [2]: (a) adhesive failure and (b) cohesive failure.

3.2. Modes of micromechanical damage: Failure characters

System adhesive-adherend was characterized not only from the point of shear strength of adhesive-bonded joints but also on the basis of the character of their failure. On the basis of the discussion in the previous sections and the past works, we can distinguish three kinds of failure [i.e., 2, 48, 109, 113]: (a) adhesive (or quasiinterfacial) failure (see Fig. 17a) (rupture of the adhesive bond, such that the separation appears to occur along one of the two adhesive-adherend interfaces) [2, 64], (b) cohesive failure (see Fig. 17b) (rupture of the adhesive bond, such that the separation appears to be within the thickness of the adhesive layer) [2, 64, 109], and (c) mixed failure (crack goes partly between adhesive and adherend and partly through adhesive and/or adherend) [64]. For a given bond, transitions between adhesive and cohesive modes of debonding are often observed when changing the geometry of the assembly, the loading configuration, or the rate of debonding extension. Correspondingly, the strength of the bond, expressed in terms of a failure stress or in terms of a steady state debonding toughness, can differ widely depending on the debond extention mode. It is commonly observed that the transition from a cohesive mode at low rate to an adhesive mode at high rate which is commonly reported in the literature for rubbery copolymer adhesives, adhesive tapes, or pressure sensitive adhesives.

The difference between a design decifiency and a processing decificiency can often be determined by inspection of the failure surface [2]. A design deficiency is characterised by fracture of the adhesive (cohesion failure) with residues on both surfaces (Fig. 17b). This is the typical failure surface observed from adhesive strength tests such as lap-shear or peel tests. The experimental data surveyed [i.e., 22–24] show that the cohesive characteristic of the boundary layer are also affected by the contact thermooxidation reactions of the polymer catalyzed by iron surface compounds. The adhesive would also contain minimal voids and obvious defects. Processing deficiencies are usually characterized by interfacial failure (adhesion failure) (see

Fig. 17a) of the bond such that there will be areas where the adhesive remains on only one of the adherend surfaces, with the matching surface being free of adhesive, or by the presence of voids or other bondline defects in the adhesive. Although interfacial failures occasionally occur due to contamination, the most usual cause of in-service adhesion failures is poor environmental durability due to the inadequacy of the surface preparation used when the bond was formed.

The cohesive failure within the adhesive layer or in the surface layer of the adherend matrix may occur by brittle fracture or by a rubbery tearing, depending on the type of adhesive used [60]. This results in cracks perpendicular to the load and causes a reduction in the load-transferring capability of the joint. Cohesive failure are analyzed using two general approaches [106]: (a) the continuum mechanics (CM) approach, and (b) the fracture mechanics (FM) approach. CM assesses the nature and magnitude of the stresses and strains within the adhesive joint, often predicted by finite element analysis (FEA). The criterion that is used varies between (a) maximum values of stress [103, 116], (b) strain [116] or (c) plastic energy density [103]. However, to reduce FE model complexity, sharp corners are often modelled at bi-material interfaces, e.g., at the ends of the adherends which introduce singularities (a point of theoretically infinite stress) (Ref. [106]). Clearly, the maximum value failure criteria become meaningless as these values are a function of how well the singular field is modelled, i.e., the refinement of the mesh.

Balkova *et al.* [64] have investigated the failure modes of the glass fiber/polyester composites joints (the adhesives used for joining are all two-part epoxy based adhesives: EPOXY 371, P11, LETOXIT LX 012, LEPOX UNIVERSAL 11) under the various environmental conditions (i.e., exposed to air at room temperature and 60°C, and cool water) using the single- and double- lap shear tests. They have observed mixed failure in all the joints studied . The separation appears to be at the adhesive-adherend interface and partly within the adhesive. Cohesive failure reached nearly 60% of the whole bonded area during aging processes at room and elevated temperatures. The longer time the joints were stored in water the weaker the bonds become, especially at the joints stuck with LEPOX UNIVERSAL 11, and the adhesive failure prevailed. Only in the case of LETOXIT LX 012 the adhesive as well as cohesive bond of the adhesive was stronger than cohesive bond of the adherend and that is why this was torn up. Damaged adherend area increased from 50 to 80% of the whole bonded area for joints stored at room and elevated temperature and decreased up to 10% for joints stored in water. The delamination in the composite was not observed for any type of adhesive joint.

Whilst the locus of failure of unaged structural joints usually involves a cohesive-type fracture process in the adhesive layer where the adhesion at the interface remains high, after environmental attack failure often occurs at or very close to the interface between the adhesive and the metallic adherend [29, 117]. Generally, it is known that whilst the bonding in the boundary zone between a polymer and metal surface is of high strength, it is not necessarily stable against the effects of water [118]. However, whether the failure path is at the interface or whether it is in the oxide, in a weak boundary layer or within the primer (if used) is a matter of some controversy [32]. The exact failure path probably depends upon the particular joint under examination [119]. As a consequence of the difference in adherend thickness, the stress distribution developed in a relatively thin steel adherend used in the automotive industry and the the stress distribution developed in a thick steel adherend for a marine application may produce apparently different failure processes before and after environmental aging [29].

4. Quality control tests: Assessment of bonding quality

A successful test would be one in which there was virtually no disbond growth at all, and one in which there were absolutely no interfacial failures [10]. The most important thing to note about durability testing of adhesively bonded joints is that the mode of failure is more important than the failure load. The measured strength might be of significance in comparing different cohesive failure modes, but the presence of any adhesion failure at the interface would transcend all other considerations. As Hart-Smith pointed out [10], the great danger with any bonded durability test is that, if a load can be measured, there will be some who base the accept/reject decision on the magnitude of the load, thereby totally undermining the purpose of the test.

4.1. Standard test methods

Assessment of bonding structures are usually made by carrying out routine tensile lap shear (pr EN 2243-1) and peel tests (BS EN 2243-2) for metal to metal and BS EN 2243-3 for metal to metal honeycomb) to determine the strength. In addition, early bond loads of particular assembly are assessed for a long period of time by tensile lap shear and pull test pieces based on the component adherend form [12].

The following standard mechanical tests methods have been used widely for quality control and durability performance (i.e., mechanical or environmental stability) of adhesive joints in metallic and composite materials adherends: (a) single-lap shear test, (b) double-lap shear test (c) Thick-adherend shear test (TAST), (d) floating-roller peel test, (e) Double-cantilaver beam test, (f) Wedge-crack test, (g) Floating-roller test, (h) Short-beam shear test.

4.1.1. Thick-adherend shear test (TAST)

Applications for structural adhesive in a marine environment will generally involve much thicker adherends than used in some other industries such automobile industry. As a consequence of the difference in adherend thickness, the stress distribution developed in a relatively thin steel adherend used in the automotive industry and the stress distribution developed in a thick adherend for a marine application may produce

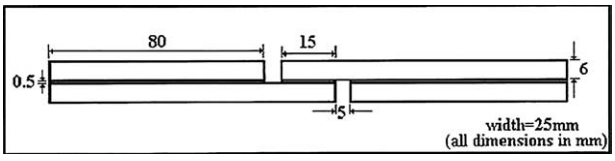

Figure 18 The standard thick adherend shear test (TAST) specimen.

apparently different failure processes before and after environmental aging [29]. Therefore, in order to simplify the stress distributions present in the tensile lap shear specimens, the thick-adherend shear test (TAST) specimen (see Fig. 18) has been proposed by Althof [120] and Krieger [121]. In these specimens, by using a thick adherend and a short overlap, the specimen rotation and the adherend compliance under load are largely eliminated, rendering a state of stress in the adhesive almost entirely dominated by uniform shear [65]. However, since the complience of the adherend under load is not totally eliminated [70], this makes measuring the shear modulus difficult, because it necessitates accurate measurement of small displacements and correcting for adherend deformations over a thin adhesive layer. Even so, the method is adequate for determining maximum strains and stresses, as pointed out by Maheri and Adams [65].

On the other hand, although structural adhesive test specimens such as the lap-shear and TAST specimens are almost always used for testing under static conditions, the adhesive material can show a degree of viscoelastic behavior such that its mechanical properties under dynamic (or impact) loading can be significantly different from those under static loading. Since many structural adhesives are used in transport applications where the bonded joints are subject to dynamic as well as static loading, the adhesive dynamic properties can be of significance [65]. An early work [122] on determining the dynamic moduli of thin, constrained adhesive films showed that dynamic moduli could be slightly higher than those obtained in static tests, the difference decreasing for more brittle, structural epoxies.

4.1.2. Double-cantilaver beam (DCB) and wedge-crack tests

Literature survey and a review of standard test methods revealed [123] that the double cantilaver beam (DCB) and wedge-crack tests (schematic illustration of this test method shown in Fig. 19a are well suited to

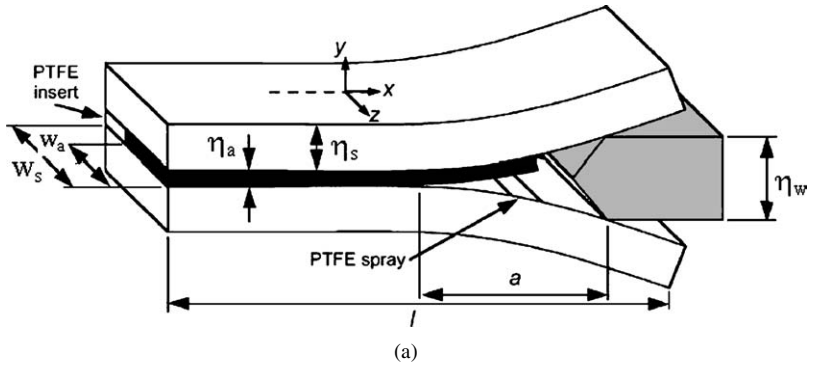

(a)

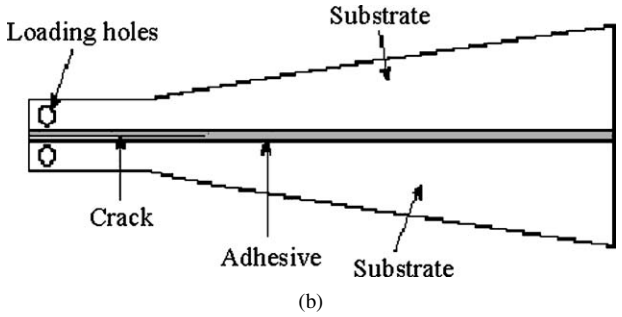

(b)

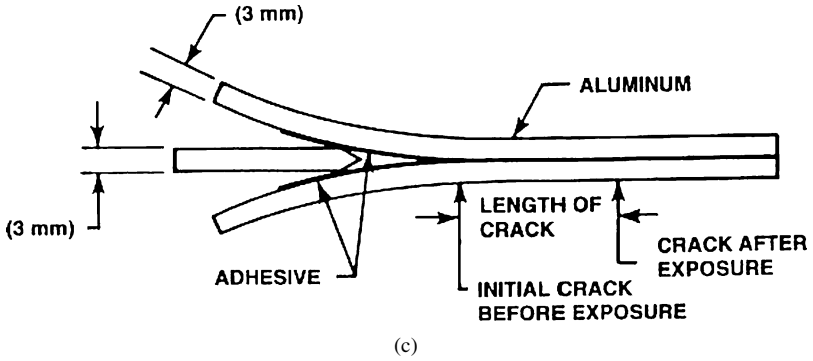

(c)

Figure 19 Double-cantilaver beam (DCB) and wedge-crack tests: (a) principle of the wedge-opened double cantilaver beam (DCB) test with definition of the notations [124], (b) Tapered double cantilaver beam (TDCB) test specimen [134], and (c) Boeing wedge crack durability test for bonded metal structures [10].

evaluating the short- and long-term durability adhesive bonds [125–128]. In the DCB test, a bonded sample is pulled apart, at a constant test machine crosshead velocity, by fixture (hinges or pinned blocks) at the end of the beams. The specimen is loaded and unloaded until the crack has propagated entirely through the sample.

The wedge-opened double cantilaver beam (DCB) test is one of the simplest methods for the application of fracture mechanics to the testing of crack extension in adhesive joints or composite laminates [129, 130]. The simplicity of the test rests on the facts that the debond extension is intrinsically stable and that no load cell is needed [124]. The principle of the test is sketched in Fig. 19a. Two plates, taken in the present case as having the same thickness, η_s, are bonded face to face with an adhesive layer of thickness η_a. The width, w_s, of the plates can be larger than the width, w_a, of the bonded area. A wedge thickness η_w inserted between the plates induces the extension of a decohesion crack up to a distance "a" from the wedge. If the plates remain purely elastic, the "debonding toughness Γ" of the bond is equal [124] to the strain energy release rate G. If we assume that the assembly is free of residual stresses and that the contribution of the adhesive layer to the strain energy of the system can be neglected, G can be expressed on the basis of a simple beam bending model as [124]

$$G = \frac{3\ \Delta l^2 E_s\, \eta_s^3\, w_s}{16 a^4 w_a} \tag{17}$$

where E_s is the plates Young's modulus and the displacement at the wedge is $\Delta l = \eta_w - \eta_a$. Several more refined expressions of G have been proposed.

The application of fracture mechanics to adhesive joints dates back to the 1960s when Ripling *et al.* [131] and later Mostovoy *et al.* [132] studied experimental methods to determine the plane-strain fracture toughness (K_{Ic}) of bonded metallic joints. This work led to an ASTM standard [133] which used a simple shear-corrected beam theory (SBT) to deduce the values of adhesive fracture energy G_{Ic} from either adhesively bonded double cantilaver beam (DCB) (see Fig. 19a) or tapered double cantilaver beam (TDCB) (see Fig. 19b) test specimens [134]. The double-cantilever-beam peel test coupon suffers from the limitations that each such coupon can be tested only at a time, tying up a combination of test machine and environmental chamber for an appreciable time per coupon. As suggested by Hart-Smith [10], this might explain why a major aircraft manufacturer relied on this test to choose between different surface treatments by through pre-production testing, but has not implemented such a test in production. Perhaps the greatest drawback of the double-cantilever beam coupon for tests like this is that the opportunity to measure and vary the prying force, raises the temptation of assessing the quality of the bond in terms of the prying force rather than the mode of failure [10].

Unfortunately, there is a lack of standard test procedures for measuring the bond strength of adhesively bonded composite materials. ASTM test methods researched cover either adhesively bonded metals or interlaminar failures in composites. The specimen used for the DCB and wedge crack tests is based on those of ASTM D3433, ASTM D3762, and ASTM D5528-94a Standard Test Method for Mode I Interlaminar Fracture Toughness of Unidirectional Fiber-Reinforced Polymer Matrix Composites.

The man responsible for the first reliable and simple specimen with which to predict in the short term whether or not a bond would fail interfacially in service was Bert Bethune, of Boeing (Ref. [10]). His wedge-crack durability test for bonded metal structures (see Fig. 19c) is now an integral part of virtually all manufacturing programs. The Boeing wedge test for bonded metal structures can be performed with the same specimen as in DCB test, but an angled wedge is driven into the crack opening to stimulate crack growth (see Fig. 19c for schematic illustration). Then, the sample is observed (often in an environmental exposure chamber) and the crack tip propagation is recorded. As in the case of DCB test, wedge-crack test is also used to evaluating the short-and long-term durability adhesive bonds [123]. The reason to develop the Boeing-wedge crack test (Fig. 19c) was to apply a sustained peel load in a humid environment. The bonded metal coupon would split apart rapidly whenever the surface preparation was one of those which had failed in service, but there would be little or no crack growth for the durable processes and materials, and whatever fracture did occur would be cohesive. As Hart-Smith [10] points out, any sign of interfacial failure should be interpretated as having failed the test.

A wedge is driven into the end of the bond at room temperature, and the coupon and wedge are then inserted into a hot-wet environment, to see whether the initial disbond will grow under the peel load and, if so, in what manner. It could grow cohesively (leaving roughly half the adhesive on each adherend) or interfacially (showing no sign of adhesion between the adhesive and the adherend) [10]. A small amount of cohesive growth may be permitted. The mechanism of this accelerated failure, if it occurs, is a sustained peel load in the presence of moisture. In the wedge –crack test, the specimens are subjected to elevated temperature and humidity, which is a reliable short-term method to predict bond integrity of a joint over long periods of time in service, as detailed in the literature [123, 125, 126, 135–139].

As noted by Hart-Smith [10], the need for a bonded composite durability test is just as great as it was for metal bonding 20 years ago. So to devise a durability test-coupon for composite structures as reliable as the wedge-crack coupon has been for metal bonding. When used with composite laminates, the wedge-crack specimen must be made from unidirectional (0°) tape plies. The reason for using all-0° adherends is that transverse surface fibers (at 90° to the length of the specimen) are so weak in the interlaminar tension and shear that the tip of the delamination would be diverted away from

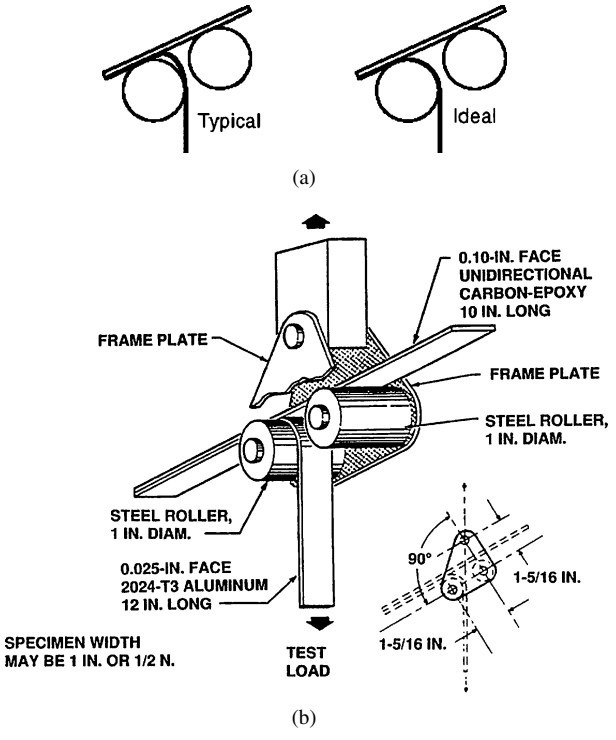

Figure 20 Floating-roller peel test: (a) typical and ideal floating roller test [123] and (b) adoption of floating-roller peel test for evaluating bonded composite Structures [10].

the bond surface into the laminate at a far lower peel stress than should be withstood by a structurally sound bond [10].

4.1.3. Floating-roller peel test

Fig. 20a shows the schematic illustration of floating-roller peel test method for typical and ideal cases [123]. As this test method is usually used to test for durability of bonded metal structures, it is mounted on the test machine in ambient environment and a drop of water is applied to the tip of the initial disbond. Poor surface preparations result in an instantaneous switch to interfacial failures, which spread rapidly [10]. One can not use this same test for composite adherends, because they will not bend enough. The initial approach utilized floating roller tests on woven fiberglass and carbon fiberglass samples [123]. The ASTM D3167 test is designed for a thick adherend bonded to a thin metal adherend that bends arounds the roller during peeling. Because they bend at too tight a radius of curvature and fractured before the bond could be broken (see Fig. 20a), this test method was abandoned in favor of other bond strength tests that do not require such extreme strains on the adherends to the fracture the bond.

The concept of this test might be adapted by trying to peel off a thinner strip of aluminum alloy, properly treated and bonded to a thicker all-0° carbon-epoxy laminate [10]. The coupon will bow, because of the thermal unbalance, but this should not affect the usefullness of the test unless the bowing were so great that the specimen could not be installed in a test rig. The test would be invalidated by having the adhesive separate from the aluminum instead of from the composite, but past experience with metal-to-metal bonding indicates that this will not occur if the aluminum strips are properly anodized and primed. (Using aluminum for this purpose would even reduce the specimen cost.) [10]. Fig. 20b illustrates the adoption of floating-roller peel test for evaluating bonded composite structures [10].

4.1.4. Short-beam shear test

The short-beam shear test specified in ASTM D2344 uses three-point bending where failure occurs in shear mode parallel to the fibers in the midplane as shown in Fig. 21a. The maximum shear stress τ_{max} (normally called the interlaminar shear strength, ILSS) is related [74] to the applied maximum load P_{max} and specimen dimensions, according to the simple elastic beam theory: $\tau_{max} = 3P_{max}/(4w\eta)$, where w and η are width and thickness of specimen. Because of the simplicity of the test method and minimum complication in specimen preparation, it has become one of the most widely used methods to determine the quality of both polymer and metal matrices composites [140]. Unfortunately this test has an inherent problem in that meaningful results can not be obtained for very thin specimens [140]. The high stress concentration and damage by crushing in severe cases at the loading points with a very short span (normally five times the specimen thickness) may induce premature failure and complicates the interpretation of test results. To avoid this problem four-point bending of a long beam may be used.

In order to solve a manufacturing problem caused by the use of released nylon peel plies, the short-beam test was adopted by Fischer, in Austria [10] (see Fig. 21b for this adoption). The short-beam shear coupon was made by bonding together two thinner pieces of laminate, using various surface preparations. One skin was precured, and the other co-cured with the adhesive

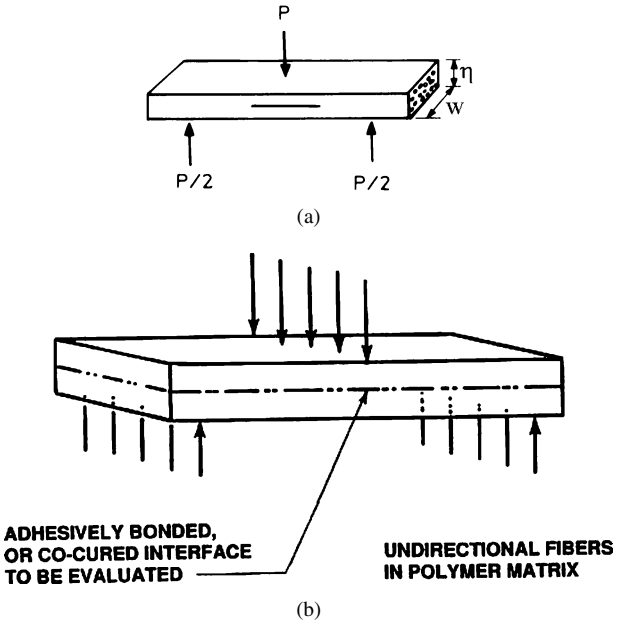

Figure 21 Short-beam shear test: (a) Schematic specimen geometry and loading configuration for short-beam test (140) and (b) Fisher modification of short-beam shear coupon to test durability of composite bonded structures [10].

layer. Even with short-term testing, the released nylon peel-ply surface resulted in a loss of 50% of the strength, with respect to the equivalent coupon in which the peel-ply surface had been thoroughly sanded before bonding [10]. The failures to the unabraded nylon peel-ply surfaces were clearly the result of poor adhesion between the precured laminate and the adhesive layer, occuring at a stress of 30–40 N/mm^2. The failures were interlaminar outside the adhesive layer for both a non-released polyester peel ply, without sanding, and the thoroughly sanded nylon peel-ply surface, occuring at a shear stress of 50–60 N/mm^2. Only short-term tests were run, so the relative durability of the two successful techniques was not established, although it was recognised that this specimen could be used for this purpose.

4.2. Novel test methods

Last ten years the new test methods have been developed (see for example, Refs. [33, 48, 90, 110, 141, 142]) in order to better quantify the mechanical properties of adhesive joints under static and dynamic loadings. These new test methods have been developed to study the effects of various factors including time dependance, surface treatment, aging, characterisation of an interface between two pieces of the same polymer material, and dynamic loading on the durability performance of the adhesive joints.

Existing laboratory constant peel rate tests [48, 143–145] evaluate mainly mechanical load endurance of the bonds and are suitable for quickly performed overload excursions. In these tests, the bonds are stressed over short times and researchers have little or no time to observe, study or document the initiation or progression of failure [143]. The tests are used for the design, quality control and inspection purposes of the bonded components and are unable to detect slow time-dependent failure of the bond which may occur over long times in service [144]. Furthermore, in these tests, failure often takes place within the adhesive if a strong bond is formed, and away from them immediate vicinity of the bonded interface [145]. In service where some rubber-to-metal bonded components fail unexpectedly soon, sometimes failure takes place at or near the bonded interfaces. The inability of current tests to detect time-dependent failure can produce misleading results for products intended for long service life. Therefore, because of these problems faced in practice, Ansarifar and co-workers [48, 49, 110, 141] developed a new constant-load peel test method, which was utilized to produce failure with the rubber adjacent to the bond, similar to that occurring in service. Fig. 4a illustrates the test piece used to assess rubber-to-metal bond failure. Preliminary studies [110, 141], using peel test pieces (Fig. 4a) prepared by bonding unfilled and carbon black filled natural rubber compounds to mild steel with commercial solvent-based bonding agents, indicated that if a constant force of sufficient magnitude was applied to the peel leg, time-dependent mechanical failure near to the bond was observed. The failure locus appeared to lie slightly within the rubber (typically at a depth of a few tenths of a milimeter) and was ascribed to cohesive failure in the elastomer [110]. It appears that cavitation like processes might also occur in the highly stressed peel front region during bond failure, and it was argued [110] that if such processes could occur in a time-dependent manner, this could account for the occurrance of time-dependent failure in a strain-crysllazing elastomer. There were indications [48, 49, 110] that rates of crack-growth from different test-piece geometries could be related to the strain energy release rate. This suggested that the relationship between the rate of failure and the strain energy release rate might be characteristic, geometry-independent property for a particular rubber-metal bond system. Using this new test method, it was observed [48] that the rate of failure increased rapidly with energy level showing about a sixth-power dependence, a very strong dependence for the system studied. As was claimed by Ansarifer and co-workers [48, 49, 110, 141] this new test method, therefore, offers a more consistent and accurate means of assessing integrity of the bond and measuring its strength than the existing constant rate peel tests.

Knox and Cowling [33] have developed a novel method, called scrap test method in order to investigate the influence of surface treatment on durability performance. The aims of designing this test method were twofolds: (a) the effect of aging on the adhesion strength of an adhesive at the interface, and (b) distinguishing amongst the durability performance of various surface pretreatments. In this test, a relatively short period of time is used. To investigate the effect of aging on the adhesion strength of an adhesive at the interface, a jig was designed (see Fig. 22a), to strip a thick

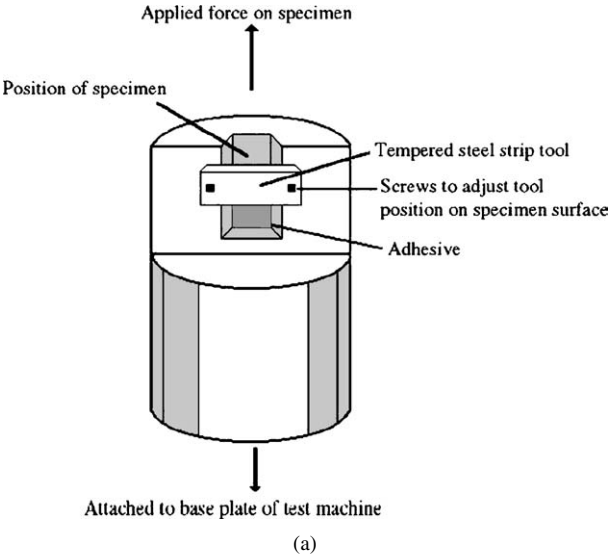

Figure 22 A novel method called scrap test method [33]: (a) design of scrap jig (not to scale) and (b) scrap test specimen (not to scale).

film of adhesive from an adherend (see Fig. 22b). The force required to remove the adhesive after the sample has undergone aging is recorded. In order to test this method, the specimens were prepared by hot curing a single part paste adhesive (AV119) on a mild steel substrate to form a thick film. Knox and Cowling [33] have used the following procedure to fabricate the scrape test specimens: (a) the required area on the substrate is prepared for bonding, including shot blasting of the surface, solvent degrease and followed by pretreatment with a primer if needed, (b) after applying adhesive to the adherend surface, heat resistant masking tape is used to give a clean working edge and control the film size, (c) then the specimen is laid in a jig (see Fig. 22b) with an adjacent surface, sprayed with PTFE, placed against the adhesive film to maintain a constant thickness.The specimens were subjected to accelerated environmental aging (i.e., at 30°C and 100% relative humidity), and then tested immediately wet at half-week intervals at laboratory ambient temperatures. It was suggested [33] that the scrap test method appears to be very useful for rapidly detecting changes in interfacial strength of an adhesive/adherend system, and for distinguishing amongst the durability performance of various surface pretreatments.

Schüller and Lauke [142] have proposed another novel method for characterization of an interface between two pieces of the same polymer material by the interfacial transverse strength. However, they suggested that the basic idea of this test method is not limited to such situations but can be applied also to bimaterial composites. Fig. 23 shows this new test arrangement proposed by Schüller and Lauke [142]. The specimen consists of two halves, each with a single-edge notch. They are glued together to form a double-edge notched specimen. The notches are semicircular. Therefore, the production of such samples is quite simple. The specimen is then tested in a tensile testing machine. Due to the notched shape, the stress state is not purely tensile in the plane of the interface. It has a transverse component, which is generated by the notched shape. This allows the optimazation of the interfacial stress state by changing the geometry of the specimen. Optimazation means, here, avoidance of stress components in the thickness direction and generation of a uniform tensile stress at a large interface portion. Recently, these basic ideas of this arrangement were applied successfully to determine the adhesion strength between a single fiber and a matrix material [146]. It was claimed [142] the main advantages of the test are the simple preparation of the samples, the simple experimental set-up as well as the data-reduction scheme. The test applies a nearly uniform transverse tensile stress to the interface. Therefore, it allows the application of the strength concept on interfaces without simplifications forced by complex stress fields and without introduction of additional parameters like a characteristic length. The method is not constrained to glued interfaces, even other preparation methods are possible, for instance, two-component injection molding or welding. The test provides the possibility of measuring a real material property, which is (nearly) independent of the specific testing arrangement. The main disadvantage of testing bimaterial joints [142] is the creation of a well-known stress distribution along the interface. The strength concept also requires a uniform transverse stress at the joint. Finally, the interfacial stress must not have concentrations at the edges of the specimens to avoid surface effects. The stress analysis revealed [142] that the stress state in the center of the specimen is biaxial, it has an in-plane tensile component and a transverse tensile one. All other components are nearly zero. The ratio of the two remaining components depends on the specific geometry. The use of the maximum stress criterion for this situation seems reasonable as a first step [142].

The toughness of an adhesive joint may decrease considerably under dynamic- or impact-loading [147]. This arises because adhesives are polymeric materials that exhibit plastic and viscoelastic deformations, and thus their fracture behavior may be very dependent upon the rate of loading and temperature [90]. Hence, for applications such as in the automotive industry, for example, when adhesives are being used increasingly in safety-critical areas, it is necessary to evaluate any possible decrease in performance that may occur when the adhesively-bonded joints are subjected to impact loading. A new test method for the dynamic loading has been developed by the automotive industry [90, 148, 149] to evaluate the fracture behavior of adhesive joints when subjected to relatively high rates of test

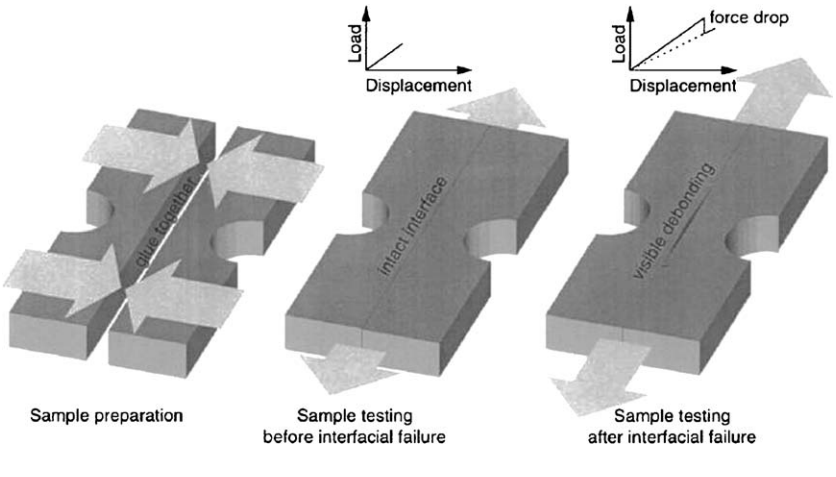

Figure 23 Schematic view of the new test arrangement and expected load-displacement Curves proposed by Schüller and Lauke [142].

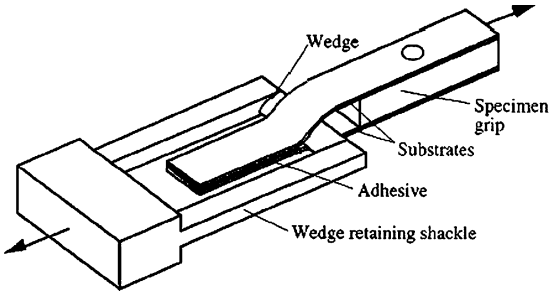

Figure 24 The impact wedge-peel (IWP) test specimen [90].

at various test temperatures. This is the impact wedge-peel (IWP) test, for which an International Standard (ISO 11343) test method [150] was recently adopted. A schematic of the IWP test is presented in Fig. 24. The specimen is shaped like a tunning fork, and a wedge (of a specified shape) is drawan through the bonded portion of the specimen, as indicated in Fig. 24. The International Standard [150] specifies that specimens should be 90 mm long and 20 mm wide, and made using sheet-metal adherends of between 0.6 and 1.7 mm thick. The adherends should be bonded over a length of 30 mm, the unbonded arms being formed to give the "tuning fork" profile. No starter crack or notch is used with these specimens. The wedge velocities reccommended by the ISO are 2 m/s for steel adherends, and 3 m/s for aluminum-alloy adherends. The more detail about the application of this test method is given in Ref. [90].

5. Stress concentrations in adhesively bonded joints

In bonded joints, the adhesive is critical to the transfer of load from one adherend to another. The adhesive joint is characterized by stress peaks (both shear and peeling components) due to the peculiar structure of the joint: geometrical and stiffness factors are concurrent in determining the entity of these peaks [61]. Joints are sources of stress concentrations which diminish the overall efficiency of a structure [3]. In strength critical components it becomes imperative to reduce these stress concentration factors so as to increase structural efficiency. Stress concentrations in bonded joints arise from abrupt changes in adherend/adhesive thicknesses and from differences in elastic moduli [70, 151] under static [152] and dynamic [63] loadings. The actual magnitude of the stresses depends on many geometric and material property parameters. Single-lap joints are widely used in most studies due to their simplicity and practical applications. However, they have stress concentration on both edges [72]. Thus, it is necessary to reduce the stress concentration by means of changing the adherend configurations. For example, tapered lap joints (see Fig. 12h) and scarf joints (see Fig. 12c) are useful to reduce stress concentration for static loading [63]. However, it is not known whether these configurations are effective or not under dynamic condition.

The primary considerations in the design of structures are the stiffness and strength (particularly with respect to weight). Without proper joints, it is not possible to take full advantage of the high stiffness and strength of the structures. As pointed out by Li and Lee-Sullivan [46], the use of adhesive bonding in primary structural applications has been somewhat limited because of the difficulty in (a) defining and predicting joint strength, and (b) designing the joint geometry to optimize strength and reliability. Since these problems are mechanical in nature, stress analysis is required to understand how the force loads are distributed along the adherends and adhesive layer. The stress analysis of adhesively bonded joints is complex because the joints rarely see simple or pure loading of any type (e.g. shear, tension, or compression) but, rather, are usually subjected to some bending. Moreover, the flexibility and geometry of the adhesive layer affects distortion, and thus, the overall stress distribution [46]. As a result, rather than rigorous analysis of stress distributions for complex geometries in the initial design stage, simple geometries such as the lap and scarf joints are first analyzed numerically and tested experimentally. The results from these simple tests provide insight and can also be extrapolated for designing more complex and practical geometries with the aid of sophisticated computational tools such as finite element analysis (FEA) method.

Rather limited work can be found to date in the use of finite element analysis (FEA) optimisation on adhesively bonded joints [i.e., 3, 153, 154]. Groth and Nordlund [154] studied optimum shapes of adherends with the intention of minimising the Tsai-Hill factor (objective function) along the adhesive overlap. The Tsai-Hill yield criterion is a general orthotropic form of the Von Mises isotropic yield hypothesis. Joint types included in this analysis were: (a) single-lap, (b) double-lap, (c) double-strap and (d) a console bonded to a rigid wall. The adherends for both the single- and double-lap joints had to be pre-profiled so that the mesh distortions would not make the analysis unfeasible.

Adams and Peppiatt [155] have studied the effect of spew fillet size. The spew can be considered as the result of the adhesive squeezed out of the lap region at the moment of the joint manufacture. The effect of the fillet size was studied by assuming 45° fillet and changing its size. The magnitude of principal stresses obtained from such analysis showed a large difference when compared to results obtained from analysis which assume the adhesive to have a square edge. The highest principal stress was found to lie on the corner of the unloaded adherend. This correlated well with observed failure characteristics during testing. The inclusion of a triangle spew (45°) decreased the magnitude of the maximum principal stress by 40% when compared to a square end adhesive fillet.

Crocombe and Adams [152] included the effect of additional parameters such as material and geometric properties. In this analysis, the stress distribution across the adhesive thickness was not assumed constant. Their results for a lap joint with a spew fillet indicate that the averaged maximum adhesive stress increased with decreasing modulus ratio (increasing adhesive stiffness) up to a limiting value, after which they decreased again. Variations of overlap length, adhesive thickness were also included in their analysis.

Dorn and Weiping [156] performed a number of FEM analysis and some experimental measurements in order to study the effect of spew fillets for joints with different couples of plastic and metal parts. In that work the spew angles are not considered design variables, their values are assumed at the beginning and maintained fixed for the whole article. Hildebrand [157] studied different shapes (obtained by tapering, rounding or denting) of the extremities of the adhesive layer in joints of metal with fiber-reinforced plastics parts; also in this case, the analysis was performed by the FEA method. He considered the shape of the extremities as design variables and developed an optimazationn study. A comparative analysis of the effect of the spew geometry considering triangular and rounded profiles, has been developed by Lang and Mallick [158] by the FEA method. Detailed analysis has been devoted to study the effect of the adhesive thickness, while the effect of the spew angle is only addressed briefly and their conclusions on the subject do not explain the reported maximum peel stress dependency. Recently (159) they also investigated the effect of a recess (i.e., lack of adhesive in the central portion of the lap) in the joint. In both studies the joint concerns adherends equal in material and thickness.

In recent years, the strength of the adhesive joints under impact (i.e., dynamic) loading has become important because their use expands to the aircraft and automobile industries [63]. For these applications, the crash worthiness of the structures should be proved, so that the dynamic strength of adhesive joints used in the structures should be predicted analytically. For example, the dynamic strength of the adhesive bond was investigated intensively by Adams and Harris [160, 161], Kinloch *et al.* [162], Latailade and Cayssials [163, 164], Yokoyama [165], Bezemer *et al.* [166], Blackman *et al.* [90]. However, a few investigations on the stress distribution and its variation with time in joints have been performed by Zachary and Burger [167], and Sato and Ikegami [63]. Sato and Ikegami [63] have recently investigated the dynamic deformation and the stress concentration in single lap joints, tapered lap joints and scarf joints using analytical and experimental techniques. They simulated the deformation and stress distribution in these joints under impact loading using the finite element method.

Therefore, based on above discussion and the literature, we can conclude that the various factors have been taken into consideration to analyze and optimise the adhesively bonded joints. These factors include the (a) thickness and length of the adhesive layer, (b) adhesive and adherend elastic properties(such as elastic moduli, flexibility of the adhesive) (c) plastic yielding behavior of adhesives [14], (d) geometries of joints [such as tapering, rounding, denting, scarf, spew fillet, recessing [62] etc], (e) type of static loading to be transferred (i.e., shear, comprerssion, tensile bending), and (f) dynamic or impact loading [63, 90, 160–165].

5.1. Load transfer in adhesively bonded joints

The joint must be carefully analyzed because it represents a discontinuity in the material, and therefore resulting high stresses often intiate joint failure. There are many useful studies on the analysis of bonded joints (see for example, Ref. [125–128, 135–139]). Analyses have been carried out for various joint configurations and for different properties of the adherends and adhesives using closed form or numerical analysis methods. As mentioned previously, the primary function of a joint is to transfer load from one structural member to another. In most bonded joints the load transfer takes place through interfacial shear. For example, as shown in Fig. 25a, in composite materials, the interfacial shear gives rise to high interlaminar normal and shear stresses for a single-lap joint. As pointed out in the previous section, the actual magnitude of the stresses depends on many geometric and material property parameters, such as the thickness and length of the adhesive layer compared to the corresponding values for the adherend material, flexibility of the adhesive and type of load to be transferred (i.e., simple loading of shear, compression; complex loading such as bending). As seen in Fig. 25a both interlaminar normal and shear stresses have a large stress concentration near the end of the joint. In the rest of the joint they are uniformly distributed. Because of this high stress concentration in the adhesive layer, high stresses are produced in the adjacent plies of the adherend laminates [60]. Therefore, failure may initiate in these plies. It was suggested [168] that an effective way of reducing the local high stresses in the plies adjacent to the adhesive layer is to interleave the plies of the adherend laminates so that adhesion takes place in many layers and, consequently, stresses are distributed in many plies. As pointed out by Agarwal and Broutman [60], interleaving is particularly desirable when the number of plies in the laminate is large.

The influence of load transfer depends on the stiffness of the bondline. Heslehurst [80] has recently investigated the load transfer along the adhesive bondline. The elastic distribution of shear stress over the bondline of a double-lap joint is now recognized as being non-uniform, with peaked ends and a shallow trough [80] (smilar to Fig. 25a), The distribution can be modelled as a hyperbolic function [169]:

$$\tau(x) = A \sin h(\lambda x) + B \cos h(\lambda x) \tag{18}$$

$$\tau(x) = \frac{\tau_{\mathrm{av}}(\lambda l_{\mathrm{a}}/2)}{\sin h(\lambda l_{\mathrm{a}}/2)} \cos h\left(\frac{\lambda x}{2}\right) \text{ for } -\frac{l_{\mathrm{a}}}{2} \leq x \leq +\frac{l_{\mathrm{a}}}{2} \tag{19}$$

where l_{a} is the joint length,

$$\lambda^2 = \frac{2G_{\mathrm{a}}}{E_{\mathrm{s}}\ \eta_{\mathrm{s(o)}}\ \eta_{\mathrm{a}}} \tag{20}$$

E_{s} is the adherend Young's modulus, G_{a} the adhesive shear modulus for the elastic/plastic shear stress/strain model, $\eta_{\mathrm{s(o)}}$ is the outer adherend thickness, η_{a} is the adhesive thickness, τ_{av} is the average shear stress over the joint length ($=P/2l_{\mathrm{a}}$) and P is the axial load per unit width, l_{a} is the joint length. Heslehurst [80] studied the effect on the elastic shear stress distribution with a variations in adhesive shear modulus. Using the data

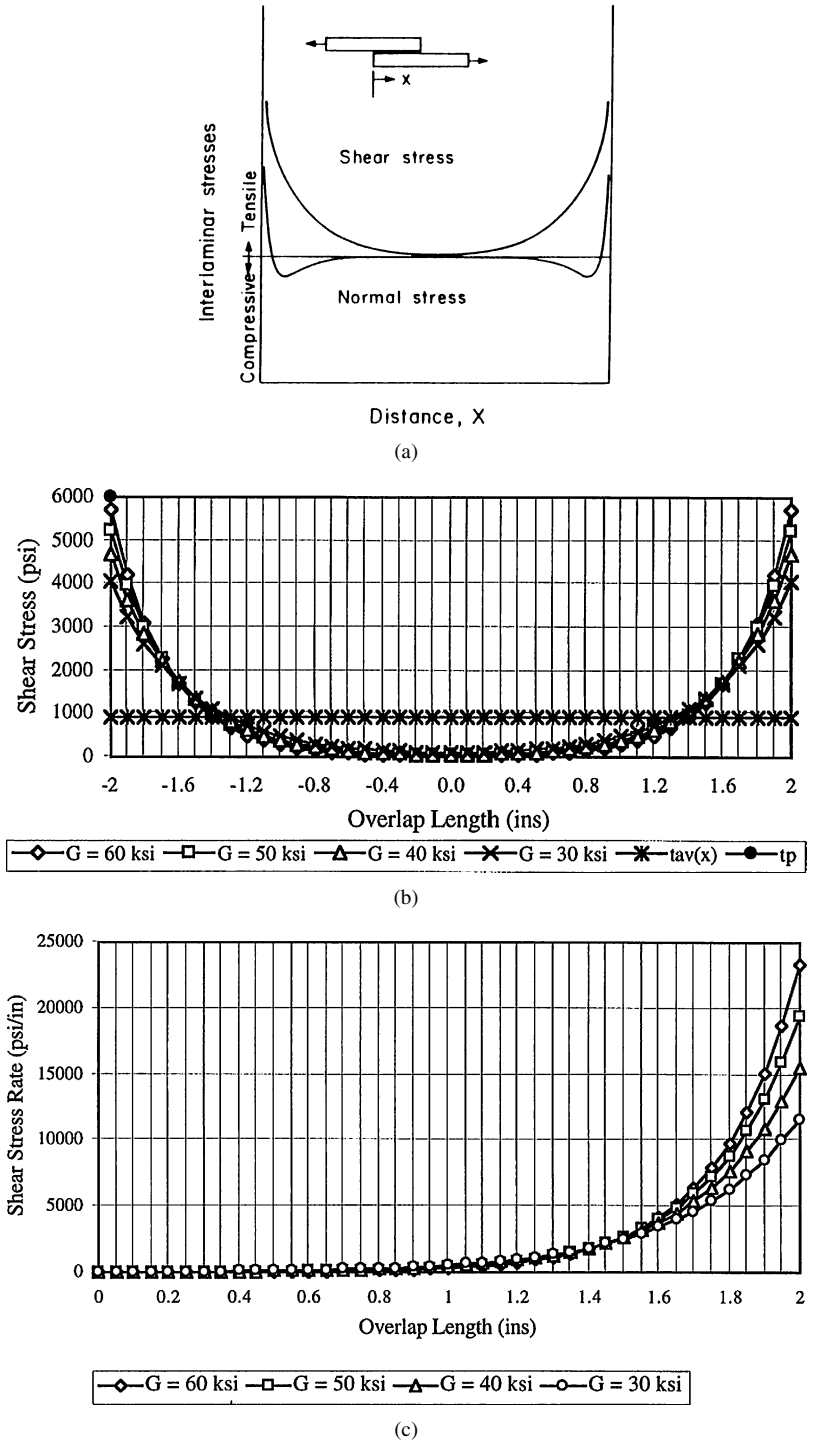

Figure 25 Stress distributions (or concentration) along the overlap length: (a) variation of interlaminar normal and shear stresses for single-lap joint [60], (b) effect of adhesive stiffness on the adhesive shear stress distribution [80], and (c) effect of adhesive shear modulus on the shear stress (load transfer) rate [80].

for an elastically balanced, thermally matched double-lap joint, a plot of the shear stress distribution for an overlap length l_a of 100 mm and applied load/unit width (P) of 1313.5 kN/m), shows the classical stress distribution, as seen in Fig. 25b. This shear stress distribution is based on the adhesive elastic-plastic shear stress/strain model [169]. The adhesive is a ductile type with shear modulus of 414 MPa. If the adhesive mechanical properties are reduced (i.e., shear modulus) the elastic stress distribution is modified by significant reduction in peak stress at the overlap ends, but only marginal increase in the shear stresses over the central portion of the overlap length [80]. This is clearly shown in Fig. 25b. Note, the average shear stress (τ_{av}) and the areas under each of the curves remains the same.

The rate of change of the elastic shear stress distribution (or the rate of load transfer) is thus given as [170]:

$$\frac{\partial \tau(x)}{\partial x} = B\lambda \sin h(\lambda x) \tag{21}$$

where

$$B = \frac{\tau_{av}(\lambda\, l_a/2)}{\sin h(\lambda\, l_a/2)} \tag{22}$$

A comparative study for a double-lap adhesively bonded joint, using the same data as in Fig. 25b, gives the shear stress rate of transfer over variations in adhesive shear modulus. This is shown in Fig. 25c. Thus, from this figure it was concluded [80] that with a higher shear modulus the load transfer rate is significantly greater. Therefore, with a higher rate of load transfer there is a concentration of load at the joint end that induces problems. Such problems will ultimately lead to a failure at the joint end. However, stiffness losses in the adhesive do have an advantage, but a corresponding loss of strength will also be evident [170].

6. Stress analysis using 2-D and 3-D finite element analysis methods in adhesive joints: Geometricly-linear and nonlinear adhesive design

Stress analysis provides the connection between the applied load and the created interfacial stress as well as the optimal specimen geometry. The determination of the best geometry is very complex problem. Structural optimazation of a joint tries to modify the geometry of the adhesive layer and also of the adherend parts, with the scope of reducing the intensity of the stress peaks and therefore increase the strength of the joint [61]. This approach has been made possible by the numerical analysis to treat cases with geometrical features that are beyond the analytical approach, such as fillets introduced at the ends of the overlap zone. This line of research has been explored over the last two decades [i.e., 70, 156–159, 171, 172], accounting also for the non-linearities occurring during collapse (material inelasticity, large displacements). The effects occurring at the ends of the overlap are extensively discussed in detail in Ref. [70], on the basis of previous paper of Adams and co-workers.

Since the 1970s, finite element analysis (FEA) methods have increasingly been used to analyze the various adhesively bonded joints. Wooley and Carver [98] made one of the first finite element analyses of a single lap joint. They used plane stress elements, and their results were comparable with those from the Goland and Reissner [72] solution, the seminal work in the field. Countless studies of various joints have followed this first work. The computational approach is now considered a necessary and cost effective tool for obtaining simulations and also for validating analytical solutions. The relatively large amount of work in this field can be found (see for example, Refs. [98, 105, 116, 152, 155, 173–181]). However, in many of the work, the boundary conditions at the two unbonded adherend ends are assumed to be hinged at one joint end and a roller on the other. The horizontal tensile force is then applied at the roller end. Moreover, a two-dimensional (2D) plane strain condition is usually employed in the FEM simulations as the adherend width is much larger than its thickness. The applied boundary conditions are considered as rotation boundary conditions since the two unbonded adherend ends can rotate during tensile loading [46]. Mostly, analytical solutions also assume plane strain conditions since the analyses are based on beam theory principles [182]. It would therefore be useful to compare the differences between plane strain and plane stress conditions for simply supported (rotation) and fully fixed (non-rotational) boundary conditions for joints with relatively thick adherends in comparison to the adhesive layer [46]. As compared to the theoretical and FEM studies, there is even less published experimental work in this area. The experiments usually consist of strain gaging joint specimens and/or the measurement of adhesive strains using the full-field Moire interferometry technique [173–176].

In the FEA model quadrilateral (i.e., a flat shape with four sides such as a square or a rectangle) elements require a very fine mesh for adequate accuracy [91]. For this reason efforts have been made to reduce the size of the models. The first approach was made by Yadigari *et al.* [183] who modeled the adhesive layer using only one row of six-node plane elements. Carpenter and Barsoum [184] modeled the adherends using two-node beam elements and the adhesive layer by a linear plane element with offset nodes. The number of degrees-of-freedom is reduced appreciably by this approach because the adherends and the adhesive use the same nodes. Previously, Amijima and Fujii [185] developed a similar model but they required that the displacements in the adhesive-adherend interfaces be compatible. Taylor [186] used a similar approach to model three-dimensional (3-D) adhesive joints; in this case, the adhesive was modeled using solid 3-D brick elements and the adherends were represented by plates. Naboulsi and Mall [187] modeled the adhesive layer and adherends using shell elements; this approach considers the contribution of the bending stiffness of the adhesive layer.

Andruet *et al.* [91] have recently developed a special 2- and 3-D finite element analysis (FEA) methods for stress and displacement analyses in bonded joints. Both the 2-D and 3-D elements were used to model the whole adhesive system; adherends and adhesive layer. In their two-dimensional finite element analysis (2-D FEA), Andruet *et al.* [91] have used Bernoulli beam elements to represent adherends, with axial deformation and the adhesive layer by plane-stress or plane-strain elements. The nodes of the plane stress-strain elements that lie at the adherend-adhesive interface are rigidly linked with the nodes of the beam elements, resulting in offset nodes which coincide with the midplanes of the adherends. On the other hand, the 3-D elements consist of shell elements that represent the adherends and solid brick elements to model the adhesive. The resulting mesh can represent arbitrary beam- or plate-like geometries, which are a larger part of adhesive joint designs. This model can include debonds as well as cracks within the adhesive, therefore it can be used for durability analysis of adhesive joints. Their models (the 2-D and 3-dimensional formulations) included (a) geometric nonlinearities, and (b) the temperature and moisture effects. In their formulations the reason to include the geometric nonlinearities was to account for large displaments in the 2-D and 3-D adhesive elements.

On the basis of above discussion and literature, we can therefore clarify and summarize the various

conditions used in the FEA methods: (a) 2- or 3-D formulations, (b) plane-strain or plane-stress condition, (c) geometrically linear and non-linear analyses, (d) types of loading (i.e., static or dynamic loading), (e) temperature and moisture effects, (f) boundary conditions (i.e., rotational or non-rotational), (g) geometric shapes of joints (i.e., single- or double-lap joints, tapering, scarf, fillet, spew, chamfer, recessing etc), (h) linear elastic behavior of the joint components, (i) non-linear or plastic yielding behavior of joint components (i.e., large rotation, plasticity).

As mentioned above, in designing 2-D geometric non-linear adhesive, Andruet *et al.* (2001) [91] have modelled the adherends as Bernoulli/Euler beam elements with axial and bending deformation modes. The adhesive is a standard plane-strain quadrilateral element except that the nodes are offset to coincide with the midplane of the corresponding adherend. The beams and special adhesive elements are shown in Fig. 26a. (In this figure, u and v are axial and transverse displacements, respectively). The formulation is similar to that of Carpenter and Barsoum [184], except that the interpolation functions for the adhesive elements were chosen to be compatible with the deformation of the beam-truss elements. This element converges faster than those with non-compatible displacements in the adhesive-adherend interface, as shown by Taylor [186]. Adherends were modelled using the large-displacement Bernoulli-Euler beam elements. The formulation of this element can be found in the literature [188]. Using this formulation Andruet *et al.* [91] obtained the folowing finite element model for the adherends as

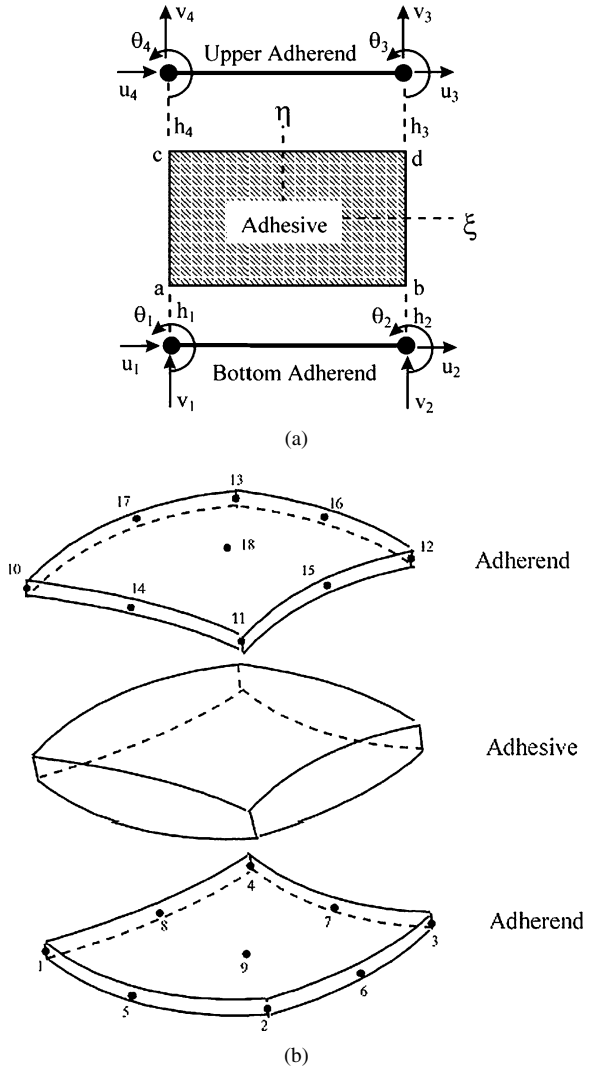

Figure 26 Finite element configuration using the geometrically-nonlinear adhesive [91]: (a) 2-D adhesive finite element and (b) 3-D sandwich-type configuration of the adhesive element.

$$[K_{\text{Adher}}(\{\Delta\})]\{\Delta\} = \{F\} \tag{23}$$

where $\{\Delta\}$ is the nodal displacement vector, $\{u_1, u_2, s_1, s_2, s_3, s_4\}$, $K(\{\Delta\})$ the stiffness matrix and $\{F\}$ the nodal load vector.

Andruet and his co-workers [91] have formulated the adhesive layer as a plane-stress/strain solid element with offset nodes. In order to make the displacements in the adhesive-adherend interfaces compatible, special interpolation functions were used [186]. The finite element discretization, coordinates of any point in the adhesive can be expressed as a function of the nodal coordinates of the element

$$\{x\} = \sum N_{\text{i}} x_{\text{i}} \tag{24}$$

where $\{x\} = \{x, y\}$ are the coordinates of a generic point in the adhesive, $\{x_{\text{i}}\} = \{x_{\text{i}}, y_{\text{i}}\}$ the nodal coordinates and N_{i} the linear shape functions of local coordinates ψ and φ (see Fig. 26a). The displacements of the adherends were expressed as a summation of polynomial functions. The expression for the displacement of the bottom adherend is

$$\{u_{\text{adhes}}\} = [N_{\text{i}}]_{\text{adhes}}\{u_{\text{i}}\}_{\text{adhes}} \tag{25}$$

where

$$\{u_{\text{adhes}}\} = \begin{Bmatrix} u \\ v \end{Bmatrix}_{\text{adhes}}$$

$$\{u_{\text{i}}\}_{\text{adhes}} = \{u_1, v_1, u_2, v_2, u_3, v_3, u_4, v_4\}_{\text{adhes}}$$

and $[N_i]_{\text{adhes}}$ are interpolation functions in the adhesive layer.

In order to have displacement continuity in the adhesive-adherend interfaces, appropriate interpolation functions for the adhesive layer must be found. For this, $[N_{\text{i}}]_{\text{adhes}}$ are obtained by imposition of equal displacement of the adhesive and the adherends at both interfaces *ab* and *cd* (Fig. 26a),

$$\begin{aligned} \{u_{\text{adhes}}\}_{\text{ab}} &= [N_{\text{iab}}]_{\text{adhes}}\{u_{\text{i}}\}_{\text{adhes}} = \{u_{\text{adher}}\}_{\text{b}} \\ &= [N_{\text{i}}]_{\text{adher}}\{u_{\text{i}}\}_{\text{adher b}} \end{aligned} \tag{26}$$

$$\begin{aligned} \{u_{\text{adhes}}\}_{\text{cd}} &= [N_{\text{i cd}}]_{\text{adhes}}\{u_{\text{i}}\}_{\text{adhes}} = \{u_{\text{adher}}\}_{\text{u}} \\ &= [N_{\text{i}}]_{\text{adher}}\{u_{\text{i}}\}_{\text{adher u}} \end{aligned} \tag{27}$$

where $[N_{\text{i ab}}]_{\text{adhes}}$ and $[N_{\text{i cd}}]_{\text{adhes}}$ are the interpolation functions for the adhesive evaluated at the ab and cd

interfaces, respectively. From these expressions the displacements in the adhesive layer were obtained as function of the nodal displacement of the adherends

$$\{u_{\text{adhes}}\} = [N_{\text{i}}']\{u\}_{\text{adher}} \tag{28}$$

where $[N_{\text{i}}']$ are the interpolation functions of the displacements in the adhesive layer with respect to the adherend nodal displacements.

From these equations Andruet *et al.* [91] obtained cubic and quadratic interpolation functions for the vertical and horizontal displacements, respectively, in the direction of the axis of the joint, the ψ axis in Fig. 26a. In the direction transverse to the axis of the joint, axis φ in Fig. 23a, linear interpolation functions are used. The constitutive law for the adhesive is

$$ {}_{\text{t}}C_{\text{ijrs}} = D = \underbrace{\frac{E_{\text{a}}}{1-\nu_{\text{a}}^2}\begin{pmatrix} 1 & \nu_{\text{a}} & 0 \\ \nu_{\text{a}} & 1 & 0 \\ 0 & 0 & \frac{1-\nu_{\text{a}}}{2} \end{pmatrix}}_{\text{Plane Stress}} $$

or

$$ D = \underbrace{\frac{E_a}{(1+\nu_a)(1-2\nu_a)}\begin{pmatrix} 1-\nu_{\text{a}} & \nu_{\text{a}} & 0 \\ \nu & 1-\nu_{\text{a}} & 0 \\ 0 & 0 & \frac{1-2\nu_{\text{a}}}{2} \end{pmatrix}}_{\text{Plane Stress}} \tag{29}$$

where E_{a} is the elastic modulus and ν_{a} the Poisson ratio.

Substituting Equations 28 and 29 into Equation 1 in Ref. [91], they obtained the finite element model of the adhesive

$$[K_{\text{Adhes}}(\{\Delta\})]\{\Delta\} = \{F\} \tag{30}$$

and the model of the adherend-adhesive system is the summation of the stiffness matrices of the adherend and adhesive:

$$[K_{\text{Adher}} + K_{\text{Adhes}}]\{\Delta\} = [K]\{\Delta\}\{F\} \tag{31}$$

Equation 31 can be expressed as follows:

$$[K_{\text{L}} + K_{\text{NL}}]\{U\} = \{F\} \tag{32}$$

where K_{L} and K_{NL} are matrices representing the linear and nonlinear stiffness of the model, respectively, and U is the displacement vector. The nonlinear Equation 32 is solved by means of the modified Newton-Raphson method:

$$\left({}_{\text{t}}^{\text{t}}K_{\text{L}} + {}_{\text{t}}^{\text{t}}K_{\text{NL}}\right)\Delta U^{(\text{i})} = {}^{\text{t}+\Delta\text{t}}f^{(\text{i}-1)} \tag{33}$$

where $\Delta U^{(\text{i})}$ is the displacement vector for the ith iteration and R-F is the unbalanced force vector for the $t + \Delta t$ step. The solution of Equation 33, $\Delta U^{(\text{i})}$, was used to obtain an improved prediction of the equilibrium configuration.

In their study, Andruet *et al.* [91] have also taken into account the effects of thermal and moisture by defining an initial strain ε_{o}, which is a function of the thermal and moisture coefficients and the temperature and moisture variations relative to the initial times. This initial strain does not produce stress, accordingly

$$\sigma = D(\varepsilon - \varepsilon_{\text{o}}) \tag{34}$$

Andruet *et al.* [40] have also formulated a 3-D finite element model for geometric nonlinear design, which is an extension of the adhesive element developed by Taylor [186]. This model of the adhesively bonded joint has two main components: (a) the adhesive layer and (b) the adherends. These components are combined in a sandwich-type configuration as shown in Fig. 26b. The model consists of two adherends represented by general shell elements and the adhesive layer modeled as a solid element with offset nodes in the mid-planes of the adherends. In the work by Taylor [186], the adherends were modeled by Mindlin plate elements. Since cuved structures are modeled better with shell than with plate elements, the newly formulated element enhances the rate of convergence for practical joint configurations [91]. Using the modelling of the adherends as shell elements, formulation given by Bathe [189], Andruet *et al.* [91] have formulated the displacement vector, and that they presented the constitutive relation for the 3-D geometric nonlinear design as follows:

$$C = \begin{bmatrix} E_{11} & E_{12} & 0 & 0 & 0 & 0 \\ E_{12} & E_{22} & 0 & 0 & 0 & 0 \\ 0 & 0 & 0 & 0 & 0 & 0 \\ 0 & 0 & 0 & G_{12} & 0 & 0 \\ 0 & 0 & 0 & 0 & \frac{5}{6}G_{23} & 0 \\ 0 & 0 & 0 & 0 & 0 & \frac{5}{6}G_{21} \end{bmatrix} \tag{35}$$

The third row and colomn are empty because σ_{33} is negligible for plates and shells.

They modelled the adhesive layer as 3-D solid brick elements, with nodes offset to the shell midplanes [91]. This is equivalent to condensing out the degress of freedom of the continuum elements into the degrees of freedom of the adjacent shells that model the adherends. Using the displacement continuity at the adhesive-adherend interfaces improves the accuracy of relatively coarse meshes. Quadratic interpolation functions were used in the planes of the element parallel to the adherend mid-planes in order to have compatibility of the displacements in the adhesive/adherend interfaces [91]. In the thickness direction, linear interpolation functions were used. Quadratic and linear Lagrange polynomials are used. Analogous to the two-dimensional element, the coefficients of the interpolation functions for the adhesive were obtained by imposition of equal displacements of adherends and adhesive in their interfaces. Isotropic and orthotropic constitutive laws were used.

Similar to the 2-D case, in 3-D geometric nonlinear adhesive design, thermal and moisture effects were taken into account by definition of an initial strain ε_{o}, which is a function of thermal and moisture coefficients

and the temperature and moisture variations relative to the initial times. Using the D parameter in Equation 35, Equation 34 can be used in the present case. This initial strain does not produce stress, accordingly.

Gonçalves *et al.* [92] have developed a new 3-D FEA method of adhesive joints. The model considers geometric and material non-linerarities as in the case of Andruet *et al.*'s work [91] and used solid brick elements as well as specially developed interface elements. The main objective was to calculate the stresses at the interfaces between adherends and adhesives, which are considered critical regions in these structures. They formulated an equilibrium equations of a structural problem involving contact as minimization of the potential energy subjected to certain kinematic constraints. Contrary to continuum elements where stress-strain relationships are used, interface elements are governed by stress-relative displacements relationships. The vector of relative displacements between two homologous points were obtained from the displacements fields associated with the element faces (top and bottom). Then the stresses at the interfaces were obtained from the relative displacements (δ) as follows

$$\begin{aligned} \tau_{sn} &= k_s \delta_s \\ \tau_{tn} &= k_t \, \delta_t \\ \tau_{nn} &= k_n \delta_n \end{aligned} \tag{36}$$

where s and t represent the tangential directions and n the normal direction. or Equation 36 can be written in matrix form

$$\sigma = D\delta \tag{37}$$

where

$$D = \begin{pmatrix} k_s & 0 & 0 \\ 0 & k_t & 0 \\ 0 & 0 & k_n \end{pmatrix} \tag{38}$$

The parameters k_s and k_t are the shear interface stiffness and k_n is the normal interface stiffness. Their units are N/m^2 and they represent the penalty parameter introduced by the user. Note that these parameters need to be carefully chosen in order to obtain a good performance of the model; small values induce large interpretations incompatible with the physical reality while large values produce numerical problems.

7. Application of 2-D and 3-D finite element analyses methods on optimizing the adhesive joints

At the adhesive joint ends, the analytical solution (i.e., finite element analysis) of stresses can display singular behavior (i.e., approach infinite values) [62]. An infinite stress is of course a mathematical anomaly, and in practice does not exist. To avoid any adverse effects from the singularity point several approaches have been undertaken. One of these approaches is based on the fracture mechanics principles of energy release rate and stress intensity factors. Groth [190] formulated a fracture criterion based on a stress intensity factor derived from bi-material singularities at the ends of bonded joints. In another approach, Crocombe *et al.* [191] ignored the final element incorporating the singularity point and extrapolated to the corner to obtain the peak stress values. Adams and Harris [192] reasoned that, in practice, sharp corners at the end of the lap joint are always rounded slightly during manufacture. Therefore, to deal with singularity behavior they used rounded corners, which produced a uniform stress field.

7.1. Stress and strain analysis under static and impact loadings

Schüller and Lauke [142] have analyzed the stress state of a newly developed test specimen with a semicircular notch (see Fig. 23) using the 3-D finite-element anlysis model. As seen in Fig. 23, the two halves in the specimen were treated as homogeneous solids connected by an ideal interface. It was assumed [142] that this simplification of the complex structure of a real interphase is reasonable as long as the interphase is thin compared with the whole specimen and does not influence strongly, the stress field. The average tensile stress in the smallest cross-section is $\sigma_{av} = P/(2w_r\eta)$, where P, w_r and η denote the applied load, the remaining width of one notched specimen half and the specimen thickness, respectively. Due to the symmetry of the specimen, all shear components vanish in the center of the specimen. Finite-element results for a necked specimen published in [193] suggest that plane-stress condition is a good approximation for the stress field leading to the assumption that the stress state in the center of the specimen is approximately biaxial. Assuming the linear-elastic material, all non-zero stress components are proportional to the applied load and also to σ_{av}. As stated by Schüller and Lauke [142], then, the normalized interfacial transverse stress σ_{it}/σ_{av} and the combined loading ratio σ_{ip}/σ_{it} completely describe the biaxial stress field, where σ_{ip} denotes the in-plane component. These ratios depend on the specific geometry. The notch also causes a stress concentration at its ground. It was suggested [142] that if this stress concentration exceeds the linear-elastic limit of the polymer material during experiment, this analysis would not be valid. Therefore, even the stress ratio σ_{it}/σ_{eqv} is an important parameter describing a specific geometry. σ_{eqv} is the maximum equivalent stress at the neck ground. The ratio expresses the highest attainable interfacial stress within the limit of linear-elastic theory. The variation of the notch radius R_N and each shape is uniquely characterized by the shape parameter R_N/a.

The three-dimensional model finite element analysis allows evaluating even the variation of the interfacial stress in the direction of thickness. The model is parametric, which makes the evaluation of different specimen shape very convenient. The interfacial transverse stress σ_{it} is equal to the stress component σ_x at the interface ($x = 0$). The interfacial transverse stress has a wide maximum between the notches that reaches $\sigma_{it}/\sigma_{av} = 0.24$ for this geometry ($R_N/w_r = 1$, $\eta/w_r = 1$). It is slightly higher at the surface of the specimen but does not show any concentration or even

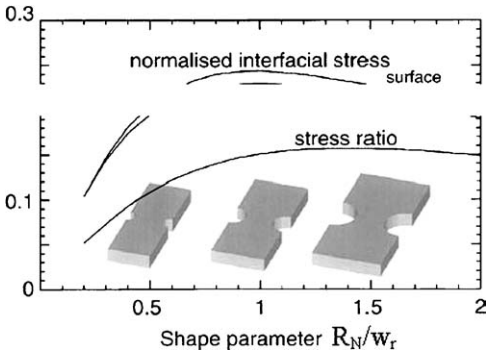

Figure 27 Normalized interfacial tranverse stress σ_{it}/σ_{av} (above) and stress ratio σ_{it}/σ_{eqv} (below) versus shape parameter R_N/w_r [142].

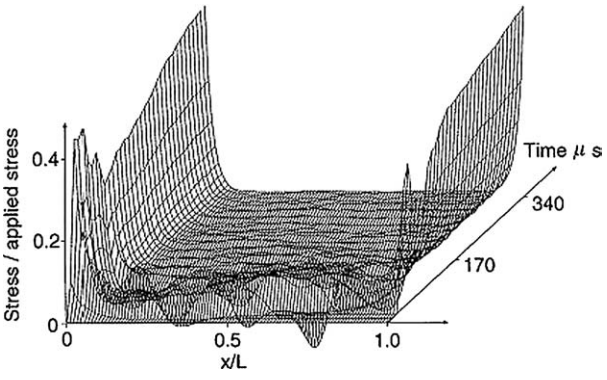

Figure 28 Variation of stress in the adhesive layer of single lap joint under step loading ($L = 100$ mm) (Ref. [63]).

singularity. The variation of the interfacial stress along the thickness indicates the stress state is really three-dimensional and that the specimen thickness influences the stress field. The shear components σ_{xy}, σ_{xz}, σ_{yz} and also σ_y are small compared with σ_x. The ratio of biaxiality is $\sigma_{ip}/\sigma_{it} = 3.5$. The influence of the shape parameter R_N/a on the normalized interfacial transverse stress σ_{it}/σ_{av} and stress ratio σ_{it}/σ_{eqv} was shown in Fig. 27. The highest attainable interfacial transverse stress is reached for a shape parameter $R_N/w_r \approx 1.5$. Nevertheless, Schüller and Lauke [142] recommended to use $R_N/w_r = 1$ because the interfacial transverse stress σ_{it}/σ_{av} has a maximum there and the stress ratio σ_{it}/σ_{eqv} is nearly the same. The wide maximum of σ_{it}/σ_{av} prevents impression of sample preparation (especially imprecise shape parameter R_N/w_r) from having large effects on σ_{it}/σ_{av}.

The strength of the adhesive joints under impact (or dynamic) loading has become important because of the important industrial applications such as the aircraft and automobile industries. The dynamic strength of adhesive bond was investigated by many researchers (i.e., for example, Refs. [160–167]). Sato and Ikegami [63] have recently investigated the stress distribution and the time variation of stress and strain in the joints under tensile impact loading using the 2-D finite element method with plane strain condidions, considering the viscoelastic properties of the adhesive in the single lap joints, tapered joints and scarf joints. The joints studied consisted of aluminum alloy and epoxy resin. The element thickness of the adherends was changed gradually in the tapered part so that the acute angle of the adherend could be described. The adhesive layer was treated as a single element layer because the adhesive layer was very thin.

As shown in Fig. 28, there was stress concentration at both edges of the adhesive layer in the single lap joint. At the initial stage of loading, the stresses increased and showed peaks at both the edges in the adhesive layer. The peak value of a shear stress at the left edge (stress-wave-imput side) was the greatest in the stress components (see Fig. 28). The maximum value of the shear stress was over 0.4 MPa when the applied stress was 1 MPa. At the right edge, there was also a great peak of a normal stress in the y-direction, and the value was over 0.4 MPa. After the peaks, the stresses in the single lap joint decreased. The stress distributions during the initial stage were greatly different from those of static loads. For instance, the distributions of dynamic stress were not symmetric although those of the static stress were symmetric. Stress distributions in single lap joints under static loading depended on the distance between the joints and the load applying points, i.e., on the adherend length without the joint length [63]. If the distance increased, the bending deformations and the stress concentration also increased. Similar phenomena occurred during the impact test. As the flexural waves propagated outward in the adherends, the region of bending deformations was spread out. It was equivalent to the increasing of the adherend length at static tests. Then the stresses at the edges increased gradually as shown in Fig. 28.

They also studied the stress distributions and the time variation of the stresses in the adhesive layer of a tapered lap joint, which has the same lap length of 100 mm as the single lap in the joint. These joints showed similar phenomena to the case of the single lap joint, i.e., there were transient variation and gradual increase. The stress values at both the edges of the tapered lap joint were less than half of those of the single lap joint which has the same lap length. Therefore, tapering of adherends in lap joints was effective to reduce stress concentration.

Finally, in the scarf joints investigated (i.e., which had the same lap length of 100 mm as the single lap joint and the tapered lap joint), the stress values and the stress concentration were smaller than those in the other joint configurations discussed in this work. As pointed out by Sato and Ikegami [63], scarf joints do not have a geometrical offset of the adherends. Thus, a bending moment and a flexural wave, which often cause stress concentration in lap joints, are not induced because stress waves propagate smoothly in the joints. Calculated results of the dynamic deformation of the joints in the present FEM analysis showed good agreement with the experimental results [63] (see Section 8 for more detail).

7.2. Effects of geometric linear and non-linearity, T-joints, fillets, spews, chamfer size, and recessing on the strength of single-lap joints

7.2.1. Geometrically linear and non-linear analysis in 2-D finite element method

Li *et al.* [73] have studied the effects of processing variables such as bonded length, adhesive thickness,

and adherend thickness on the static stiffness (i.e., linear and rotational stiffnesses) of the adhesive bonded T-joints using the linear elastic 2-D FEA method. The adhesive joint consists of a right angle plate bonded to a rigid plate using adhesive (i.e., T-joint) [see for example, Fig. 4a ($\theta = 90^\circ$). Both adherends bonded are mild steel with a modulus of elasticity of 210 GPa and Poisson's ratio of 0.29. An epoxy resin adhesive was used having a modulus of elasticity of 3.48 GPa. Because of the discontinuous nature of the joint geometry and material properties in the interface between adherend and adhesive, large stresses and strain may exist around these regions. For this region, a gradual mesh refinement was used to concentrate elements around te adhesive layer.The joint model with plane strain condition was subjected to two linear loads and one bending moment. It was assumed that the adhesive and adherends had linear elastic properties.The analysis of such joints is complicated by the geometric complexity and by the discontinuous nature of the adherend/adhesive interface. The linear FEA element method has been shown to give good agreement with experimental results for T-joints [70] and was therefore used.The deflections along the P_x and P_y load directions in the T-joints with dimensions are shown in Fig. 29. The maximum deflections generally occur in the directions in which the loads are applied and they decreased towards to the joint region.The linear stiffness (in Nmm^{-1}) of the joint was calculated from the slope of the load/deflection curves in the direction of application of P_x and P_y. The rotational stiffness (in Nmm) was calculated from the ratio of the applied moment M and the corresponding rotational angle at the top point of the central axes of the vertical and the horizontal plates.

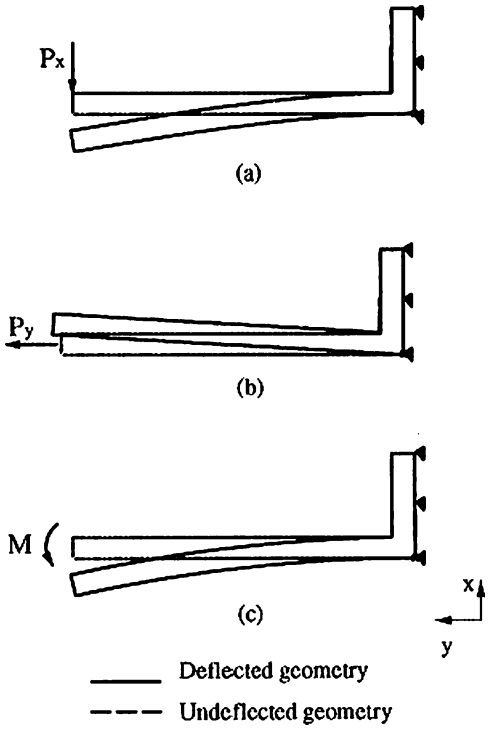

Figure 29 The deflections of the joints [73]: (a) loading in the x-direction P_x, (b) loading in the y-direction, and (c) loading in the moment M.

As shown in Fig. 30a, the linear stiffness is affected by the bonded length for the case of loading P_x, and the effect becomes less as the bonded length is increased. In comparison between a bonded length of 10 and 16 mm the linear stiffness increases by only 0.1%, but the increase is 0.7% between length of 6 and 10 mm. However, for the case of the loading direction P_y, when the bonded length increases from 6 to 10 mm, the linear stiffness increases by 1.8%.The rate of increase continuously gets less, and the linear stiffness increases only 0.19% as the bonded length increases from 10 mm up to 16 mm. It is very clear that the absolute stiffness in the y direction is considerably higher than in the x direction. The effect of the different bonded lengths on the linear stiffness is plotted in Fig. 30a. For the case of effect of bonded length on the rotational stiffness, between bonded length of 6 and 10 mm, increasing the bonded length results in increase of 0.4% in rotational stiffness and between a bonded length of 10 and 16 mm, the increase is 0.2% [73]. Therefore, a bonded length of 10 mm can be used without significant loss of the joint stiffness compared with using any higher values. Li *et al.* [73] have also analyzed the effect of adhesive thickness on linear and rotational stiffnesses. Fig. 30b indicates the effect of adhesive thickness on the stiffness of the T-joint (rotational stiffness in the bending moment M), stiffness increasing by 6.14 between adhesive thickness of 0.05 and 0.5 mm. The variation of linear stiffness in the y-direction shows similar trends, the stiffness decreasing by 37.64% between adhesive thickness of 0.05 and 0.5 mm. It can be noted that the stiffness in the y-direction is much higher than in the x direction. Therefore, it can be concluded that the joint stiffness was reduced when the adhesive thickness was increased.

Fig. 30c shows the effect of the adherend thickness on the stiffness in the x direction lineraly increases by 88% between adherend thickness of 2–4 mm. The variation of linear stiffness in the y-direction shows different trends, the stiffness increasing 57% between adherend thickness of 2 and 4 mm. It can be found that the stiffness in the y direction is also much higher than in the x-direction. The variation of rotational stiffness shows similar trends with that in the x direction, and the stiffness is increasing by 88% between adherend thickness of 2 and 4 mm. Therefore, It is clear that the joint stiffness was increased when the adherend thickness was increased.

In summary, the bonded length, adhesive thickness and adherend thickness of the joint have marked effects on the T-joint stiffness. It was also found that the linear stiffness in the y-direction and rotational stiffness under bending moment loading are much higher than the linear stiffness in the x direction for all conditions.

Andruet *et al.* [91] have analyzed a single lap joint using the 2-D finite element analysis methods. The principals of these methods were presented in Section 6. Note that the single lap joint geometry used was popular in industrial applications as a benchmark test and the bibliography for this joint is very extensive; there are many analytical solutions and test results. Peel and shear stresses were obtained performing a linear

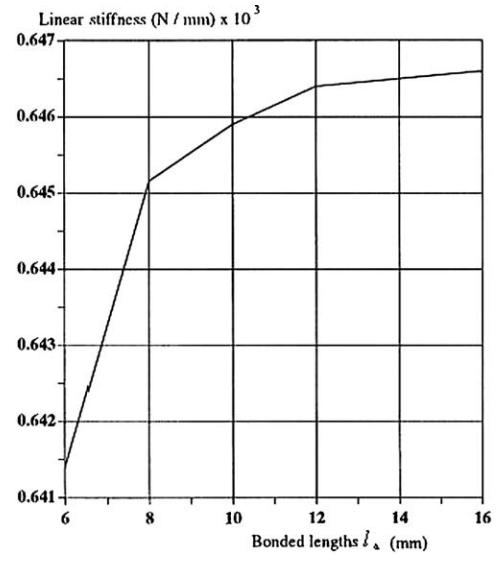

(a)

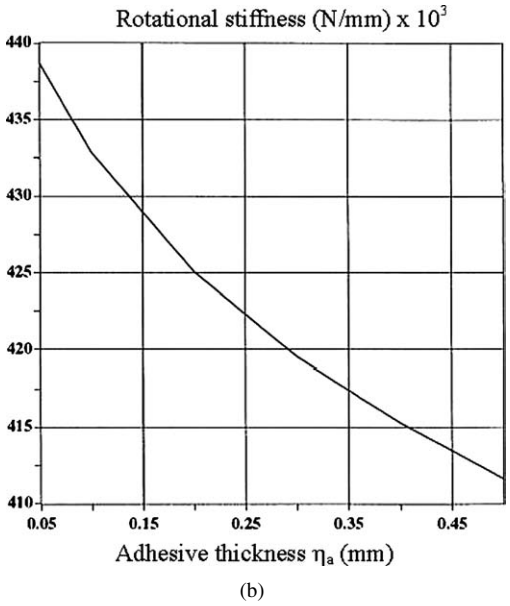

(b)

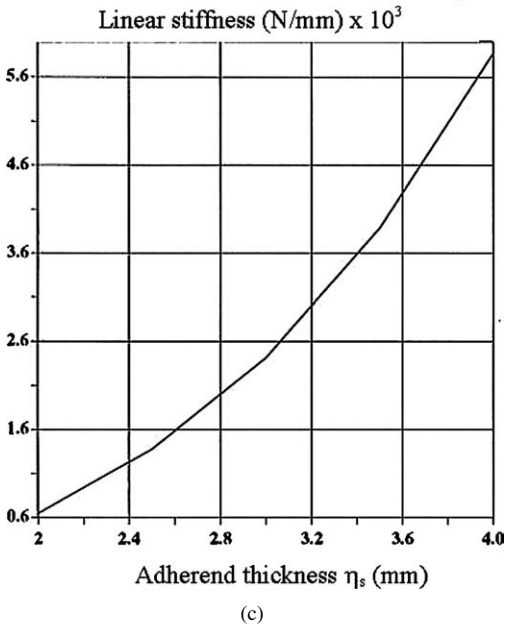

(c)

Figure 30 Effects of bonded length, and adhesive and adherend thicknesses on the stiffness of the T-joint [73]: (a) the linear stiffness versus bonded length, (b) the rotational stiffness (in the bending moment M) versus adhesive thickness, and (c) the linear stiffness (in the x-direction) versus adherend thickness.

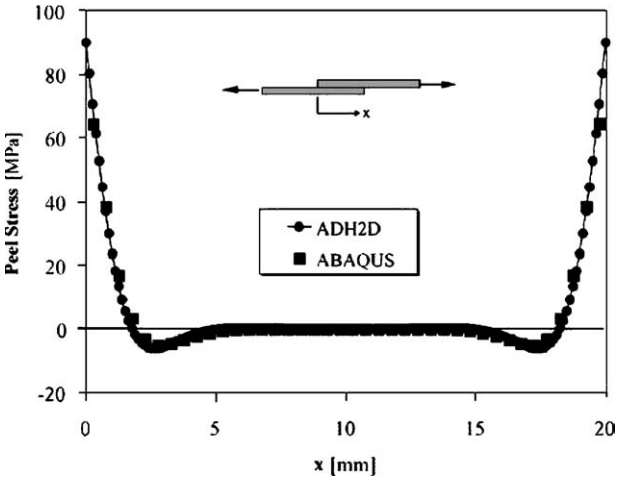

(a)

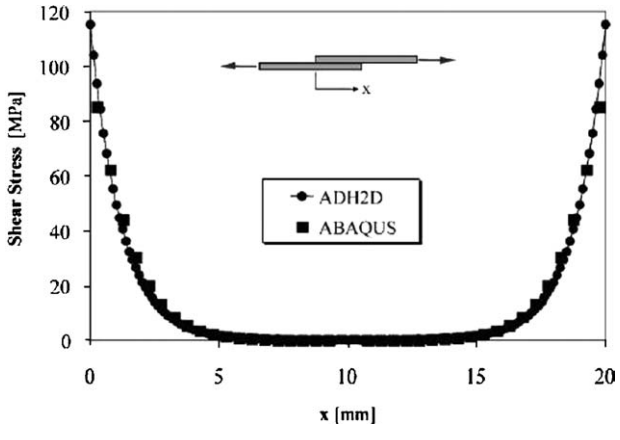

(b)

Figure 31 Stress distributions for a single lap joint with linear analysis [91]: (a) peel stress and (b) shear stress.

analysis with a ADH2D, and that they were compared with those from a finite element analysis with ABAQUS [ref. 194], using 2-D plane-stress finite elements (see Fig. 31a and b).

The same specimen was also analyzed with geometric nonlinearities. This time the whole structure was modeled, so the moments at the beginning of the overlap are no longer required. The specimen was subjected to different levels of load. σ_{av} is the average adherend stress, or the total load divided by the thickness and the width of the adherends. Fig. 32a and b show the effect of the nonlinearity in the peel and shear stress distributions. Also, these figures show that stress concentrations decrease as the load increases. This is the result of the reduction of the moment arm of the two eccentric loads as their magnitude increases [91]. There is a physical limit for that reduction of the moment arm, which is when the two loads are colinear. Therefore, it was suggested [91] that the change in the stress concentration between two load levels becomes less important as the load increases. The results for $\sigma_{av} = 400$ MPa from the ADH2D model are in good agreement with those from the ABAQUS [ref. 194] model as shown in Fig. 32a and b.

Li and Lee-Sullivan [46] have studied an adhesive joint with relatively thick adherends in tension under both plane strain and plane stress conditions using

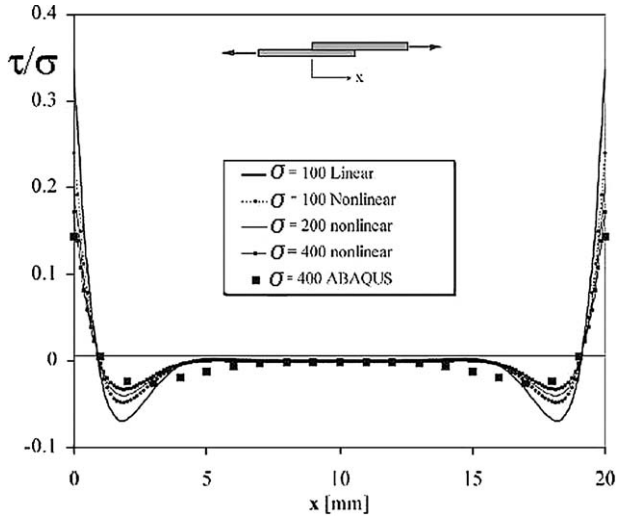

(a)

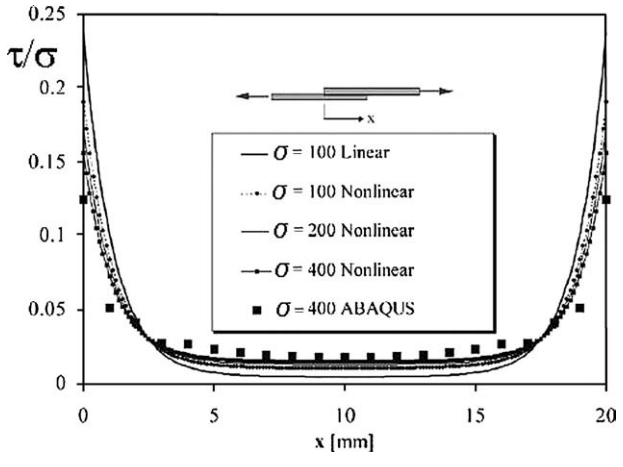

(b)

Figure 32 Stress distributions for a single lap joint [91]. Geometric non-linearities included. Dimensions of stresses are MPa: (a) peel stress and (b) shear stress.

2-D FEA method with the inclusion of a geometrically non-linearity. Furthermore, the additional influence of other factors, such as boundary conditions, overlap end geometries, and adhesive modulus, on the bending moment factor at the overlap edge, k, and adhesive stresses (see Equation 1 in Section 1.2) has also been investigated. The bending moment factor, k, relates the bending moment on the adherend at the end of the overlap to the in-plane loading (see Section 2.4 for more detail). In order to assess the accuracy of the FEM simulations, experimental testing which included measuring the strain distributions along the overlap region of the adherend was also performed. The strain variation between the upper and lower surfaces of the unbonded adherend section adjacent to the overlap was measured. In the FEM studies, filleted and unfilleted joints bonded using two different types of epoxy adhesives (i.e., rigid and flexible) were simulated. The higher modulus resin was referred to as the rigid adhesive [46]. The adherend material was aluminum 6061-T6. In this study, two different boundary conditions [i.e., as rotation (R) and no-rotation (NR)] and FEM meshes were used for both the filleted and unfilleted joints. In setting the rotation boundary condition, only concentrated force is applied

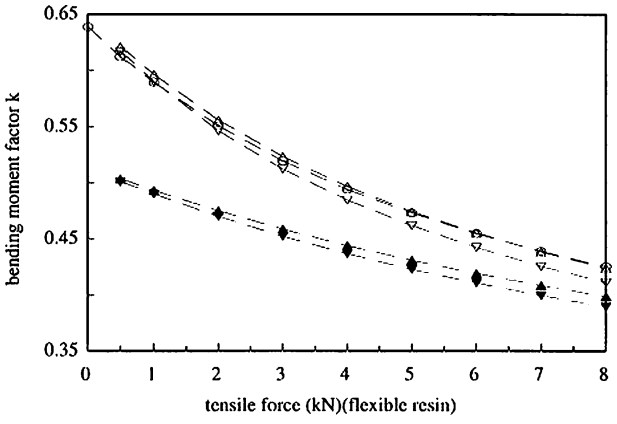

Figure 33 A comparison between FEM results and Oplinger's solution for bending moment factor (k_{op}) values for an unfilleted joint bonded with the flexible adhesive [46]: (○): Oplinger (plane strain), (▲): 2D plane strain FEM—No rotation, (▼): 2D plane stress FEM—No rotation, (△): 2D plane strain FEM—Rotation, and (▽): 2D plane stress FEM—Rotation.

at the center node at the right roller adherend end. Most of the analytical work [e.g. 72, 103, 104] applies boundary conditions which allow for rotation. In the present study for non-rotation boundary condition, the equivalent nodal load was applied to every surface node based on the iso-longitudinal strain condion, i.e., all the nodes at the unbounded adherend end have the same longitudinal strain, and the surface load or force can be determined. The corresponding nodal nodes can therefore be determined based on the equivalent principle of static forces from the finite element theory. Rotation is restricted by not allowing vertical deflection at the last two nodes along the adherend centerline.

Fig. 33 compares the FEM results on the variation in the bending moment factor, k, for unfilleted joints with the theoretical solution proposed by Oplinger (see Equation 10 in Section 2.3 for more details). As this figure shows, the 2D plane strain FEM simulations for rotation boundary conditions give the upper-bound values of k while plane stress and no-rotation boundary conditions give the lower-bound values. The Oplinger's solution [102] (see Equation 16) using plane strain condition agrees very closely with the k values predicted by both plane strain and plane stress FEM simulations for rotation boundary conditions. The good agreement should be expected since the analytical model implicitly assumes end rotation. These results suggest [46] that the boundary conditions at the adherend ends have a greater effect on k than the stress state of the joint, i.e., whether plane strain and stress conditions. However, for same boundary conditions, the plane strain condition would give slightly larger predictions of k than plane stress.

Fig. 34 compares the effect of fillets on the variation of k as obtained by FEM simulations. It is seen that the k values of the unfilleted joint results are slightly higher than those for the filleted joints under the same boundary conditions. Some of the difference is probably due to the slightly different planes of analysis chosen. It is seen in both Figs 33 and 34 that the k predictions between the filleted and unfilleted joints become increasingly closer with increasing tensile force. Additionally,

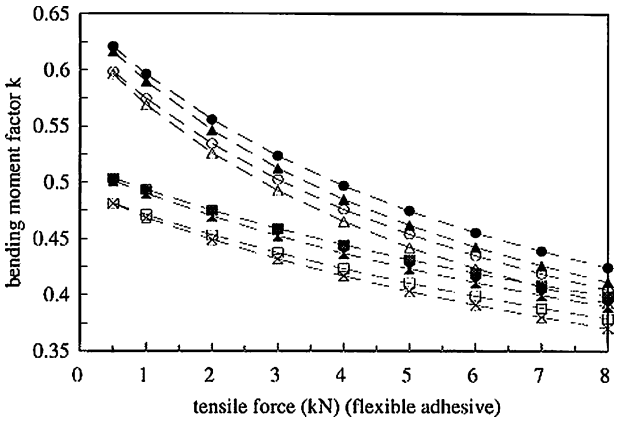

Figure 34 The variation of bending moment factor k as a function of the tensile force for the filleted and unfilleted joints with the flexible adhesive. *N* and *R* refer to no-rotation and rotation boundary conditions used in FEM simulations [46]: (○): plane strain FEM—R (with fillet), (△): plane stress FEM—R (with fillet), (⧖): plane stress FEM–N (with fillet), (●): plane strain FEM—R (no fillet), (▲): plane stress FEM—R (no fillet), (■): plane strain FEM—N (no fillet), and (⧗): plane stress FEM—N (no fillet).

the differences in predictions due to different boundary conditions, i.e., rotation and no-rotation, also decrease with increasing tensile force. It is expected that the predictions will ultimately converge at increasingly higher tensile forces [46].

Lang and Mallick [62] have investigated the bonded single-lap joints using the 2-D FEM method (in plane strain condition) under tensile loading by extending the work done by Mazumdar and Mallick [195, 196]. However, they produced the single-lap joints by removing portions of the adhesive from the interior of the overlap (i.e., recessed joints). The gap or recess in the recessed joint is centrally located in the overlap region. Full-rounded spew was selected as the spew shape, since it best represents the spew geometry [62]. The total lap length is defined as the length over which the two substrates are overlapped, while the effective or true lap length is the actual length over which the adhesive is used between the substrates. Note that the effective lap length decreases as the gap or recess in the adhesive is increased. In the limit, the effective lap length approaches zero when no adhesive is used in the overlap; spews are present at each end, which transfer the load from one substrate to the other.Both the adhesive and the substrate were assumed to behave as linear elastic materials. The loading and boundary conditions used simulate those encountered in a tensile test. The stress distributions at the adhesive mid-thickness and interface (i.e., at the interface between the adhesive and the substrate) were determined for joints with various levels of recessing, and compared to the stress distributions in continuous single-lap joints. In the Lang and Mallick's study, an approach similar to that of Crocombe *et al.* [191] was undertaken by considering stress values very close to the singularity point. By using an an extremely fine mesh around the singularity point, stress values as close as 0.04 mm away from the interface were obtained.

Lang and Mallick [62] first investigated the stresses at the adhesive mid-thickness and at the interface in a continuous single-lap joint in order to provide a baseline for comparing the stresses in recessed joints.The continuous joint had a lap length of 63.5 mm and a spew radius of 3.3 mm. This makes the total distance from the left spew (point O) to the right spew (point E) along the interface to be approximately 70 mm. The 2-D FEA of the continuous joint shows that the shear stress, peel stress and axial stress distribution at the adhesive mid-thickness is symmetric about the vertical centerline of the overlap. Across the mid-section of the overlap, the stresses are constant and have much lower values as compared to the peak stresses, which occur near spew surfaces. At the spew ends shear and axial stresses approach zero satisfying free edge boundary conditions, while peel stress decreases to a smaller non-zero value. Away from the adhesive mid-thickness the stress distributions are highly non-symmetric and the maximum stress values are highly non-symmetric and the maximum stress values are much larger at the interface than at the mid-thickness [62]. The stresses along the interface have approximately the same magnitude as the stresses at the adhesive mid-thickness. However, at the loaded end of the spew, steep stress gradients along the inteface appear with stresses approaching extremely high values at the interface corner. At the unloaded end, the stresses are much smaller and are not of much concern. As an example, Fig. 35a shows the peel variation against the distance along the overlap including spews for a continuous single-lap joint.

The stress distributions for shear, peel and axial stresses at the adhesive mid-thickness for a recessed joint with an effective lap length of 25.4 mm are shown in Fig. 35b. As this figure shows, the stress distributions at the mid-thickness are the same on each side of the recess, and near the lap ends they are similar to those observed at the adhesive midd-thickness of the continuous joint (see Fig. 35a). For instance, all three stresses show maximum values close to the spew ends and immediately reduce to lower values away from the spew as the mid-section of the overlap is approached. However, near the ends of the recess, steep stress gradients appear for shear, peel and aqxial stresses. The shear stress near the recess end increases to 50% of the peak stress and then decreases to zero at the free edge of the recess. The peel stress has a steep compressive value, while the axial stress decreases to zero from the interior of the overlap to the free edge of the recess.

Lang and Mallick (1999) [62] have also investigated the effect of recessing on maximum stresses, as shown in Fig. 35c. This figure displays the stress distribution of shear, peel, and axial stresses along the interface for various effective lap lengths. As can be seen in this figure the peak stresses at the loaded end, near the interface corner, do not increase significantly as the effective lap length decreases. This is seen more clearly in Fig. 35d, which depicts the variation of shear, peel and axial stresses found at the interface corner (point E) as the effective lap length is reduced. Fig. 35d shows that all three stresses stay constant, and increase only slightly as the zero effective lap length is reached. One should note that the stresses used in Fig. 35d were taken at the interface corner, which is a singularity point. Therefore,

to avoid portraying unrealistically high stress values, interface stresses one and two nodes away from the singularity point were determined [62].

7.2.2. Geometrically linear and non-linear analysis in 3-D finite element method

Andruet *et al.* [91] have also studied the single lap joint specimen using the 3-dimensional version of the adhesive finite element (ADH3D) (see Section 6 for the basis of this analysis). The model of the adhesively bonded joint has two main components: The adhesive layer and the adherends. These components are combined in a sandwich-type configuration as shown in Fig. 26b. Even though symmetry conditions could be used, the whole structure was modeled, including the two lateral shells, to avoid any kind of assumption or simplification in the model. The thickness of the adherends is 1.6 mm, the adhesive layer thickness is 0.102 mm, and the specimen's width is 25.4 mm. The aluminum adherends and epoxy adhesive layer were used in this study. In this work, the finite element model of the single lap joint was taken to be composed of 1190 nodes and 252 elements. The mesh is finer in the overlap than in the lateral shells. Since the most important effects occur at the overlap ends, refinement of the mesh in this region would improve the accuracy of the model.

Peel stress distributions at the mid-plane of the overlap region are shown in Fig. 36. 3-D effects can be observed; specifically, the peel stresses are largest at

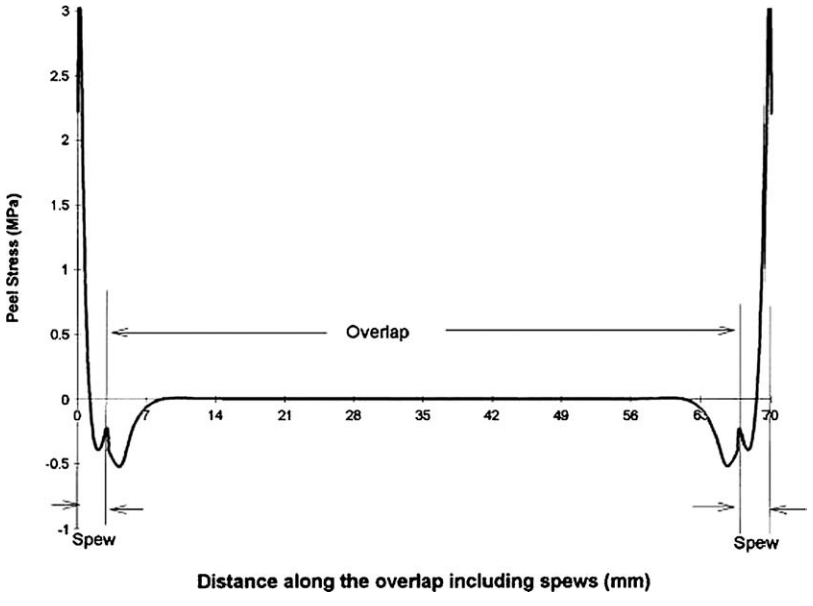

(a)

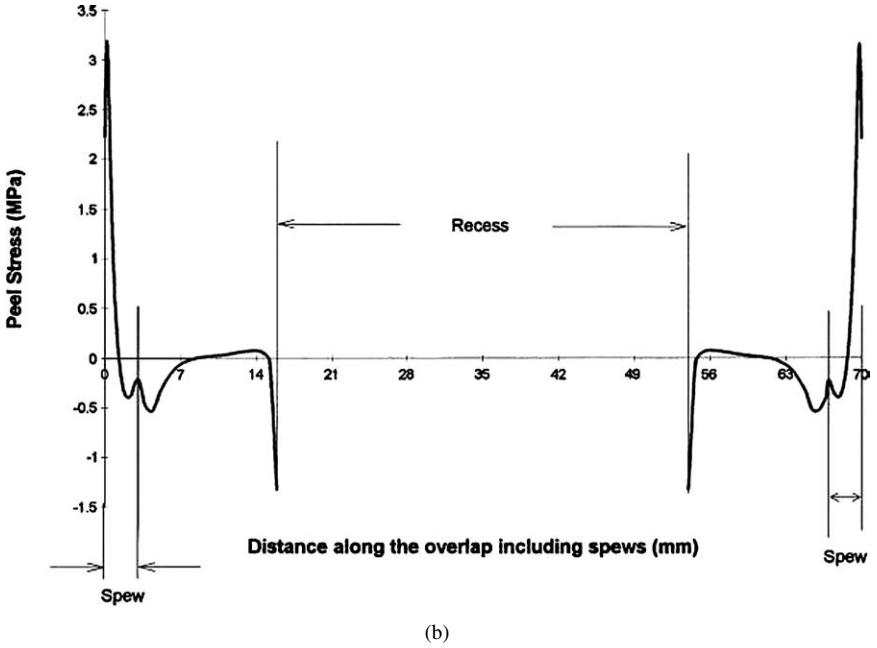

(b)

Figure 35 Peel (σ_{yy}), shear (τ_{xy}), and axial (σ_{xx}) stresses for continuous and recessed (including spews) single-lap joint [62]. Load = 6.90 MPa; Adhesive thickness = 0.762 mm; (Total) lap length = 63.5 mm: (a) variation of peel (σ_{yy}) stress against the distance along the overlap including spews for a continuous single-lap joint at the adhesive mid-thickness. (b) Peel stress (σ_{yy}) variation for recessed single-lap joint at the adhesive mid-thickness. Effective lap length = 25.4 mm. (c) Shear stress (τ_{xy}) variation at the interface for a single-lap joint with various lap lengths. (d) Variation of shear (τ_{xy}), peel (σ_{yy}), and axial (σ_{xx}) stresses at the interface corner as the effective lap length is reduced. (*Continued*)

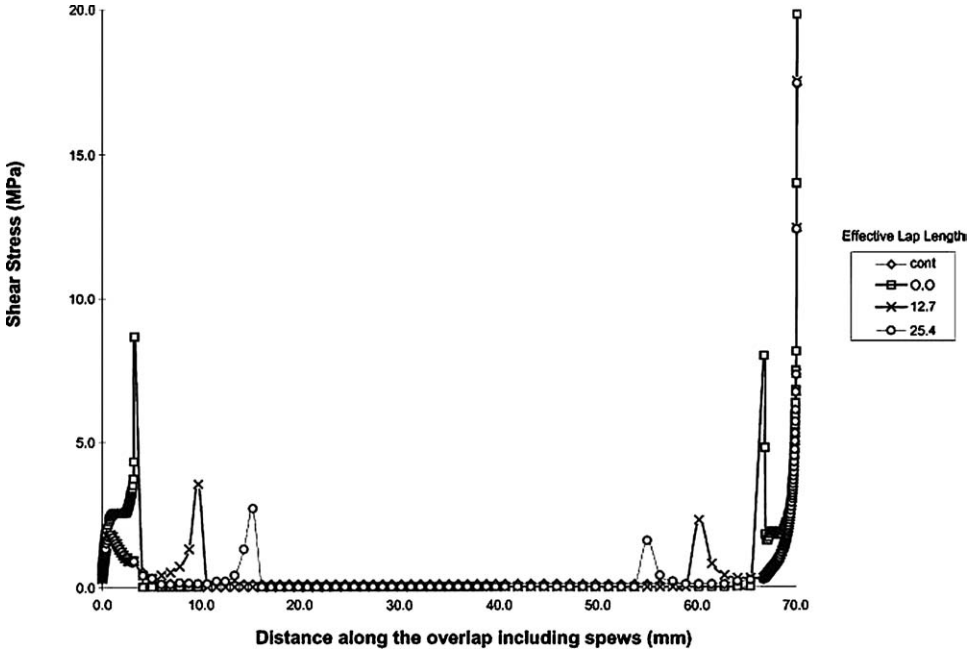

(c)

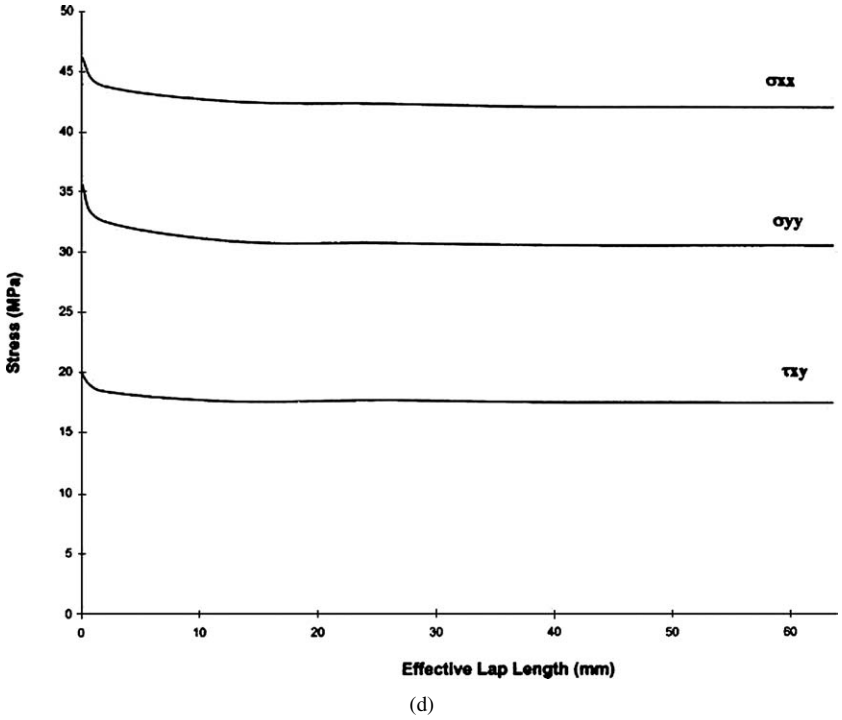

(d)

Figure 35 (*Continued*).

the center of the joint and decrease at the edges. This behavior is in qualitative agreement with experimental results of Adams *et al.* [197]. This is due to the Poisson effects and the anti-elastic bending of the adherends. The shear stress distribution in the yz direction (τ_{yz}) shows strong stress concentrations at the two corners in the free edge of the overlap, but the maximum absolute values are on the order of the maximum values of the other components of the stress tensor [91]. This stress distribution clearly shows 3-D effects.

To optimize the adhesive lap joints, Belingardi *et al.* [61] have investigated the effects played by the joint geometry, namely the spews (see Fig. 12d) (i.e., shoulders of adhesive connecting the unloaded ends of the adherends) and of chamfers (see Fig. 12e) at the ends of the adherends, on the stress field of a steel/fiber-reinforced plastic single-lap joints in order to optimise the design, identifying the geometrical configuration that minimizes the stress peaks. The study has been performed numerically, by means of the 3-D FEA method, assuming plane strain and linear elastic behaviors of all the joint components. The latter limiting assumption was justified by the argument that, even if it is well known that the ultimate strength of the joint largely depends on non-linear phenomena (e.g., large rotation, plasticity), the reduction of the elastic stress peaks is often beneficial in case of low ductility and essential in case of fatigue loading [61].The plates used as adherends are made of different materials, namely a steel for plate 1 (i.e., adherend 1) and fiber-reinforced

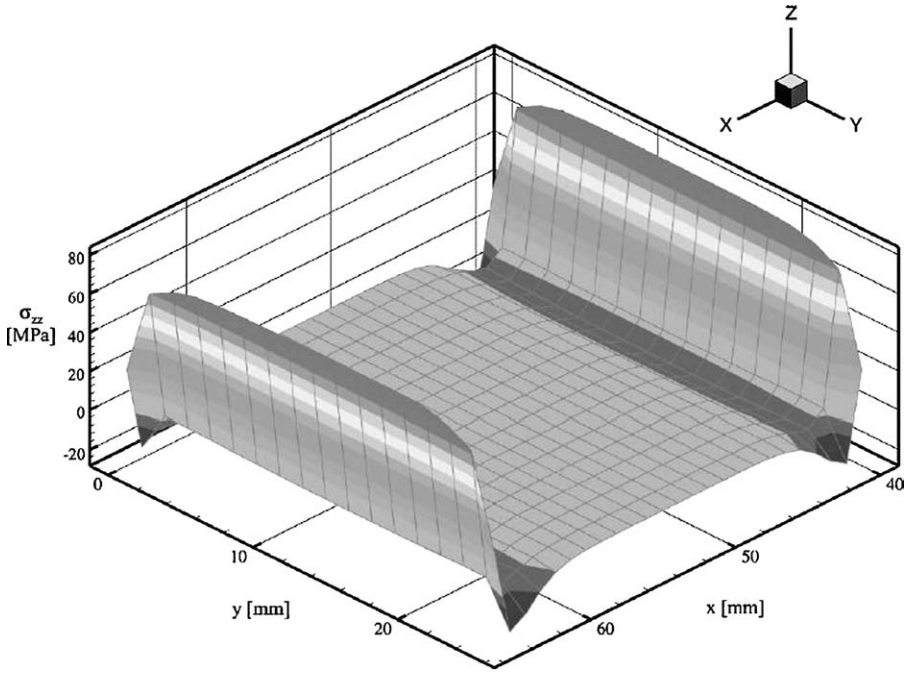

Figure 36 Distribution of peel stresses (σ_{yy}) in the midplane of the adhesive layer of the single lap joint [91].

plastics for plate 2 (i.e., adherend 2), and have different thickness. The adhesive is an epoxy resin. The tensile load applied to the joint corresponds to 10 MPa in the steel plate. The four-noded element type 42 has been used for all zones. The total number of finite elements is about 10.000, the adhesive layer contains six elements along its thickness (0.1 mm). For comparison, mainly to assess whether the level of mesh refinement was enough to give correct results, also the simplified solution of Bigwood and Crocombe [97] has been calculated in this case. In order to accomplish this, Belingardi *et al.* [61] have used the following two equations:

$$\frac{d^4\sigma_y}{dx^4} + 4K_5^4\sigma_y = 0 \tag{39}$$

$$\frac{d^3\tau_{xy}}{dx^3} - K_6^2\tau_{xy} = 0 \tag{40}$$

where σ_{yy} and τ_{xy} are the peel (i.e., σ_a) and shear stress (i.e., τ_a) components, K_5 and K_6 are constants related to the material properties and to the thickness values. Equations 39 and 40 hold exactly if the adherends are identical, in the present case they are reasonably approximate since the stiffness values of the adherends are not too different. In order to differentiate the effects of fillet and spew on the adhesive joints, peel and shear stresses were also evaluted for the basic configuration of the single lap joint. Fig. 37 shows the behavior of the peel and shear stresses in the continuous single-lap joints. The stress fields were shown on two levels: (a) the interface between steel and adhesive, (b) the interface between adhesive and composite. In general terms, the stress field is affected by the typical peaks at the ends of the overlap zone, both for the peel and for the shear stresses. On each interface (adhesive-steel, adhesive-composite) the highest peak occurs at the overlap end corresponding to the loaded adherend. This is particularly true for the peel stress.

Starting from the basic configuration, both solutions in which a fillet made of adhesive covers the end of the adhesive layer only (see Fig. 12f), and solutions in which a spew made of adhesive covers the end of the adhesive layer and of the adherend (see Fig. 12d) have

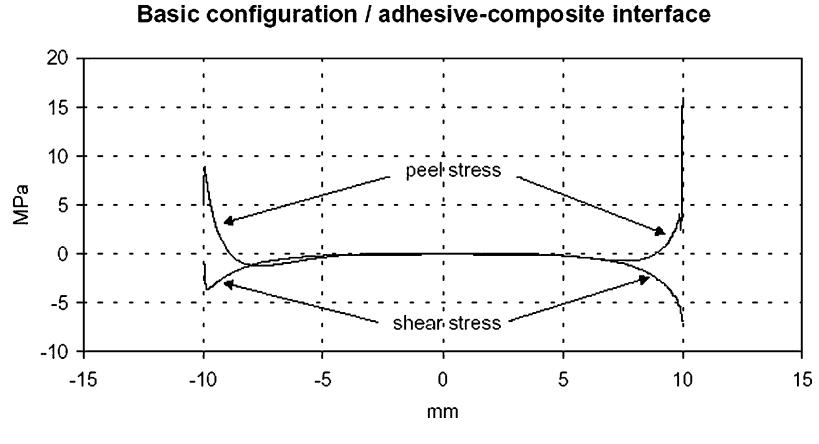

Figure 37 Basic configuration [61]: peel and shear stresses in the joint and comparison with the simplified theoretical solution.

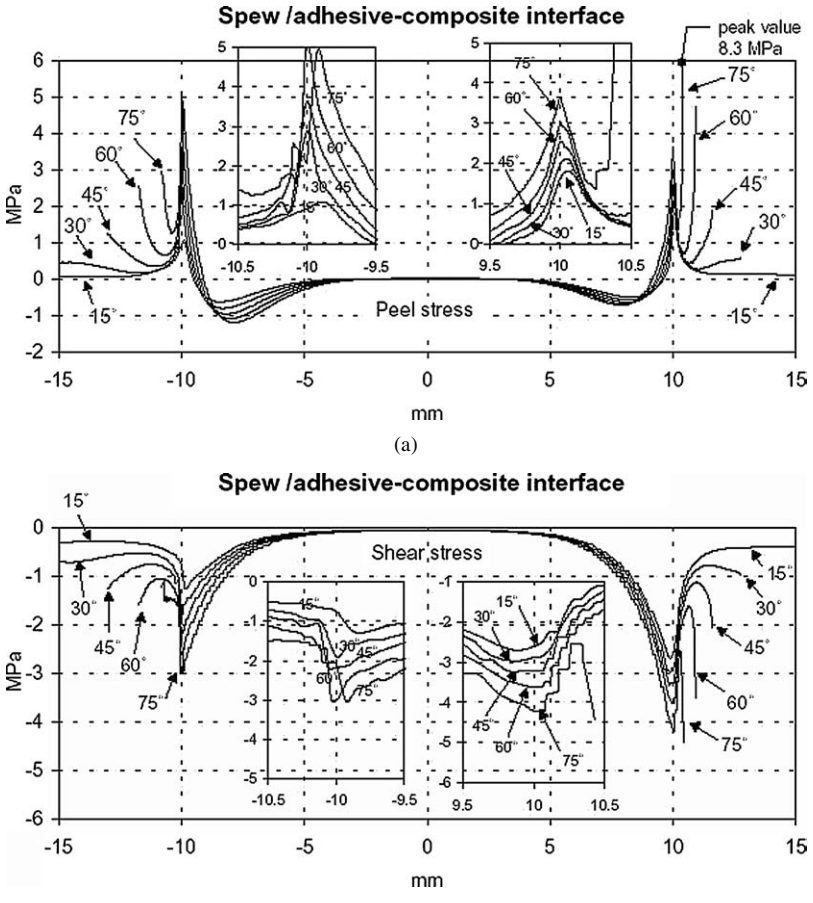

Figure 38 Effects of spew on the peel and shear stresses along the adhesive-composite interface [61]: (a) peel stress and (b) shear stress.

been analyzed similarly to [157, 159, 198]. Belingardi *et al.* [61] first focused on the spew case, to identify the spew angle α that minimizes the stress peaks.

Fig. 38a and b show the effects of spew on the peel and shear stresses along the adhesive-composite interface, As seen in this figure, the effect of the adhesive spew on the stress field can be appreciated. In general terms, the amplitude of the stresses with α under high values of α the additional stress peaks that occur at the ends of the spews can even exceed the peaks occurring at the ends of the overlap, when α is lower such additional stress peaks tends to disappear. Nevertheless, the dependence of the stress on the spew angle α is fairly complicated [61]; Belingardi *et al.* [61] have summarized the effects of spew angle α on the peel and shear stresses: (a) considering the peel component on the adhesive-steel interface, the highest stress peaks always appear (except for the case 15°) at the left overlap end or at the left spew end, i.e., at the loaded end, as in the basic configuration (see Fig. 37 for comparison); b) conversely, for the peel component on the adhesive-composite interface the highest stress peaks (see Fig. 38a) usually appear (except for the case 15°) at the unloaded end, that is, again at the left end; only in the case 75° the right spew end causes the highest peak; (c) as far as the shear component is concerned, on three interfaces the highest peaks appear always at the right end. It can be noticed [126] that, with respect to the basic configuration (see Fig. 37), the stress reduction due to the spew is more pronounced for the peel than for the shear component, being about five times for the peel stress and two times for the shear stress (see Fig. 38). As a synthetic rule, it can be concluded that for α equal to 45° the stress is well reduced and the additional peaks at the ends of the spew do not exceed those at the ends of the overlap.

In order to further reduce the stress peaks, an improvement that has been tested in addition to the spew, Belingardi *et al.* [61] have also considered the chamfering in the the unloaded ends of the adherends on the inner side, as shown in Fig. 12e. This idea, yet considered in [157], was here further developed by Belingardi *et al.* [61] to find the best configuration. For the sake of simplicity, the same angle value was adopted both for the spew and for the chamfer, the latter concerns two-thirds of the thickness, whilst the remaining third is square. Fig. 39a and b show the effects of the chamfer and of the spew on the peel and shear stresses along the adhesive-composite interface, respectively. As seen in these figures, each peak is shifted inwards, at the location where the chamfer starts. For the shear component on the adhesive-composite interface (see Fig. 39b) the highest peaks always appear at the right spew end (α high) or right overlap (α low). The highest peaks in peel component appear at the left spew end on the adhesive-steel interface [61], and at the right spew end on the adhesive-composite interface (see Fig. 39b), that is, they are always at the loaded end (for low-angle values the peaks tend to be equal and very small). With respect to the case of spew only it can be concluded

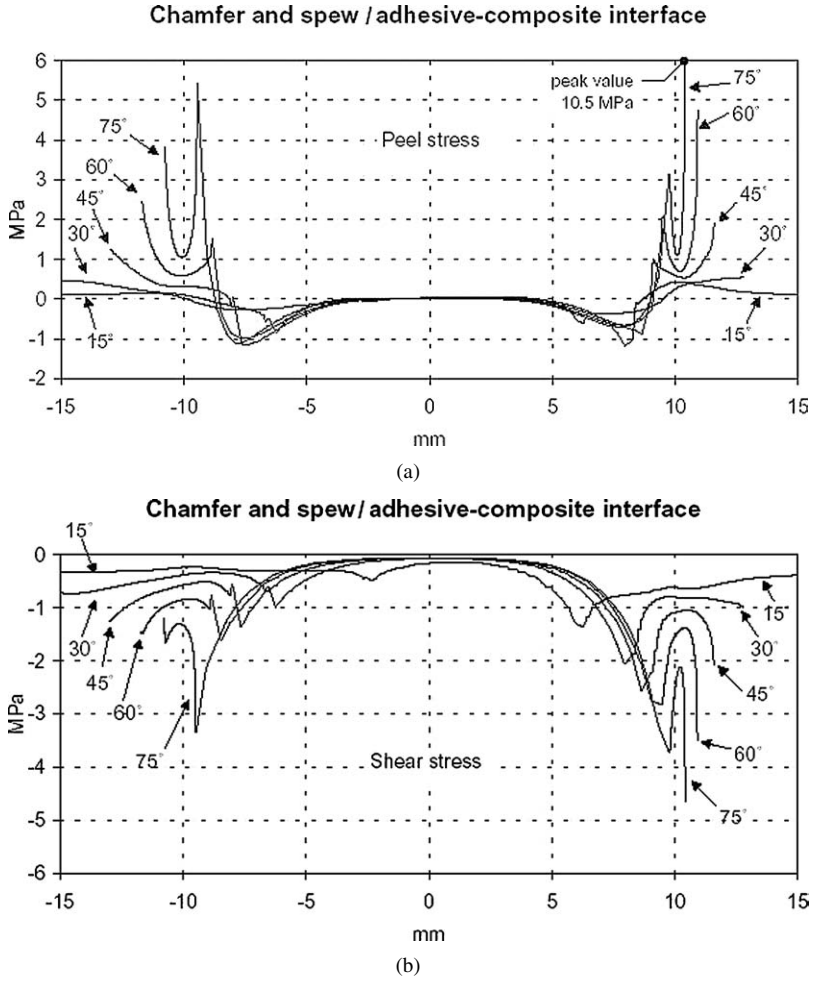

Figure 39 Effect of the chamfer and of the spew on the peel and shear stresses along the Adhesive-composite interface [61]: (a) peel stress and (b) shear stress.

[61] that: (a) the stresses are, in general, lower; (b) when the angle α assumes values below 45° the peaks of the peel stress occurring at the ends of the spews tend to zero and those at the ends of the overlap even disappear. The latter result is of considerable relevance, since these stress peaks are the most harmful for the joint.

Gonçalves *et al.* [92] have investigated a new model for 3-D FEA of adhesive joints considering geometric and material nonlinearities and used solid brick elements as well as specially developed interface elements using a single-lap joint (see Section 6.1.2 for the description of this new FEA method). They used the following two different analyses approches for both the adhesive and adherends in this model: (a) linear elastic, and (b) elasto-plastic material models. Geometric nonlinearity was considered in all analyses. Gonçalves *et al.* [199, 200] have previously developd an interface FEA model for 3-D analysis. It consists of 18 nodes distributed in two faces. Contrary to continuum elements where stress-strain relationships are used, interface elements are governed by stress-relative displacements relationships [92]. The main objective of this work was to calculate the stresses at the interfaces between adherends and adhesive, which are considered critical regions in these structures [92].

Using the linear-elastic materials model, the stress distributions at the middle of the adhesive thickness were evaluated for the various normalized stresses including σ_{xx}, σ_{yy}, σ_{zz}, τ_{xy}, τ_{xz}, and τ_{yz}. Fig. 40a depicts the stress distributions for the normalized stresses σ_{xx}, τ_{xy}, τ_{xz}, where each graph in this figure represents the longitudinal distribution of a normalized stress component along the overlap length in several longitudinal planes. The average shear stress at the adhesive (τ_{av}) was used to normalize the stress components. In Fig. 40a, the σ_{xx} normal stress component is plotted. Its maximum value occurs close to the ends of the overlap, at the longitudinal plane that is nearest to the symmetry plane ($z = 0.176$ mm). The σ_{xx} distribution is almost constant across the joint width but decreases significantly near the edge ($z = 12.324$ mm). That effect is also verified for the σ_{yy}, and σ_{zz} components. The σ_{yy} stresses at the ends of the overlap and in the plane closer to the longididunal symmetry plane are higher than the other stress components. The σ_{yy}, and σ_{zz} stresses are of the same order of magnitude. Fig. 40b shows the distribution of the shear stress τ_{xy} . This stress distribution does not change significantly across the joint width, which means that this stress component is less sensitive to the 3-D effects. Whereas the stress τ_{xz} is zero at the longitudinal symmetry plane. For other planes, there are peaks near the ends of the overlap. These peaks are increasingly higher for longitudinal planes closer to the joint edges. The stress τ_{yz} is also zero at the longitudinal symmetry plane and the peak increases with the z

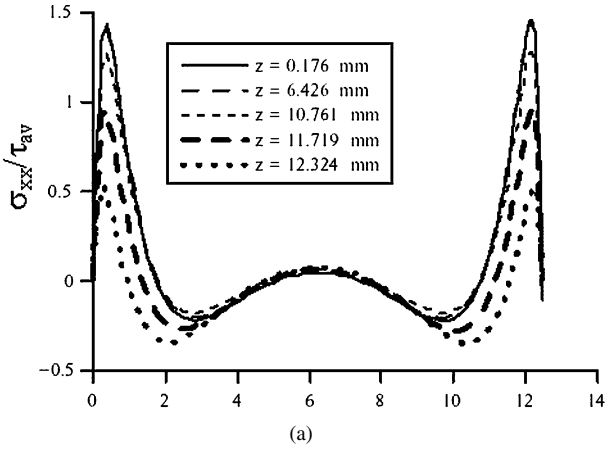

(a)

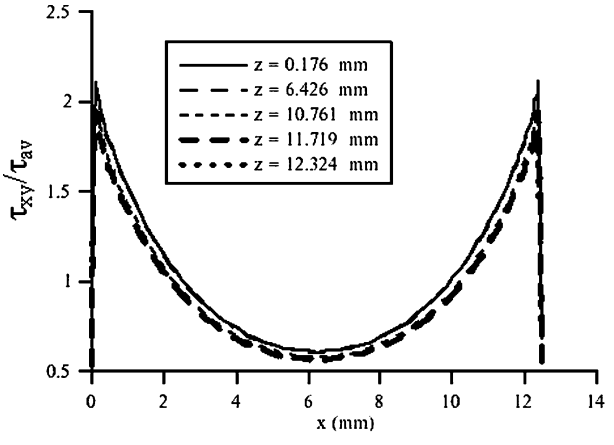

(b)

Figure 40 The longitudinal distribution of a normalized stress component along the overlap length in several longitudinal planes at the middle of the adhesive thickness using the linear elastic material [92]: (a) normalized stress (σ_{xx}) and (b) Normalized stress τ_{xy}.

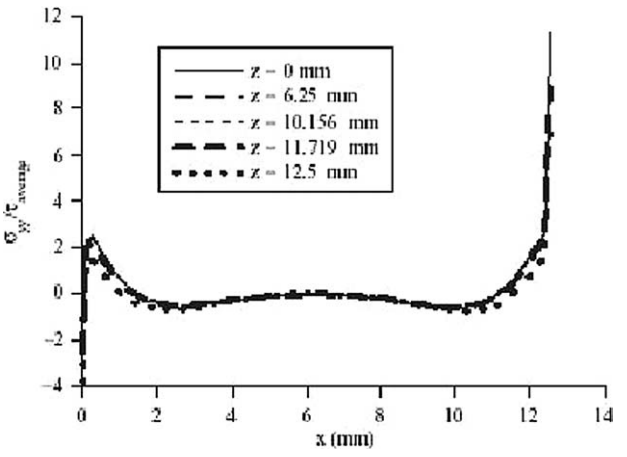

(a)

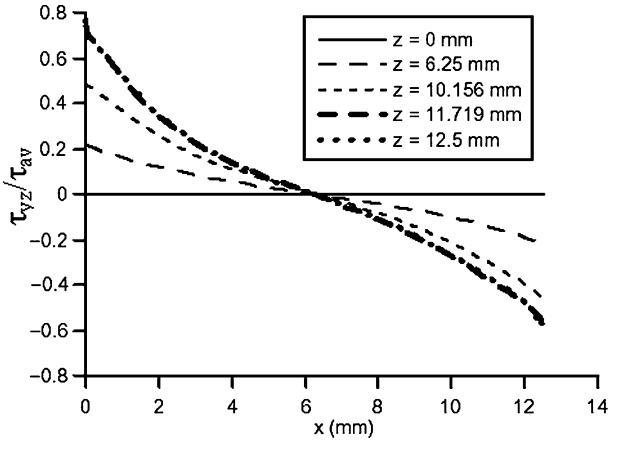

(b)

Figure 41 Distribution of normalized stresses at the interface using the linear-elastic material [92]: (a) normalized stress σ_{yy} ($y = 0.125$ mm) and (b) normalized stress τ_{yz} ($y = 0.125$ mm).

coordinate. It should be noted that the 3-D effect for the two last stress components (i.e., τ_{xz} and τ_{yz}) is present across all the joint's width. This is contrary to what happens with the normal stress components where the 3-D effect is only present near the edges.

Gonçalves *et al.* [92] have also studied the stresses at the interfaces for linear elastic materials (see Fig. 41a and b). It should be noted that the stresses were plotted along the longitudinal planes that are different from the ones in Fig. 40. As can be seen in Fig. 41 the peak stresses at the interfaces are much higher than at the middle of the adhesive layer (see Fig. 40). This explains why the interfaces are critical regions regarding adhesive joints failure [92]. As observed for the normal stress components in the middle of the adhesive layer, the normal stress σ_{yy} at the interface is almost constant across the joint width, but decreases near the edges. In Fig. 41a it can be seen that the maximum stress σ_{yy} occurs at the end of the overlap and at the symmetry plane ($z = 0$ mm). The shear stress τ_{xy} has a similar behavior. It must be noted that these two stress components have peak values that are much higher than the ones in the middle of the adhesive layer. The shear stress τ_{yz} at the interface (see Fig. 41b) and in the middle of the adhesive layers have similar distributions.

Gonçalves *et al.* [92] have also performed a material and geometric nonlinear FEA using the elasto-plastic materials' behavior.The von Mises yield criterion and Raghava *et al.* [201] parabolic criteria were used for the adherends and adhesive, respectively. In the Raghava *et al.* criterion a ratio of 1.3 between the compression and tensile strengths was assumed. From this analysis, the maximum normalized stresses σ_{yy} and τ_{xy} at the upper interface ($y = 0.125$ mm) for different load levels were determined, and are presented in Fig. 42. It can be stated that the peak normalized stresses decrease as the

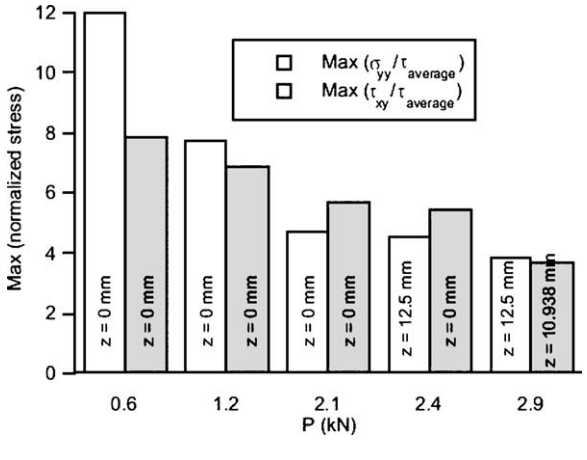

Figure 42 Change of the maximum values of normalized stresses σ_{yy} and τ_{xy} at the interface using the elasto-plastic material behavior [92].

applied load increases. Also, for the higher load levels the peak normalized stresses shift from the symmetry plane to the free edge.

8. Mechanical joint analysis using the experimental methods

8.1. Peel and shear stresses, yielding behavior and bending under static loading

Li and Lee-Sullivan [46] have studied adhesive stresses (i.e., peel and shear) and compared them with the FEA results. The adhesive peel and shear stress distributions along the centerline of the bond layer using Equation 1 in Section 1.2 are shown in Fig. 43a and b for tensile loads up to 5 kN for the filleted and unfilleted rigid joints, respectively. Li and Lee-Sullivan [46] concluded from these plots that: (a) for the same boundary conditions, plane strain and plane stress FEM simulations give quite similar adhesive stress didtributions; (b) adhesive stresses are not significantly affected by the nature of the adherend end boundary conditions, i.e., rotation or no-rotation boundary conditions; (c) the peel and shear stresses are influenced by the modulus of the bonding adhesive-the stiffer adhesive, the higher the stresses; (d) the analytical solution for peel stresses agrees quite well with FEM simulations but is higher for shear stresses; (e) the main effect of having fillets is the decrease in the adhesive maximum peel stresses while the maximum shear stresses slightly increase.

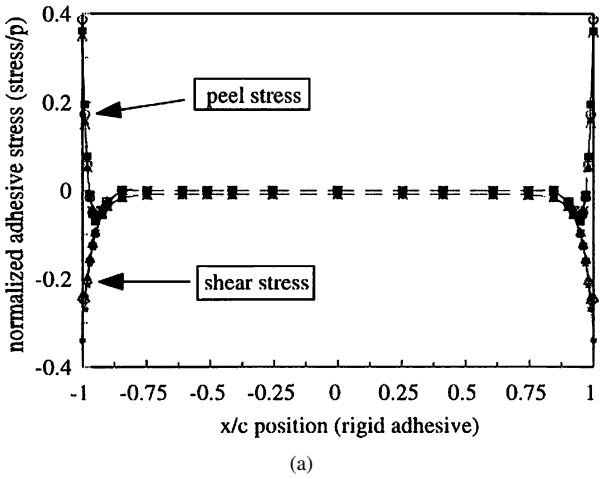

(a)

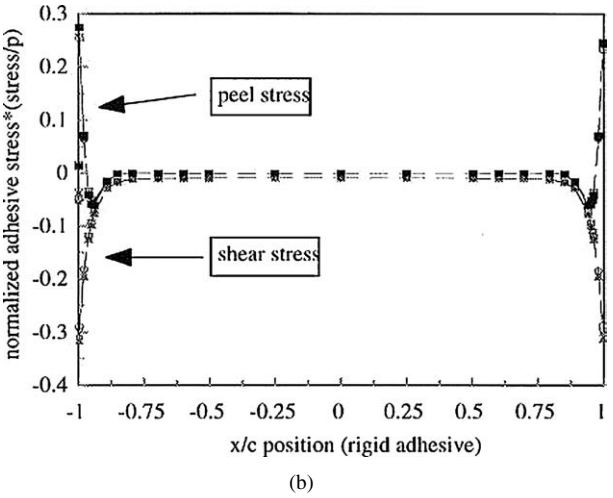

(b)

Figure 43 The variation of adhesive stresses along the bond centerline when the applied load is 5 kN for [46]. (a) The unfilleted rigid joint: (■): Oplinger, (▲): plane-strain FEM—No-rotation, (△): plane-stress—No-rotation, (○): plane strain FEM—Rotation, and (▽): plane stress FEM—Rotation. (b) The filleted ridid joint: (■): Plane strain FEM—Rotation, (▲): Plane stress FEM—Rotation, (○): Plane strain FEM—No-rotation, and (▽): Plane stress FEM—No-rotation.

Wang and Chalkley [14] have studied experimentally the plastic yielding behavior of a rubber-toughened film adhesive (FM73) (i.e., widely employed in the aerospace industries) subjected to triaxial stresses. The adherends used were made of Aluminum alloy 2024-T3. The specimen used to evaluate the yield behavior in the presence of combined stresses is the modified Iosipescu specimen [202, 203]. Note that Iosipescu specimens were originally designed for use with fiber composite materials. Experiments were conducted under various combination of tension, compression and shear-loading to determine the yield locus of the film adhesive over the full range of hydrostatic stress. The Iosipescu specimen was modified by Broughton [202] to allow a compressive load P_β to be applied at an angle β to the longitudinal axis of the bondline. A biaxial stress state subsequently develops in the adhesive bondline with the stresses σ_x and τ_{xy} being given by, referring to Fig. 44 for coordinate and notations.

$$\sigma_x = \frac{-P_\beta \sin(\beta)}{S_b} \tag{41}$$

$$\tau_{xy} = \frac{-P_{\beta\alpha} \cos(\beta)}{S_b} \tag{42}$$

where P_β is the compressive load, S_b denotes the bondline area, σ_x is the through-thickness tensile stress and τ_{xy} the shear stress.

Using the experimental results, the applicability of several yield criteria (i.e., the modified von Mises yield criterion [15, 16], the modified Tresca yield criterion [15, 16] and the Druker-Prager criterion [16, 17]) commonly employed to characterize neat adhesives was first critically assessed. However, according to Wang and Chalkley [14], these three yield criteria suffered the same deficiency: Over-predicting the beneficial effect of compressive hydrostatic stress. To overcome this difficulty, Wang and Chalkley have adopted the following modified Drucker-Prager/Cap plasticity model [14, 194], developed mainly for determining the

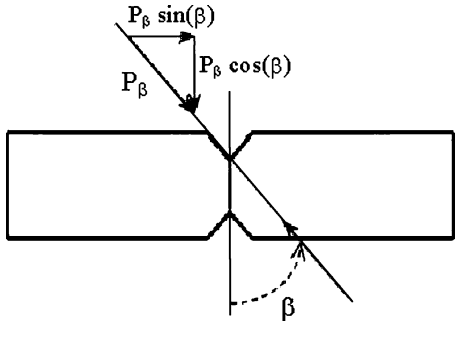

Figure 44 The modified Iosipescu specimen under combined loading [14].

pressure dependent yield failure of cohesive geological materials, to model the pressure-sensitive yielding behavior of adhesives. There are three parts to this model: (a) The first part uses the Drucker-Prager model [14, 16, 17] to describe the yield surface corresponding to predominantly shearing behavior. (b) The second part is a transition yield surface that has a constant radius in the meridonial plane, ensuring the continuity of the overall yield locus. (c) The third part is a "cap" yield surface which has an elliptical shape with constant eccentricity in the meridonial plane and also includes dependence on the third stress invariant, through the deviatoric stress σ_d in the deviatoric plane. Therefore, the yield surface consists of three surfaces given by

$$F_s = 0 \tag{43}$$

$$F_t = 0 \tag{44}$$

$$F_e = 0 \tag{45}$$

where F_s, F_t and F_e are

$$F_s = \sigma_d - p\tan\Phi - \sigma_c = 0 \tag{46}$$

$$F_t = \sqrt{(p - p_a)^2 + \left[t - \frac{\cos\Phi - a}{\cos\Phi}(\sigma_c + p_a\tan\Phi)\right]^2} - \beta[\sigma_c + p_a\tan(\Phi)] \tag{47}$$

$$F_e = \sqrt{(p - p_a)^2 + \left[\frac{\Lambda\sigma_d}{1 + \beta - \beta/\cos(\Phi)}\right]^2} - \Lambda[\sigma_c + p_a\tan(\Phi)] \tag{48}$$

where

$$\sigma_d = \frac{q}{2}\left[1 + \frac{1}{Y} - \left(1 - \frac{1}{Y}\right)\left(\frac{r}{q}\right)^3\right] \tag{49}$$

$$q = \sqrt{3J_2} \tag{50}$$

$$r^3 = \frac{27}{2} = \frac{(2\sigma_1 + \sigma_2 + \sigma_3)(2\sigma_2 + \sigma_3 + \sigma_1)(2\sigma_3 + \sigma_1 + \sigma_2)}{2} \tag{51}$$

where σ_1 and σ_3 are the maximum and minimum principal stresses.

$$\sigma_c = \left(1 - \frac{1}{3}\tan\Phi\right)\sigma_e^o \tag{52}$$

Here q is the von Mises equivalent stress and r is the third invariant of the deviatoric stress. The use of the deviatoric stress measure σ_d is to allow the model to match different yield-stress values in tension and compression in the deviatoric plane. The constant Φ is the material angle of friction, σ_c is the material cohesion stress, and the parameter Y controls the shape of the yield surface in the deviatoric plane. The value of Y is equal to the ratio of the flow stress in triaxial tension to the flow stress in triaxial compression. For example, Y and Φ can be expressed in terms of the ratio of uniaxial compressive yield stress to uniaxial tensile yield stress $\vartheta(\vartheta = \sigma_e^o/\sigma_i^o$, see Chiang and Chai [17],

$$Y = \frac{2 + \vartheta}{2\vartheta + 1} \tag{53}$$

$$\tan\Phi = \frac{3(\vartheta - 1)}{\vartheta + 2} \tag{54}$$

In the present case, since $\vartheta \approx 1.64$, we have $Y = 0.85$ and $\Phi = 27.8^\circ$. This friction angle β is significantly lower than what the experimental results suggest [14]. This is primarily due to the error in assuming the yield points corresponding to the uniaxial tension and uniaxial compression would lie on the same straight line. The present experimental results clearly demonstrate that this is not the case for the structural adhesive being considered [14].

The parameters β and Λ control respectively the radius of the transition yield surface and the cap eccentricity. Generally parameter β is a small number, with values typically between 0.01, and 0.05, where the value of Λ must be greater than 0 and is generally less than 1.0. The transition surface is a less important segment of the yield locus. It was developed in order to create a smooth transition between the shear failure surface and the cap surface, but is not significant in the initial stages of fitting the yield function to the experimental results, as seen in Fig. 45.

As can be seen from Equations 46, 47 and 48 there are total of six material constants that need to be identified to fully specify the entire yield envelope: Y, Φ, σ_c, β, Λ, p_a. In the present study, the parameter Y is set to be 0.778. Then by inspecting the shape of the yield contour, the parameters Φ and σ_c can be obtained by curve fitting the experimental data corresponding negative hydrostatic pressure [14]. The remaining three constants can be determined by curve fitting the experimental data

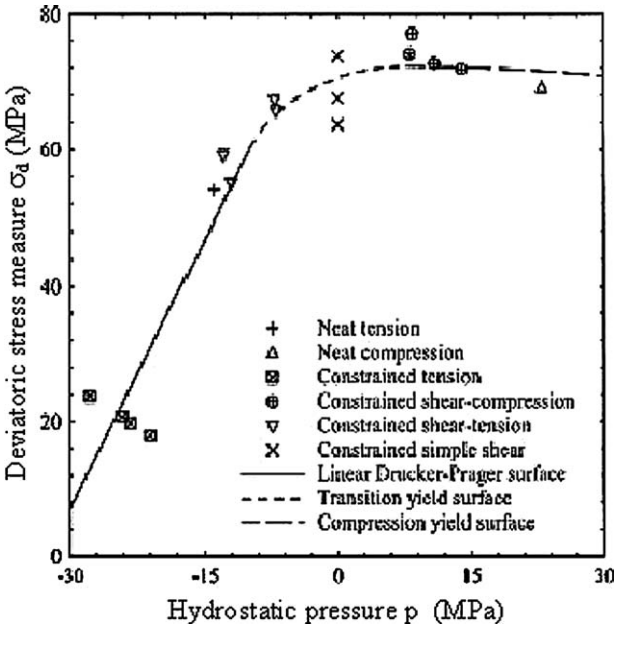

Figure 45 Modified Drucker-Prager curve fit [14].

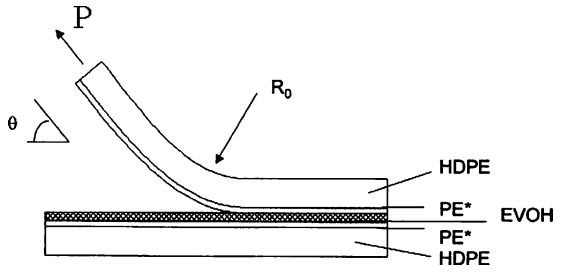

Figure 46 Peel geometry in which the peel arm corresponds to HDPE/PE* with separation occurring at the EVOH/PE* interface [36].

corresponding to positive hydrostatic pressure using the least-squares method.

Amongst modern polymeric materials, the use of multi-layer structures is becoming popular. Guiu and Shanahan [36] have studied the adhesion between two semi-crystalline polymers (i.e., EVOH and PE) using peel tests at various peel angles. This study deals specifically with a five-layer system composed of two outer strata of high-density polyethylene (HDPE) with an inner layer of an ethylene/vinyl alcohol copolymer (EVOH) (see Fig. 46). The further two layers consist of an "adhesive" between the HDPE and EVOH phases: a grafted polyethylene (PE). Both temperature and peel speed have been used as experimental variables.

Both so-called "L-peel" and "T-peel" tests have been used in this investigation, but they studied the "L-peel" tests in details. As shown in Fig. 46, seperation is initiated by a blade at the EVOH/PE interface and a peel arm consisting of HDPE/PE* is peeled away from the remaining HDPE/PE*/EVOH structure which remains essentially flat, being (adhesively) attached to aluminum backing plate (not shown in Fig. 46. Peel angle, θ, is variable; the term "L-peel" referes to the observed configuration for $\theta = 90^\circ$.

Using Equation 3 the overall peel energy was calculted at temperatures in the range of 0–70°C and for peel speeds in the range of 0.1–100 mm min^{-1} as represented by G_p versus log (v_p) (see Fig. 8). Various points are worth noting [192]: (a) Peel energy, G_p, increases with peel rate, v_p, irrespective of test temperature, (b) Two regimes of behavior are present. For temperatures above 21°C, G_p, is relatively low, of the order of 5 kJm^{-2} (although this is still a high value for peel energy) whereas for lower temperatures, larger values of G_p are obtained, typically of the order of 20 kJm^{-2}. (c) At 21°C, a transition between the two types of behavior can be observed where a jump in peel energy occurs in the vicinity of $v = 10$ mm/min. This jump is of the order of 10 kJm^{-2}. For the higher energy domain, microscopic observation of the peeled arm revealed the existence of small crazelike regions at intervals of ca. 200 μm in PE* [204]. It was suggested [205] that these highly damaged polymer regions require large energy expenditure, thus explaining the considerable jump in peel energy. Such crazing behavior was previously reported by Reynolds in polyethelene [206] and in amorphous thermoplastics by Cho *et al.* [37]. Some sort of stick-slip fracture behavior seems likely. Similar transitions in various different systems have been reported over the long history of the peel test, the first reference probably being that of Gent and Petrich [43], later examples being given in [51, 207–209].

Ansarifar *et al.* [48] have studied the bonding properties of rubber to steel, aluminum and nylon 6,6 substrates by means of peel tests. Fig. 4a shows the peel test piece (i.e., $\theta < 90^\circ$) used to assess rubber-to-metal bond failure. This new peel test method was described in Section 4.2. Peel tests were performed at an angle of 90° at 23°C, either at constant rate of grip separation (a nominal peel rate of 0.05 to ∼16.7 mm/s), when the peeling force was recorded as a function of cross-head separation (see Fig. 5) or under constant load, where the load applied to the peeling leg increased from 216 N to 483 N. The actual peel rate was was determined by recording the distance the peel advanced along the bond and dividing it with the time it took. In Fig. 5, the first peaks corresponding to the onset of crack growth, where the peeling force was still rising, and the last peak corresponding to when test stopped or leg break occurred, were ignored . The remaining peaks on the trace were utilized for calculating an average peeling force for the test piece (see Fig. 5).

After the peel experiments were completed, force values were placed in Equation 31 to calculate peeling energies for the test pieces. From constant rate peel tests, the nominal peel rate was calculated from the cros-head speed and the test-piece geometry. The peeling rate variation as a function of the peeling energy was presented in Fig. 6. The peeling energies measured for rubber/nylon combination (∼24 kJ/m^2), were noticeably higher than those calculated for the rubber/steel and rubber/aluminum combinations (∼13 kJ/m^2). Evidently, the bond strength of rubber to steel and aluminum was almost identical, and noticeably lower than the values measured for the rubber/nylon joint failure.

Ansarifar *et al.* [48] used a second alternative procedure for producing bond failure carried out on 100 mm long test pieces involved a newly developed constant load peel test method [110, 141]. In these experiments, load was applied to the peeled leg, and bond failure proceededing a time-dependent manner at or near the interface. The locus of failure was almost parallel to the bond, but visual examination of the peel front zone showed large cavities to be present over an extensive region with unbroken strands of rubber in between. The presence of cavities was attributed to dilatational stresses created in the peel front [48]. Moreover, the fracture surfaces produced in these tests were either rough, where slow time-dependent failure along the bond was recorded at rates approximately 10^{-6}–10^{-3} mm/s, or smooth, where peel propagated along the bond likewise in a time-dependent manner at rates reaching 240 mm/s (see Fig. 47). Slope of the best fit to the results in Fig. 47 showed a power law index of about 25. It is interesting that rapid time-dependent failure along the bond was present in all the constant load peel tests, irrespective of the substrates tested.

Silva and Adams [74] have studied experimentally the failure mode of loads of a variety of 90° T-joints made of mild steel/adhesive/mild steel material for a

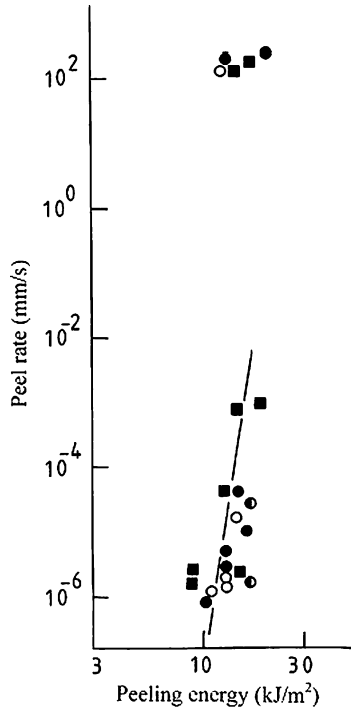

Figure 47 Time-dependent peel rate versus peeling energy relationship from constant peel tests [48]: (■): Nylon, (●): Steel, (○): Aluminum, and (◐): Aluminum ($R_a \sim 1\ \mu$m).

range of reinforcing methods, and ascertain the main parameters that influence the strength. In this study, a standard toughened epoxy paste adhesive was used. The mild steel adherend used was typical of that used in the manufacture of a car bodyshell. The geometry of the joints is illustrated in Fig. 48a. The supports consists of 90° gussets. The joints were loaded by the force P as shown in Fig. 48a, and supported by clamping some distance away from the joint area. Fig. 48b shows the failure loads of a series of T-joints on a 1.5 mm base. Joint (a) failed at the base of the vertical member by peeling of the adhesive. Joint (b) is a similar design but with a 90° gusset. The thickened vertical portion reduced the rotation and hence reduced the peel stress in the adhesive; this increased the joint strength considerably. Further improvement was obtained by combining (a) with a 90° gusset to give (c), while the strongest joint used two gussets (d). In all of these joints studied, yielding was observed in the steel base sheet, creating a plastic hinge. The designs that used two supports gussets reduced the bending moment and increased the failure load. For a simple beam fixed at both ends, the bending moment was calculated from tabulated formulae [210]. The maximum bending moment is $Pl/4$ at the middle and at the ends. Here P is the force and l is the half joint length. For the case of design (d), the bending moment is more complicated because the beam has a variable second moment of area along the span (moment of inertia I_1 and I_3).

$$M = \frac{P}{4}\left[\frac{l-(1-n)a^2}{l-(1-n)a}\right] = \frac{Pl}{4}\frac{25}{18} \qquad (55)$$

where $n = I_2/I_1 = 1/8$ and $l = 2a = 25$ mm.

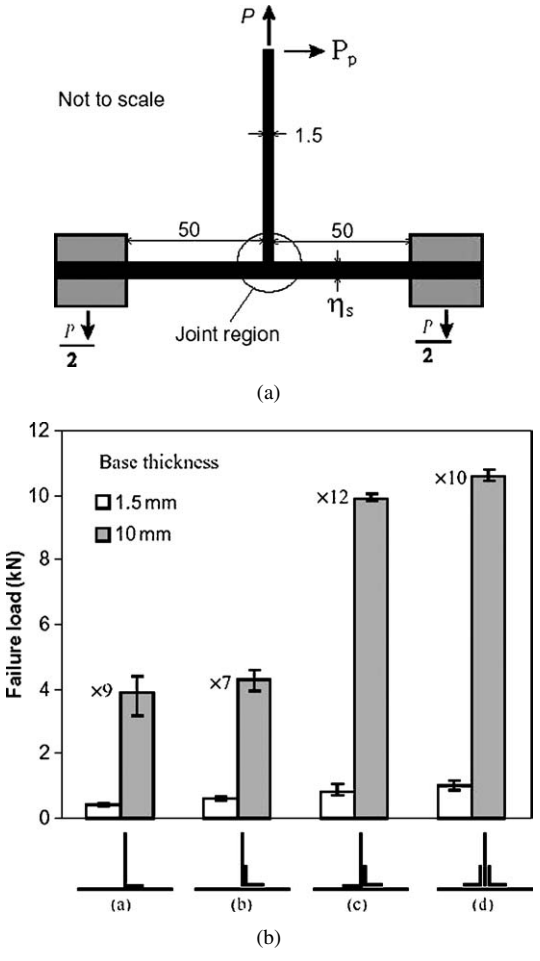

Figure 48 T-joints designs and failure loads (74): (a) Schematic diagram of T-joint test. Where P is the loading in the plane of the sheet, P_p is the tensile transverse (or peel) loading, and η_s is the adherend thickness. All dimensions in mm and (b) T-joint designs and failure loads for 10 an 1.5 mm base thickness.

Then, for the complete beam, the bending moment is given by

$$M_x = M - \frac{P}{2}x \qquad (56)$$

For a T-joint without support, the critical region is the middle of the beam where the bending moment is the highest. For a T-joint with supports, such as the gussets shown in Fig. 48b, the middle part of the joint where the supports are located is not critical anymore since the stresses are reduced by a factor of 8 ($I_2/I_1 = 8$). The transition between the base and the base plus the support is the critical part. The joint failure is dictated by yielding of the adherend base plate at this point. The bending moment is reduced in comparison with a T-joint without support and the joint will fail at a higher load.

Silva and Adams [74] have applied a FEA method with a plane-strain condition to understand the plastic behavior of the T-joint. In addition, the non-linear geometry was accounted for. The steel was allowed to yield with subsequent hardening and the adhesive was linear elastic. From the FEA results, the magnitude of the plastic deformation of the steel was determined with increasing load. The base starts to yield at 200 N near

the clamping zone. The plastic zone spreads throughout the section and eventually forms a hinge. At 575 N, the base yields near the support and an additional hinge is formed when the section is fully plastic at 1000 N. The experimental failure load for this configuration is approximately 1000 N, as seen in Fig. 48b. The failure prediction is probably dictated by yielding of the steel. Thus, the failure prediction should be around the region where the adhesive actually is. This would explain why the joint fails at a higher load.

Li and Lee-Sullivan [46] have investigated the filleted single-lap joints bonded (tested in tension) using a 2-D geometrically nonlinear FEA method under both plane strain and plane stress conditions, respectively, and verified either experimentally or theoretically. The 6061–T651 aluminum adherends were bonded using a flexible epoxy resin. The corners of the overlap were milled to a radius $r = 3.18$ mm to obtain a consistent fillet shape.The aluminum-to-aluminum joint specimen was strain gaged in two ways. In this study, gage strains (at 135°, 90°, 45°), bending moment (k), peel and shear stresses of adhesives along the bondline were determined. The first set of strain gages was mounted along the overlap region of the adherend very close to adhesive bondline. These triaxial resettes were mounted on the specimen at 135, 90 and 45°. The second set of gages was mounted onto the upper and lower surfaces of the adherend at about 7.2 mm from the corner of the overlap end. The gages were referred to as the longitudinal gages since they align with the centroidal axis of the adherend.

The filleted aluminum-to-aluminum single-lap joint was tested three times and the results averaged. The FEM results for longitudinal strains at the upper (US) and lower (LS) adherend surfaces located at 7.2 mm from the overlap end are compared with experimental longitudinal gage results, as shown in Fig. 49. The experimental results clearly fall within the range of the results generated by the FEM simulations. In order to compare the strain values predicted by FEM

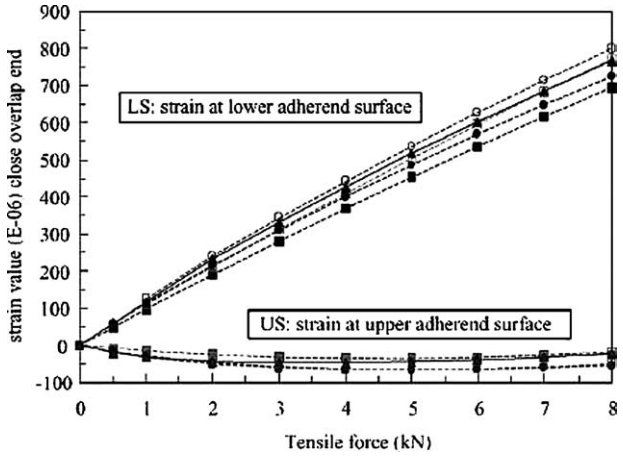

Figure 49 The variation of longitudinal strains and FEM simulations at the lower (LS) and upper (US) adherend surfaces at 7.2 mm from the overlap edge [46]. Note that the US and LS denote for the upper and lower substrates, respectively: (■): Plane strain FEM—No rotation, (●): Plane strain FEM—Rotation, (▲): Experiment, (□): Plane stress FEM—No rotation, and (○): Plane stress FEM—Rotation.

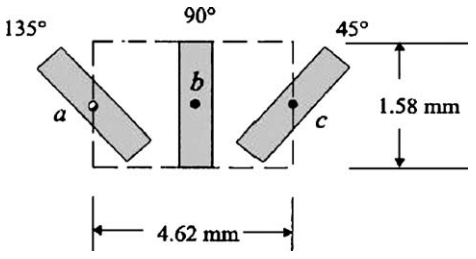

Figure 50 Rectangular area used in the averaging of FEM results obtained for the three nodes a, b, and c. The nodes represent the centers of the triaxial strain gages [46].

with the strains mesured off the rectangular rosette gages bonded along overlap edge, an averaging technique was applied. A rectangular area with dimensions 4.62 × 1.58 mm was considered in Fig. 50 in which the finite element strain at the centerline was obtained by averaging the strains at the center locations of each gage. The raw FEM data were transformed into their appropriate orientations before averaging.

Accordingly, ε_{135°, ε_{90°, and ε_{45°

$$\varepsilon_{135^\circ}|_{\text{averaged}} = \frac{\varepsilon_{135^\circ}|_{\text{at "a" point}} + \varepsilon_{135^\circ}|_{\text{at "b" point}} + \varepsilon_{135}|_{\text{at "c" point}}}{3} \tag{57a}$$

$$\varepsilon_{90^\circ}|_{\text{averaged}} = \frac{\varepsilon_{90^\circ}|_{\text{at "a" point}} + \varepsilon_{90^\circ}|_{\text{at "b" point}} + \varepsilon_{90^\circ}|_{\text{at "c" point}}}{3} \tag{57b}$$

$$\varepsilon_{45^\circ}|_{\text{averaged}} = \frac{\varepsilon_{45^\circ}|_{\text{at "a" point}} + \varepsilon_{45^\circ}|_{\text{at "b" point}} + \varepsilon_{45^\circ}|_{\text{at "c" point}}}{3} \tag{57c}$$

The strain distributions along the overlap region for the different gage orientations 135, 90 and 45° were compared with the FEM simulations. The averaged strains from FEM analyses were plotted along with the maximum and minimum values using the same markers for each position along the overlap. It can be concluded [46] that the experimental results for all three gage directions (135, 90 and 45°) agree well with FEM simulations along the overlap but there is poor agreement at the overlap end corners. See for example Fig. 51 for the 90° gage strains for the experimental and FEM simulationsin in the overlap section. It is difficult to determine which of the simulated conditions, e.g., plane strain/stress or rotation/no-rotation, give the best predictions since the error bars for the experimental results are relatively large. It is interesting, however, that the plane stress values are always higher than the plane strain values. Also, the averaged 90° gage results (see Fig. 51) which had the smallest error range, lie between the plane stress and plane strain results.

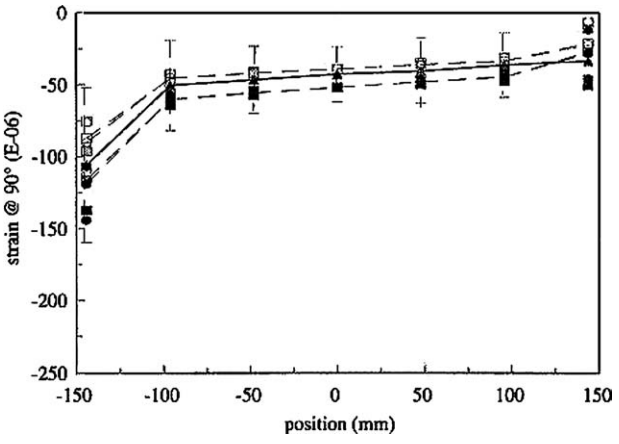

Figure 51 Comparison between the measured 90° gage strains and FEM simulations in the overlap section when applied load is 5 kN (Ref. [46]): (■): Plane strain FEM—No-rotation, (●): Plane strain—Rotation, (▲): Experimental (average), (□): Plane stress FEM—No-rotation, and (○): Plane stress FEM—Rotation.

8.2. Dynamic deformation of adhesives and joints under impact (or dynamic) loading

Since many structural adhesives are used in transport applications where the bonded joints are subject to dynamic as well as static loading, the adhesive dynamic properties (i.e., dynamic stress and strain, dynamic modulus) can be of significance. Although structural adhesive test specimens such as the lap-shear and TAST (thick-adherend shear test) specimens are almost always used for testing under static conditions, the adhesive material can show a degree of viscoelastic behavior such that its mechanical properties under dynamic loading can be significantly different from those under static loading [65]. Therefore, the durability for dynamic loading is the important subject in designing the adhesive joints.

Sato and Ikegami [63] have experimentally investigated the propagation of stress waves and the concentration of dynamic stress under tensile impact loading (i.e., dynamic deformation) in single lap joints, tapered lap joints and scarf joints, which were bonded adhesively. The joints consisted of aluminum alloy adherend and an epoxy resin adhesive. Viscoelastic properties of epoxy adhesive resin were also obtained from variation of strain waves which propagated in a rod of cured resin specimen. A compressive stress wave was generated by the collision, and propagated in the specimen. The compressive stress wave was reflected at the other end of specimen, and changed to a tensile wave. This reflection of the stress wave was repeated at both the edges of the specimen. Thus, the stress wave were propagated in the specimen repeatedly. The variation of the stress waves was measured using strain gages adherend on the surface of the specimen. The stress distribution and the time variation of stress and strain in the joints under tensile impact loading were calculated using the finite element method, considering the viscoelastic properties of the adhesive. In this study, 2-D analysis was performed assuming in-plane strain conditions. The strain wave propagation in the axial direction of epoxy adhesive specimen in the experiment were mesured. These waves could be regarded as waves measured at different points of an adhesive rod with an infinite length.

The viscoelastic parameters of the cured epoxy resin adhesive were determined using the Voight models which has three elements and five elements approaches. The relations between the complex compliance and the viscoelastic parametres of Voight model, which has three elements approach, are as follows:

$$J_1(\omega) = \frac{1}{E_o} + \frac{1}{E_1^2 + \omega^2\phi_2^2}$$
$$J_2(\omega) = \frac{\omega\,\phi_1}{E_1^2 + \omega^2\phi_1^2} \tag{58}$$

The relations of Voight model which has five elements approach are as follows:

$$J_1(\omega) = \frac{1}{E_o} + \frac{E_1}{E_1^2 + \omega^2\phi_1^2} + \frac{E_2}{E_2^2 + \omega^2\phi_2^2}$$
$$J_2(\omega) = \frac{\omega\,\phi_1}{E_1^2 + \omega^2\phi_1^2} + \frac{\omega\phi_2}{E_2^2 + \omega^2\phi_2^2} \tag{59}$$

J_1 and J_2 indicate real and imaginary parts of complex compliance. ω indicates angular frequency. The real part of the complex compliance of the adhesive decreases with respect to the frequency of the load spectrum. The imginary part of the complex compliance increases with respect to the frequency. Here, E_o, E_1 and E_2 indicate elastic constants of spring elements, ϕ_1 and ϕ_2 indicate viscosities of dashpot elements in the Voight model.

The frequency spectrum of strain variations (i.e., $\bar{\varepsilon}(x, \omega)$) can be obtained

$$\bar{\varepsilon}(x, \omega) = \bar{\varepsilon}(0, \omega)\,\exp\left[-r_d + \left(\frac{\omega}{v_s}\right)J\right]x \tag{60}$$

where x indicates position at which the strain measured, r_d and v_s indicate the decrement ratio, and velocity of the stress wave, respectively.

The calculated results of the model with five elements showed good agreement with the complex compliance obtained experimentally. The calculated results of the model with three elements deviated from the experimental results. Thus, Sato and Ikegami [63] concluded that the viscoelastic model of the five elements was sufficient to describe the viscoelastic properties of the cured adhesive.

Sato and Ikegami [63] have also carried out impact tests to verify the analytical method described in the Section 7.1. The length of the adherends was made to be 1300 mm to prolong the period until the stress waves, which were reflected at the end of specimen, eached the bonded part. The results for the strain variations with respect to time are shown in Fig. 52a–c for the single-lap, tapered lap, and scarf joints, respectively. The strain variation on the single lap joint and the tapered lap joints exhibited complicated changes because of the bending deformation. However, in the scarf joint, the smooth propagation of the stress wave occurred because the bending moment could be gnored.

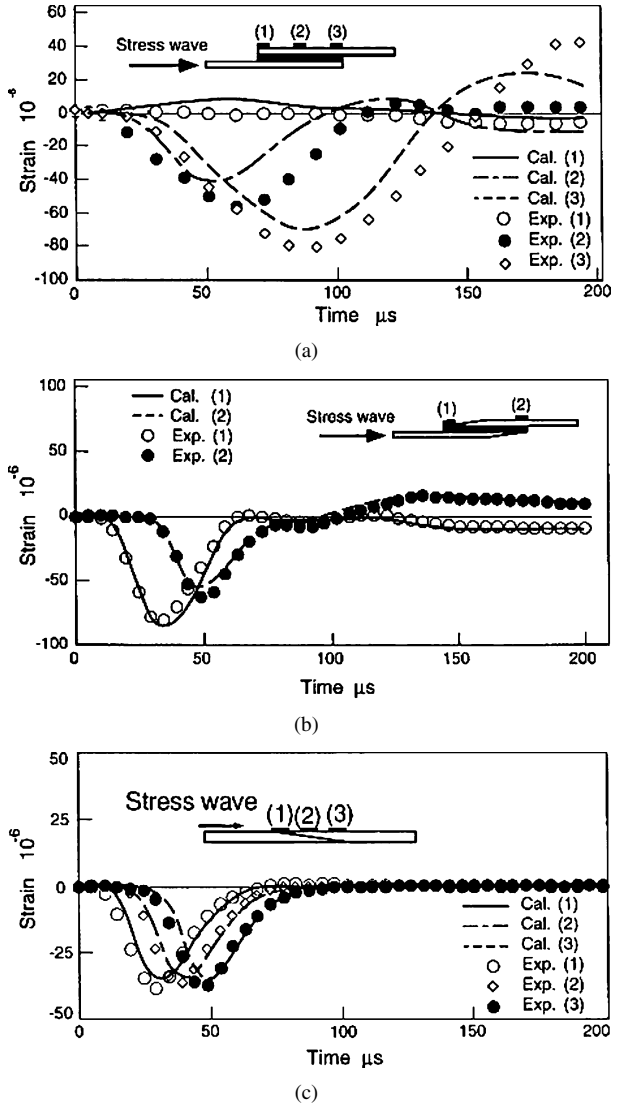

Figure 52 Comparison between experimental and the calculated (i.e., FEM) predictions of strain waves [63] for: (a) the single lap joint (over lap length = 100 mm), (b) the tapered lap joint (over lap length = 100 mm; taper length = 50 mm), and (c) the scarf joint (lap length = 100 mm). Note that calculated predictions were made for the three and five elements in Voight model, respectively [(i.e., cal. (1), cal. (2)].

In these figures, the experimental results are compared with calculated results by the analytical method (i.e., FEA) in the described above. The analytical results of the tapered lap joint and the scarf joint showed good agreement with the experimental results. The analytical results of the single lap joint almost agreed with the experimental results too. Therefore, the actual strain and stress in the joints seemed to be predicted by using the analytical method. However, in the case of the single lap joint as shown in Fig. 52a, the analytical results at the point [2] on the adherend of the stress-input side of deviated from the experimental results. The reason seemed to be due to the lack of uniformity in the adhesive thickness [63]. The joints had long adherends, so it was not easy to bond the adherends with geometrical precision. Therefore, in the joints, the thickness of the adhesive layer might have variations, which caused the deviation between the analytical results and the experimental result.

As Sato and Ikegami [63] summarized, the stress occurring in the adhesive layers of the tapered lap joint is smaller than that of the single lap joints with the same lap length. Thus, the use of tapered lap joints instead of single lap joint is effective in reducing the stress concentration not only under, static loading but also under dynamic loading. Scarf joint is the most effective shape to reduce the stress concentration in the adhesive layer not only under static loading but also under dynamic loading.

Maheri and Adams [65] have investigated experimentally the dynamic shear modulus of three structural adhesives (i.e., Araldite AV119, Araldite A420, Hysol EA956; all epoxy-based, two-part adhesives, except AV119) using the the thick-adherend shear test (TAST) specimens. In this study they used dynamic models of mass-spring and standing waves. Using the mass-spring model they determined the following expressions for dynamic shear modulus of adhesive layer for the axial and wide-wise lateral vibrations:

the axial vibration of the mass-spring model:

$$G_{\mathrm{a}} = \frac{2\pi^2 f^2 \eta_{\mathrm{a}} m_{\mathrm{s}}}{S_{\mathrm{a}}} \tag{61}$$

the wide-wise lateral vibration:

$$G_{\mathrm{a}} = \frac{2\pi^2 f^2 J_{\mathrm{o}} \eta_{\mathrm{a}}}{J_{\mathrm{A}}} \tag{62}$$

where f is the resonance frequency, η_{a} is the bondline thickness, $\mathrm{m_s}$ is the mass of one adherend, S_{a} is the surface area of the adhesive layer, J_{o} is the polar mass moment of inertia about its center o, and J_{A} is the polar second moment of adhesive layer.

The dynamic test results on bulk adhesives are tabulated in Table I. Also shown in this table, are typical values of shear modulus of each adhesives type, as obtained by using both axial and width-wise lateral dynamic tests. For each adhesive type, the resonance frequencies f of the same TAST sample was used to predict the shear modulus according to different vibration models. Nominal shear modulus values have also been tabulated for comparison. From Table I, it is clear that both the axial and the width-wise flexural results fall well short of the value of shear modulus found from tests on the bulk adhesive. The bulk adhesive dynamic test results, on the other hand, are seen to correlate well with the expected (nominal) values, and can be assumed to represent the correct value of the adhesive dynamic shear modulus. Also, if there were to be any viscoelastic effect, then the static tests should give a lower modulus [65]. It is therefore appeared that, for a standard TAST specimen where the bondline thickness is of the order 0.5 mm, the implicit assumption in the vibratory models concerning the relative dynamic compliance of the adherend was not valid. The shear stiffness $\mathrm{k_a}$ of a block of material of area, S_{a}, thickness η_{a} and shear modulus G_{a} [65] is

$$k_{\mathrm{a}} = \frac{S_{\mathrm{a}} G_{\mathrm{a}}}{\eta_{\mathrm{a}}} \tag{63}$$

For a typical adhesive, the shear modulus is of the order of 1 GPa, while that of the steel adherend is of the

TABLE I Results of dynamic tests on bulk adhesives and TAST specimens, using three different adhesives [65]

Adhesive	Nominal shear modulus (GPa)	Bulk dynamic shear modulus (GPa)	Bondline thickness (mm)	Axial freq. (Hz)	Lateral freq. (Hz)	Computed shear modulus (GPa)			
						Axial mode		Lateral mode	
						Mass-spring model	Stand wave model	Mass-spring model	Stand wave model
AV119	1.1[a]	1.14	0.460	8820	3980	0.656	0.830	0.780	0.795
A420		0.65	0.443	7450	2987	0.450	0.549	0.423	0.403
EA956	0.91[b]	1.00	0.550	8330	3452	0.699	0.873	0.701	0.690

[a] Manufacturer (Ciba-Geigy) data sheet.
[b]Determined from the quoted value of extensional modulus in the manufacturer's (Dexter Aerospace) sheet using a Poisson's ratio of 0.38.

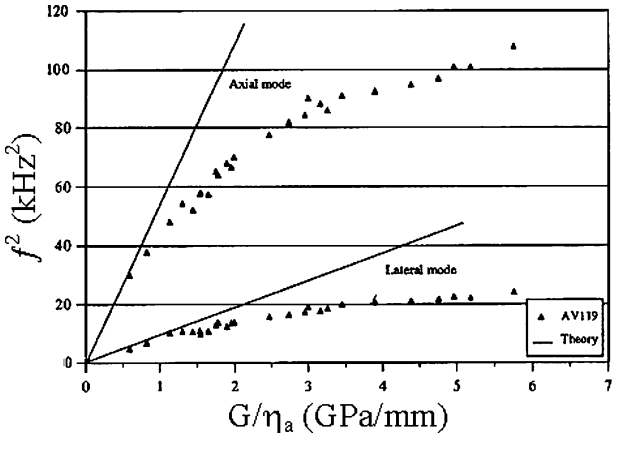

Figure 53 Resonance frequency f as a function of the adhesive layer parameter G_a/η_a (Ref. [65]).

order of 82 GPa. In the TAST joint, the adhesive and adherend (steps) thickness are 0.5 and 5.75 mm respectively. Fig. 53 shows the variation of the square of resonance frequency f with G_a/η_a for both axial as well as width-wise lateral modes of vibration for AV119 adhesive (earlier test results on standard TAST specimens with AV119 were also plotted). The points are based on the tests carried out on individual TAST specimens and show, according to Equations 61 and 62, the variation of the square of resonance frequency with the ratio G_a/η_a in which G_a is the true dynamic shear modulus of the adhesive as found from the bulk specimens tests (Table I). The solid lines are simply the graphical representation of Equations 61 and 62 for axial and lateral modes of vibration respectively, both of which predict a linear variation of f^2 with G_a/η_a. It is noted that the ratio G_a/η_a, which is proportional to the stiffness of the adhesive layer, is the only variable factor in a TAST specimen of standard dimensions. The following two expressions are cubic polynomial based on the experimental points shown in Fig. 53.

Axial mode:

$$\frac{G_a}{\eta_a} = 4.8222 \times 10^{-11} \times f^3 - 7.3454 \times 10^{-7} \times f^2 + 3.0045 \times 10^{-3} \times f \quad (64)$$

Wide-wide Lateral Mode:

$$\frac{G_a}{\eta_a} = 2.7166 \times 10^{-10} \times f^3 - 1.7967 \times 10^{-6} \times f^2 + 3.4513 \times 10^{-3} \times f \quad (65)$$

in which the units for G_a, η_a and f are (GPa), (mm) and (Hz) respectively.These empirical expressions give the dynamic shear modulus of the adhesive in a standard TAST specimen from the measured thickness of the adhesive layer, and the resonance frequency of either the width-wise lateral, or axial modes of vibration, provided that the same specimen configuration used in the present study and the same adherend material (steel) is used. The equations were applied to the test data listed in Table I, and the results are listed below in Table II. The results of dynamic tests on the bulk specimens are also shown for comparison. Therefore, the results based on the empirical relations correlate reasonably well with the bulk adhesive dynamic test results. This is to be expected for AV119 as this was used to produce the original master curves. The "unknown" adhesives A420 and EA956 were then assessed using the master

TABLE II Comparison of results based on empirical relations and bulk adhesive test results [65]

Adhesive	Bulk dynamic shear modulus (GPa)	Bondline thickness (mm)	Axial frequency (Hz)	Lateral frequency (Hz)	Predicted shear modulus (GPa)	
					Axial mode (Eq. 34)	Lateral mode (Eq. 35)
AV119	1.14	0.460	8820	3980	1.12	1.11
A420	0.65	0.443	7450	2987	0.69	0.67
EA956	1.00	0.550	8330	3452	1.06	0.92

curves and their measured natural frequencies. The results are within 8% of the previously measured bulk value, and validate the test methodology.

Sato and Ikegami [63] concluded that the use of these empirical relationships for measuring the shear modulus, G_a, of an adhesive material could also be applied to other TAST configurations. However, it would then be necessary to establish the master curves appropriate to the new parameters.

9. Effects of hot/humid environment on the durability of adhesive joints

A major concern is that the mechanical performance of adhesive joints involving metallic or nonmetallic adherends may deteriorate upon being exposed to aqueous environment [32, 211, 212]. It is the interphase of the joint, i.e., the region adjacent to the interface between the adherend and the polymeric adhesive, which is succeptible to such attack and on which attention must be focused. Various factors can affect the durability and performance of adhesive joints under the aging conditions (see for example recent studies in references [22, 28, 29, 33, 213]). Some of these important factors [29, 213] are: (a) various joint geometric factors, (b) the application of stress, (c) the joint orientation, (d) adhesives and adherend materials, (e) adhesive/adherend interfacial zone, (f) environmental effects, (g) the surface pretreatment method, and (h) elastic modulus of adherends and adhesives.

Water is the substance that presents the greatest durability problems to adhesive bond [32]. Water also has a weakening effect on the adhesives. Water may affect the adhesive properties by plasticisation and cracking. It may affect the adhesive/adherend interface by displacing the adhesive or by hydrating the metal or metal oxide surface of the adherend [213]. Many workers were devoted to study the durability performance of bonded joints (see for example, Refs. [29, 33, 83, 214–216]). Wylde and Spelt [83] used open-faced specimens in order to accelerate aging in an aluminum/epoxy double cantilaver beam. Bistact *et al.* [214] studied the durability of steel/polymer immersed in an aqueous environment (liquids such as water, salt, acid and basic solutions). Brewis *et al.* [215] proposed to use cryoblasting as a pretreatment for aluminum in order to enhance joint strength. Rider and Arnott [216] immersed aluminum alloys in boiling water followed by soaking in 1% 3-glycidoxytrimethoxysilane as a part of pretreatment. They found that the durability of bonding was notably improved in comparison with conventional pre-treatment. Knox and Cowling [29] investigated the durability performance of thick adherend steel lap shear joints and bulk adhesive using accelerated aging techniques. They also demonstrated [33] the benefits from using a surface pre-treatment prior to bonding in order to enhance the durability performance.

9.1. Effects of diffusion and oxidation

Abdel Wahab *et al.* [28] have investigated coupled stress-diffusion finite element analyses to compare with the experimental results, which were used to study the durability of adhesively bonded joints aged in hot/wet environment. Two bonded joints have been considered in this study, namely, single lap joint and butt joint. The joints were immersed in water at 60°C for up to 60 weeks. The aim of this investigation was to understand and explain the degradation in the joint strength due to water uptake in terms of the change mechanical properties and swelling using FE coupled stress-diffusion analysis [28]. Both dry and wet specimens were subjected to tensile loading and the stress/strain diagrams were obtained. Abdel Wahab *et al.* [28] have investigated the effect of the joint interface experimentally on the water uptake using a laminated "diffusion disc" consisting of cast adhesive and perforated aluminum foil (only on the upper side of the disc). Fig. 54 shows a comparison between the water uptake in this laminated discs with that in a disc of bulk adhesive having the same exposed adhesive area. It can be seen that during the early stages, the flux rate in the laminated disc is about 50% higher than that in the bulk epoxy disc. It was found that the water flux rate is higher when the interface is present during the early stages of exposure, as seen in Fig. 54. As the laminated disc has a larger diameter, it is possible that the enhanced uptake result from increased two-dimensional diffusion and not interfacial transport.

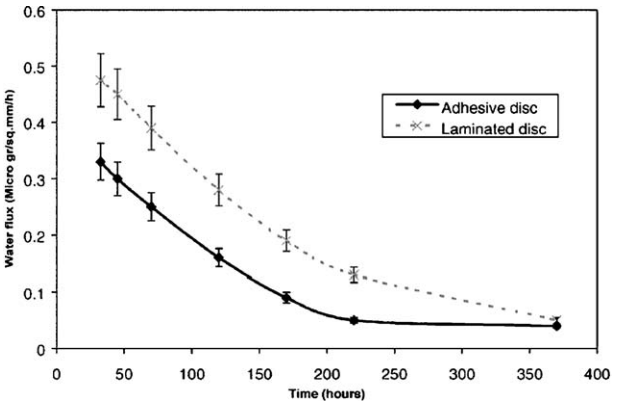

Figure 54 Effect of joint interface on water flux [28].

Abdel Wahab *et al.* [28] have analyzed the moisture distribution in the adhesive layer with coupling the diffusion-stress simulations using the transient finite element diffusion for single lap joint and butt joint. As the present finite element analysis is two-dimensional (assuming constant moisture distribution across the width of the joint), it does not consider three-dimensional effect. Additionally any moisture transport along the interface as assumed to be negligle. Therefore, it was suggested that in practise the moisture diffusion into the joint may be more rapid [28]. The aim of this analysis is to investigate modelling of this by the moisture transport process into both configurations, namely adhesive disc and laminated disc with holes. It was observed that the moisture is dissipated under the aluminum foil at the whole edge. The rate of mass uptake per quare mm (or water flux, microgram/sq. mm/h) was calculated from the finite element results using the following

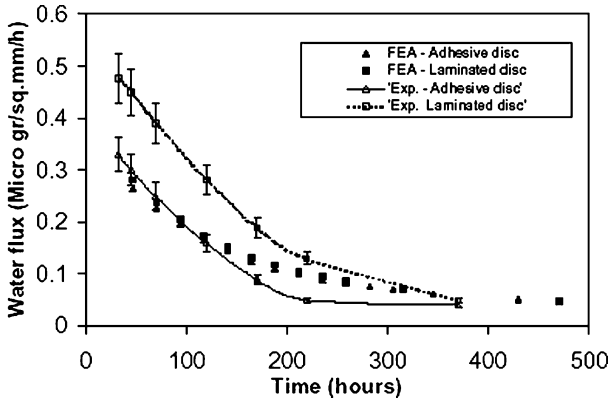

Figure 55 Comparison of water uptake for experimental and FEA results [28].

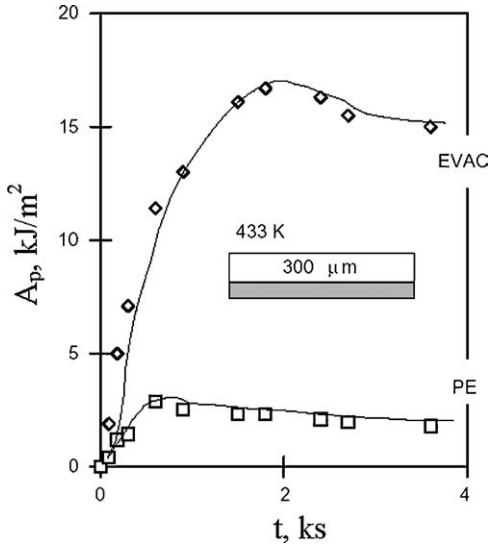

Figure 56 Peel strength A_p of PE steel and EVAC steel adhesive joints versus the contact time t at a constant temperature of 433 K in air at a free access of oxygen through the polymer melt layer [22].

expression:

$$\text{Water flux} = \frac{\sum_{i=1}^{n}(m)_i}{S_s t} = \frac{\left[\left(\sum_{i=1}^{n}\frac{C_m}{C_\infty}\right)V_i\right]_\rho}{S_s\, t} \tag{66}$$

where m is the mass uptake, C_m/C_∞ is the moisture concentration, V is the volume, S_s is the exposed area, n is the number of adhesive element, ρ is the water density and t is the time. Using this relation, Abdel Wahab *et al.* [28] have plotted the variation of water flux as a function of time for both models, as shown in Fig, 55. In this figure, the finite element results were compared to the experimental ones. Considering the FEA results, during the early stages, the water flux in the adhesive disc model calculated from FEA is slightly lower than that in the laminated disc model due to the difference in volume between the two models. However, in comparing the FEA data with the experimental results is evident that the simple diffusion model, which ignores moisture diffusion through the interface gives a significantly lower prediction of water flux in the laminated disc. Thus, observation suggests that the interface diffusion does in fact play an important role in the moisture transport process.

During oxidation in contact with steel, the iron compounds dissolve and penetrate into the bulk of a polyethlene layer [217]. The intensity of dissolution correlates with the rate of contact oxidation. Judging from the value of an efficient diffusion coefficient of the iron compounds, the process of transfer of the iron compounds was suggested to be diffusion-controlled [22]. The results of several model experiments show that the most presumable reaction of the iron compounds generation is the formation of iron carboxylates as a result of the interaction of iron oxide with the products of contact oxidation of the polymer containing carboxyl groups [217]. Kalnis and Ozolins [22] have studied the contact thermooxidation on the structure and characteristics of the boundary layer of the polyolefin adhesive (i.e., PE and EVAC adhesives) which forms the adhesion bond with steel. Note that the theoretical background about the contact thermooxidation was presented in Section 1.2. Samples of adhesive metal-polymer joints were prepared in the form of laminate panels.The samples were then held at a fixed temperature in free air for a definite time (to avoid free access of oxygen through the polymer melt layer). The change in peel strengt A_p of adhesive joints of PE or EVAC (copolymer of ethylene with vinylacetate) with steel, the thickness of a residual adhesive layer η_a on a metal substrate after a cohesive fracture of the adhesive joints were investigated as a function of a contact thermooxidation time t under conditions of catalytic contact oxidation. Fig. 56 shows the variations in the peel strength A_p with the contact time t for PE and EVAC. The characteristic of the $A_p(t)$ curves is similar. Both curves pass through the A maximum ($A_{p(max)} = A_p(t)_{|(dA_p/dt=0)}$. The greatest growth rate of peel strength for both curves corresponds to $t = 0$ ($A_p = \lim \mathrm{d}A_p/\mathrm{d}t)|_{t\to 0}$). As was experimentally proven [25], the shape of $A(t)$ function for the PE-steel adhesive joints is determined by the rate ratio of the two main competing contact thermooxidation processes which occur in the boundary layer and affect its cohesive characteristics. The processes which lead to a growth in strength of the boundary layer and hence to an increase in A_p (the accumulation of oxygen-containing groups and oxidative cross-linking), predominate before reaching the point of $A_{p(max)}$. After reaching the maximum, the oxidative destruction prevails.The coincidence of the $A_p(t)$ function for both adhesives may indicate the evidence that the contact thermooxidation process in the boundary layer are similar. The peel strength of EVAC adhesive joints grows more rapidly (A_p is higher) and reaches much greater values of $A_{p(max)}$ later than PE. These differences together with a much lower ratio of $A_{p(max)}/A_{p(max)}|_{t=3.6\ ks}$ indicate that, in the case of EVAC, the oxidative destruction processes may affect the shape of the $A_p(t)$ function less than that in the case of PE.

The fracture of adhesive joints of both polymers in the course of peeling is of cohesive character. As observed by Kalnins and Ozolins [22], the thickness η_a of the residual adhesive layers grows with contact time t.

This is an indication of the progress in the contact oxidation processes in the adhesive near the interface. The chemical changes caused by contact oxidation steadily penetrate deeper into the bulk of adhesive. The structure of the residual adhesive layer significantly differs from the bulk dhesive. Kalnins and Ozolins [22] observed that the content of a cross-linked part of the polymer gelfraction), c_{gel}, in the adhesive boundary layer grows, the content of low-molecular part, c_{lam}, increases, and the molecular weight of the polymer in the layer decreases with the contact time. This means that the competing contact oxidtion processes (i.e., cross-linking and destruction) proceed simultaneously in the adhesive boundry layer. Kalnis and Ozolins [22] have introduced an expression, which can somewhat estimate the ratio of contribution of two competing contact oxidtion processes. They suggested that this simple empirical quantity K is useful for this purpose.

$$K = \frac{1 + c_{gel}}{(1 + c_{lam})[m_{i=0}/m_i]} \tag{67}$$

where m_i is the molecular weight of the dhesive in the boundar layer at contact time t_i and $m_{i=0}$ is the initial molecular weight. In the absence of macromolecular changes, $K = 1$ (c_{gel}, $c_{lam} = 0$, $m_{i=0} = m_i$). The growth in K indicates that the cross-linking processes prevail, while the decay in K shows that the oxidative destruction predominates. The varition of K with contact time t is shown in Fig. 57. The value of K diminishes with the contact time due to the increased contribution of the process of contct oxidation destruction. Comparison between Figs 56 and 57 shows that there is no expected similarity between $K(t)$ and $A_p(t)$ curves. As suggested by Kalnins and Ozolins [22], probable reason for this may be the fact that the peel strength by itself does not probably reflect the state of strength-deformation charcteristics of the boundary layer.

Using the Kaelble's approach [57] (see Section 1.2 for detail) Kalnins and Ozolins have calculated the peel energy characteristic, $A_V = A_p/\eta$. This energy is independent of the thickness η (see Equation 4 in Section 1.1). The character of the variation in A_V

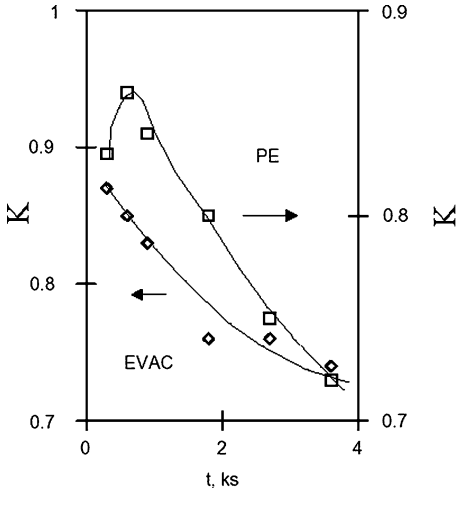

Figure 57 K versus the contact time t for EVAC steel and PE steel adhesives [22].

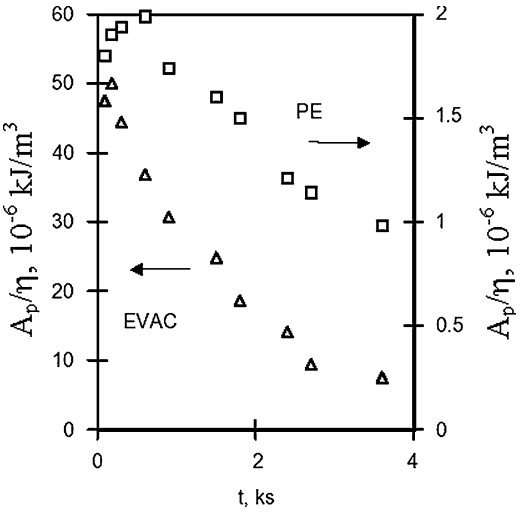

Figure 58 A_p/η versus the contact time t (Ref. [22]).

(Fig. 58) and A_p (Fig. 56) with the contact time is quite different. The values of A_V increase just at a very early stage of contact and, after reaching the maximum clearly decrease with the contact time t. It was suggested [22] that the growth in A_p with contact time occurs primarily due to the increase in the residual layer thickness η [22]. The curves $K(t)$ (Fig. 57) and $A_V(t)$ (Fig. 58) are quite similar. As observed by Kalnins and Ozolins, there is a certain correlation between the values of A_V and K for an equal contact time t. Hence, the peel energy per unit volume of the polymer adhesive involved in the deformation and consequent fracture, A_V, really depends only on the strength-deformation chacaracteristics of the adhesive (σ_B, E_a). It is of interest to consider the relation $A_v = A_p/\eta$ in the case where η depends not on the contact oxidation but on some other factor, for instance, on the peel rate (or cross-head rate). As seen from Table II, the value of η varies significantly with the peel rate. Simultaneously, at the same cross-head rates, some tensile characteristics of the adhesive (EVAC) were measured: tensile strength σ_B, elongation at break ε_B, and specific fracture energy A_B. Fig. 59 shows a good correlation between A_V and A_B measured at equal cross-head rates. This means that A_V is a quantity depending on the strength-deformation characteristics of the adhesive boundary layer, which breaks cohesively during the peel tests.

9.2. Effects of bulk adhesive, fillet, stress, surface pretreatment, and primer

Knox and Cowling [29] have studied the durability performance of thick-adherend steel lap joints and the bulk adhesive (i.e., AV119: a hot cured, one part, epoxy paste, toughened) using accelerated aging techniques (30°C, 100% relative humidity). In some cases the spew was removed by filling after cure. Fig. 60 shows the effects of accelerated aging, fillet and preload on the durability performance of AV119 bonded steel lap shear joints, which show a similar trend. The ultimate failure load decreased as the environmental aging time increased, but there is some scatter in the results. This trend is as might be expected because in the past, many

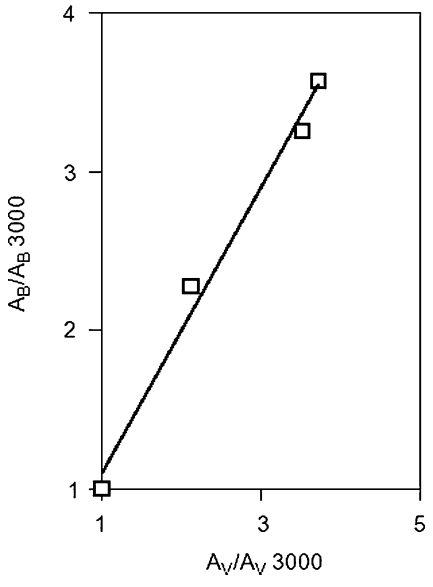

Figure 59 Correlation of A_V and A_B measured at different cross-head rates (A_V, A_B measured at a certain rate and A_{V300}, A_{B3000} at the greatest rate of 3000 mm/s) (Ref. [22]).

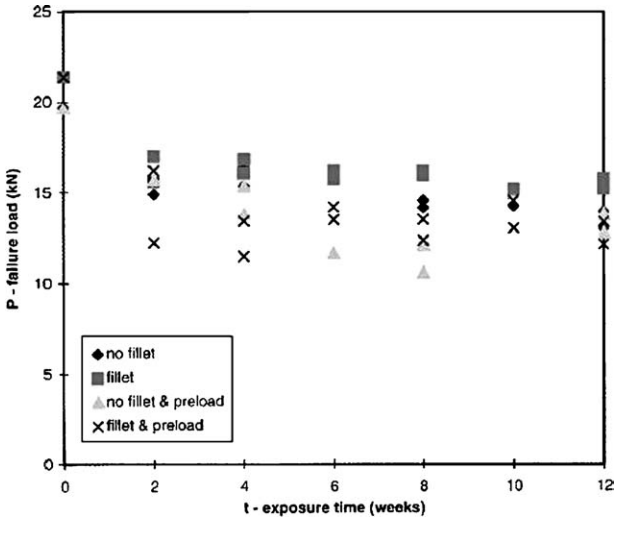

Figure 60 Accelerated durability performance of AV119-bonded steel lap shear joints showing the effect of a fillet and preload [29]. (The preload level is approximately 15% of the initial failure load.)

studies have been carried out showing the decrease of residual strength of bonded metallic substrates with epoxy adhesives after aging, in both natural environments and accelerated aging in wet or humid surroundings [32, 217–219]. This would indicate that removing the spew fillet from the joint and/or applying a load to a joint has a detrimental effect on durability performance. Others [32] also have found that a hot wet environment was by far the more hostile environment and that the presence of an applied load increased the rate of loss of strength. Know and Cowling has also observed [29] that there is a decrease in the static failure strength over a 12 week time span for all specimen types. The largest reduction in durability performance was obtained after 12 weeks from loaded specimens when the residual static failure strength had fallen to approximately 65% of the intial value [29]. The ingress of water degrades the interfacial zone and failure occurs at or very close

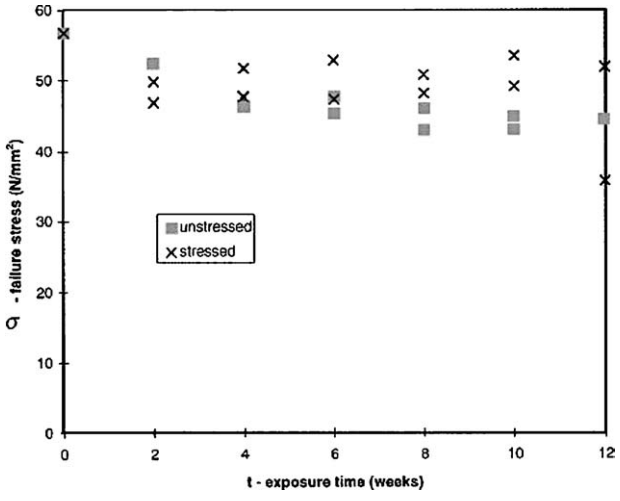

Figure 61 Accelerated durability performance of AV119 bulk tensile samples with and without a preload [29]. (The preload is 20% tensile strength 1800 N.)

to the interface. This is a classic indication of environmental attack [220]. On fracture, water is seen glistering on the adherend surface "shadows" and this area soon corrodes after exposure to air. Gledhill and Kinloch [220] established that substrate corrosion was not an operative degradation mechanism but rather a post-operative phenomenon.

The performance of the joints declined with exposure time, therefore some degradation must have occurred. Knox and Cowling [29] suggested that the loss of strength was largely due to degradation of the adhesive itself since the properties of unstressed bulk adhesive specimens also degraded over the 12 week period (see Fig. 61). However, the reduction in adhesive bulk properties over the same total time span were less (20% decrease in tensile stress and 10% decrease in Young's modulus) than in the lap shear joint (28% decrease in strength) [29]. While it can not be assumed that the bulk adhesive and the adhesive in the joint are saturated by water to the same extent, the durability performance of the joint clearly can not be attributed solely to the degradation of the bulk adhesive. It can also be demonstrated [221] that the durability performance of this type of specimen can be improved by using a surface primer. This indicates that the durability performance can be improved by the modification of the interfacial region and suggests that in the current study the same degradation is occurring in this region. Gledhill and Kinloch [220] observations also suggest that losses in joint strength are caused by adverse effects of water on the interface rather than the bulk adhesive.

Knox and Cowling [33] have investigated the use of a novel experimental technique (see Section 4.2 for more detail about this noval test) to measure the residual interfacial strength of an adhesive (i.e., AV119) to the adherend (i.e., a mild steel) after aging in a "realistic" environment (100% relative humidity, 30°C) in order to determine the effects of various surface pretreatment methods and various silanes. The residual adhesive/adherend interfacial strength was quantified by recording the required force to remove a strip of adhesive from the adherend surface using this test

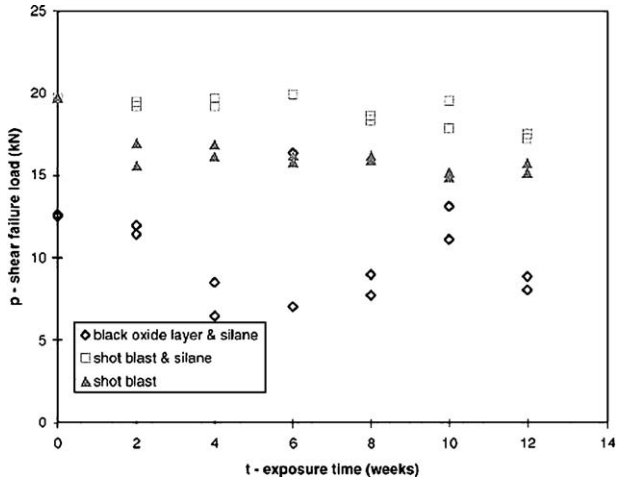

Figure 62 Accelerated durability performance of bonded steel lap shear joints showing the effect of an adequate surface pretreatment prior to the application of a primer (A 187) (Ref. [33]).

method. The geometry of the specimens enables rapid water ingress into the adhesive and interfacial zone [33]. Fig. 62 shows the effect of various surface pretreatments on the accelerated durability performance of bonded steel lap shear joints. A preliminary set of experiments reviewed the potential for a silane primer on a shot blasted surface and on an unprepared surface, i.e., with the mill scale still intact [33]. As this figure shows, for a primer to be effective, it must first be applied to a clean prepared surface. Fay and Maddison [222] found similar results when they investigated the use of Accomet C and a silane primer on thin steel lap shear joints. They concluded that these processes require application to clean surfaces, which may be difficult to attain in volume manufacturing.

Knox and Cowling [33] has also studied the effects of four primers on the accelerated durability performance of bonded steel lap shear joints (see Fig. 63). As seen in this figure, all four primers, on a shot-blasted surface, improve joint durability compared to a standard shot-blasted surface. Fig. 63 also shows that the silane-treated surfaces are superior to the standard shot-blasted samples and also the corrosion inhibitors. And,

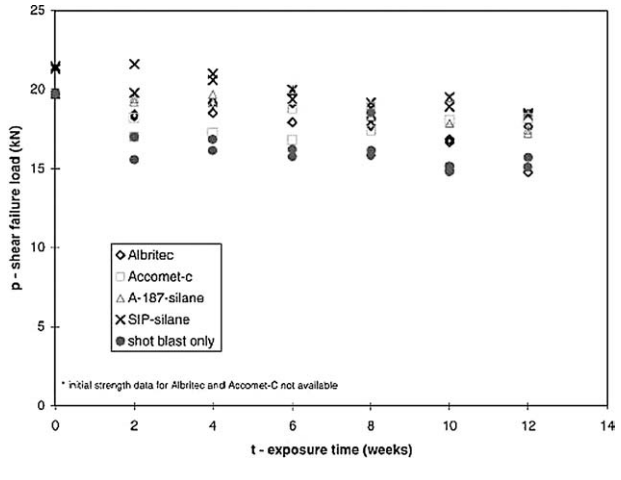

Figure 63 Accelerated durability performance of bonded steel lap shear joints showing the effect of various primers (Ref. [33]).

for a primer such as SiP, the loss in strength is negligible over the 12 week exposure period. Similar results have been found by Fay and Maddison [222], who report that stressed samples showed excellent durability performance when treated with Accomet C or a silane. The visual examination of the present aged samples by Know and Cowling showed [29] that the failure was similar in visual appearence to the unaged sample [221] demonstrating good adhesion. The effect of aging on the failure surface has very little influence. Thus, the use of a silane primer is to maintain the integrity of the interfacial zone over the test period in question [33]. The effectiveness of silane treatments is well established and it is thought to involve the formation of primary bonds at the substrate/silane interface. However, the actual mechanism by which the primer improves performance is not entirely understood and whilst silane primers do improve the water stability of adhesion on metals they do not necessarily increase resistance to bondline corrosion. When a silane is used to improve durability it has been demonstrated that they produce polysiloxane coatings on steel [223]. This may lead to a more durable interface. Throughout the work on primer selection, no consideration was given to the curing procedure, application method, layer thickness, etc. Studies [224] have shown that many processing parameters can affect the performance of the primer and, therefore, the performance of the adhesive joint.

Bhuniye and Maiti [225] have also studied the effect of the environmental conditions on the durability of the three different adherend interfaces: (a) metal-metal (i.e., Al-Al), (b) teak wood-metal (i.e., W-Al), and (c) teak wood-teak wood (W-W). The durability of adhesive materials under various harsh environmental conditions like boiling water, 5% salt water, 5% aqueous HCl and chemical mixture (i.e., toluene 30%, cyclohexane 60%, isooctane 9%, *n*-butyldisulfide 0.9%; *n*-butylmercaptan 0.1%) has been tested. Under these severe conditions only the Ciba-Geigy's hardener cured samples were treated. The retention values of the adhesive strength of polymer P-2 and standard epoxy resin on various surfaces such as wood-wood, metal-wood, metal-metal surfaces are presented in Table III. It is clear that stability of the adhesive bond of polymer P-2 under different harsh environments is inferior to that of the standard epoxy resin. After 5 days of 5% HCl treatment, it was found that the percentage of adhesive strength retention in case of polymer P-2 less than 5%. This may be due to the higher acid-susceptibility of the phospho-ester linkage of polymer which causes hydrolysis of the P-O linkage of the resin [225].

To investigate the effect of various additives on the lap-shear adhesive strength of the polymer, a mixture of 10.0% $Al_2O_3$and 10.0% silica (precipitated type) together and 10% $Al_2O_3$and 10% vinyltrichlorosilane were mixed with polymer P-2 and the standard epoxy resin before curing. Bhuniye and Maiti [225] have tested the lap-shear strength of these mixtures. In case of polymer P-2, the enhancement of adhesive strength for metal-metal interfaces is higher than wood-wood and wood-metal interfaces. Even percentage of enhancement of adhesive strength is higher than that of

TABLE III Standard retention of the adhesive strength of polymers, P-2, and standard resin after various harsh environment [225]

		Retention of adhesive strength (%)						
			5% HCl treatment		5% Salt water treatment		Chemical treatment	
Polymer code	Interfaces	Boiling water treatment (1 h)	3 days	5 days	3 days	5 days	3 days	5 days
P-2	W-W	23.0	38.0	5.0	42.0	13.0	60.0	32.0
	W-Al	20.6	22.0	2.0	37.0	7.0	51.0	21.0
	Al-Al	9.7	21.0	Nil	29.0	5.0	48.0	18.0
Standard resin	W-W	71.3	80.0	62.0	90.0	78.0	99.2	97.3
	W-Al	53.9	90.0	73.0	84.7	73.0	98.9	93.0
	Al-Al	54.0	87.3	65.0	77.6	77.0	99.0	96.0

the standard resin. It is observed that vinyltrichlorosilane is a powerful additive for enhancement of adhesive strength in each case by forming an effective bonding between epoxy polymers and metal or wood surfaces, i.e., it acts as a good coupling agent [226]. In the case, Si─O bond is generated from the hydrolysis of Si─Cl bond of vinyltrichlorosilane which strongly interacts with the metal substrate surfaces forming Si─O bond [225]. On the silane/adhesive interface, a coupling interaction arises from the polymerisation of the vinyl group of vinyltrichlorosilane under curing conditions, and the polymer thus formed interacts with the base resin. Thus using vinyltrichlorosilane as an additive the bonding between the adherends is enhanced more than in other cases.

10. Selection of adhesives

10.1. Process optimisation

Tremendous advances have been made in the development of adhesives that are stronger, easier to use, less costly and more reliable than alternative methods of joining. From early applications, such as plywood and World War II aircraft component assembly, the use of structural adhesives (where the adhesive is a load-transmitting part of the product) has grown rapidly [11]. Whenever bonding is planned, adhesive selection is of primary concern. The chemical industry has provided the user with a multitude of adhesives to choose from for any given application. Two-part, medium-viscosity, nonslumping, room-temperature-curing adhesives are the most successful because of their user-friendly properties [8]. The desirable properties [8, 227] are (a) a 1:1 mix ratio of two different-color components that combine to give a third distinct color, signifying a complete mix, (b) a uniform bond layer thickness as well as a uniform spread of the adhesive over the contact area are required with possibly no or minimum excess adhesive protruding out at the edges of the bond area. Therefore, once the adhesive has been selected the crucial task in designing the production technology remains how and where to deposit predefined quantities of this adhesive in order to achieve a bond layer of the desired quality and (c) a quick cure for rapid handling strength. Therefore, in cases where fast-setting adhesives are used, for example, cyanoacrylates, the spreading of the adhesive should be completed in the shortest time possible. Yet, the adhesive must possess a pot life sufficient enough to allow time to complete the application without rushing. There is typically tradeoff between quick cure and long pot life.

Adhesive joints are natural to consider for polymeric matric composite materials because many matrix resins are also good adhesives. For example, epoxies are used as adhesives for fiber-reinforced epoxy laminate as well as for many other materials.When the matrix material of the laminates in composites is also used as the adhesive in the joint, excellent adhesion might result [60]. However, even with the excellent adhesion, the joint does represent a discontinuity in the material, and resulting high stresses often initiate joint failure, which was discussed in Section 3. Complex composite materials found their way into high-tech industries like space travelling and aircraft construction a long time ago. However, as production methods have developed and raw material prices have been decreasing, the usage in civil engineering has increased. The pultration process offers a production method that enables polymer-based composite profiles with a sufficiently high material quality at an affordable price to be used in various construction applications [64]. The applications are tightly bound with joining of composite profiles using appropriate adhesives.Therefore, the task is to select right adhesives for bonding of composites with respect to various environmental conditions. Naturally, successful adhesive testing depends on the number of factors [64]: (a) proper surface preparation of composite adherends, (b) mixing and application of the tested adhesive, (c) clamping of the joint and curing of the adhesive, (d) test specimen preparation, and (e) final test execution. The shear properties of adhesive-bonded joints should be evaluated properly under the realistic environmetal conditions since many adhesive-bonded composite assemblies are designed to shear stresses. Therefore, single- and double-lap tensile shear tests were used for composite specimens [64]. The tested adhesives were applied to one or both bonded adherends and the joint results are compared.

A uniform bond layer thickness as well as a uniform spread of the adhesive over the joint contact are required with possibly no or minimum excess adhesive protruding out at the edges of the bond area. Therefore, once the adhesive has been selected the crucial task in designing the production technology remains how and where to deposite predefined quantities of this adhesive in order to achieve a bond layer of the desired quantitiy. In order to solve this problem, Babic [227] studied theoretically the problem of bonding rectangular plates to

substrates with a low viscosity, fast-setting adhesive. The main problem in this case is how to assure that the adhesive will (a) evenly spread over the whole rectangular contact area including the problematic four corners of the plate and (b) complete this task in the shortest time possible. Babic [227] first found an analytical solution for the case, where a drop of liquid adhesive is deposited between two large rectangular plates with a plane surface. The adhesive between the two plates initially occupies a cylinder-like volume with a radius R_o.

$$R_o = \sqrt{\frac{m_o}{\pi \rho_a d_o}} \tag{68}$$

where m_o and ρ_a are the mass and density of the adhesive deposited and d_o the initial distance between the plates. If the two plates are squeezed together, that is, if the distance d is time dependent, the radius R increases. We obtain

$$R(t) = \sqrt{\frac{m_o}{\pi \rho_a d(t)}} \tag{69}$$

and consequently

$$\frac{R(t)}{R_o} = \sqrt{\frac{d_o}{d(t)}} \tag{70}$$

with the distance d reduced for example by a factor 2, the radius R increases by $\sqrt{2}$.

Evidently, an equivalent effect can be achieved by keeping the distance d constant, that is $d = d_o$, and increasing the mass m_o, by the same factor. In this case,

$$\frac{R(t)}{R_o} = \sqrt{\frac{m(t)}{m_o}} \tag{71}$$

This simple conclusion means that the spreading of the adhesive between two parallel plates being squeezed together resembles the process of injection molding where the region between the plates represents the mold cavity and the adhesive the molten polymer, respectively [227]. As the distance d between the two plates is very small compared to the lateral dimensions L, that is $d \ll L$, in many practical cases the Hele-Shaw assumptions for the liquid flow can be adopted.

10.2. Progress in aerospace structural adhesives

Adhesive bonding has been used in the manufacture of primary aircraft fuselage and wing structures for over 50 years. As such, it is a direct competitor process to riveted structures but not as dominant. Adhesive bonding is used mainly for attaching stringers to fuselage and wing skins to stiffen the structures against buckling. It is also used to manufacture stiff lightweight structures of metal honeycomb cores inside metal skins for the flight control component structures (elevators, ailerons, spoilers, etc.). As stated by Higgins [12], the adhesive bonded aircraft structures are stable and durable and that this construction method has a lot to offer for future design programmes.

TABLE IV Comparison of physical and mechanical properties between FM® 300-2 and FM® 300 adhesive film aluminum adherends [6]

Property	FM 300-2 K cured 90 min at 121°C	FM 300 K cured 60 min at 177°C
Lap shear strength (MPa)		
24°C	38.6	37.9
121°C	26.9	27.6
150°C	15.9	18.6
Floating roller peel (kN/m)		
24°C	6.4	6.2
Honeycomb sandwich peel (Nm/m)		
24°C	74	67
Flatwise tensile (MPa)		
24°C	7.6	6.9
150°C	2.8	3.2
Flow (%)	450–550	450–550
T_g °C (TMA)	144	148

Kohli [6] has reported on the development of a new adhesive system for aeroengine bonding applications. This adhesive film designated FM® 300–2 is a 121°C cure version of 177°C curing FM® 300 adhesive film and provides similar stress-strain and mechanical performance to the FM® 300 system [228, 229]. In this work, he investigated the performance of FM® 300-2, epoxy-based adhesive, for various metal and composite bonding applications including applying this adhesive to aluminum adherends. This adhesive can be cured at 121 to 177°C and provides similar physical and mechanical properties irrespective of the cure temperature. Due to its low moisture absorption and high glass transition temperature, this shows excellent performance when bonding to wet Normex honeycomb and in bonding precured thermoset and thermoplastic composite substrates. Comparison of physical and mechanical property data between these adhesives is shown in Table IV. It is notable that the 121°C curing adhesive has a glass transition temperature of 144°C as compared to 148°C for the 177°C cured. Because of this high glass transition temperature, this film adhesive is capable of significant retention of its strength up to 150°C. The toughness properties of FM® 300-2 adhesive as indicated by peel strength are quite similar to FM® 300 . Both these systems have metal to metal peel strength of 6.4 kN/m. Because of their similar toughness and flow properties, both adhesives have similar sandwich properties. One of the key objectives in the development of this new adhesive was that it should have stress-strain properties similar to the adhesive. The 121°C cured FM® 300-2 adhesive has the same stress and strain properties as FM® 300 adhesive, not only under dry but also under hot/wet conditions up to 104°C. Therefore, the lower temperature curing adhesive can be used to minimize stresses caused by differential coefficients of expansion when bonding dissimilar substrates [6].

Higgins [12] has recently reported the adhesive materials used in the aerospace industry. In this work,

the bonding of the major aluminum alloys used as adherends in commercial aircraft structure (i.e., 2014A, 2024, 7075 and 7150) were presented. According to Higgins, the adhesive materials used for these purposes fall into three distinct groups.These are: (a) Metal/metal-hot cure, (b) metal/metal honeycomb-hot cure, and (c) metal to metal-cold cure. The hot cure adhesive materials used by the aircraft industry are mainly based on either phenolic or epoxy resin systems. Phenolic-based hot-bonded systems cure by condensation reactions which means that water vapor is generated during the cure. To prevent the bond line being pushed apart by the vapor release, high pressures need to be applied across the joint during the reaction period. This in turn effectively limits the bond widths to approximately 300 mm if optimum glue line thickness is to be achieved [12]. Large-area bonding will be required to be designed to give "windows" in the structure to allow the expanding surplus resin to spew out. The main structural phenolic and epoxy adhesives used on aircraft components, with the bonding conditions required are given [12] in Table V. The most important category of structural adhesives is that of the metal to metal hot cure types and a comparison of their room temperature mechanical properties (i.e., lap shear and peel strengths) are shown in Table VI (Ref. [12]).

TABLE V The hot cured commercial adhesive materials used by the metal to metal or metal to metal honeycomb bonding (i.e., mainly used by aircraft industry) (Ref. [12]). This table shows the bonding temperatures and bonding pressures

Adhesives	Bonding temperature (°C)	Bonding Pressure (kPa)
	Metal to metal bonds-hot cure	
Phenolic systems		
Redux film 775	145–156	480–760
CYTEC FM47	150–175	480–1380
3M Co. AF31	170–180	310–620
Epoxy systems		
Hexel redux 308A	170–180	310–380
3M Co. 163-2	115–125	200–276
	Metal to metal honeycomb bonds-hot cure	
Epoxy systems		
Hexel redux 308	180	345
3M Co. AF3109-24	180	345

TABLE VI Comparison of room temperature mechanical properties (i.e., lap shear and peel strengths) of the various hot-cured adhesives bonding to metal-to-metal adherends used in the aircraft industry [12][a]

Adhesive	Lap shear strength (MPa)	Peel strength (N/25.4 mm)
Redux 775	27–35	180–270
Redux 308A/NA	40–45	200–310
FM73	35–40	245–350
AF163-2	35–40	245–330
EA9330.1	27–35	120–155
SW9323B/A150	27–35	120–155

[a]National specifications covering these adhesives are: DTD 5577 (UK), MMM-A-132A and MIL-A-25463 (USA).
Typical room temperature values for cold cure epoxy adhesives are: Lap shear 27–35 MPa and Peel 130 N/25.4 mm.

TABLE VII Comparison of lap shear strengths at service temperature (i.e., −55°C, +80°C) for the various adhesives used in the aerospace application [12]

Adhesive	Lap shear (−55°C)	(MPa min) at (+80°C)
Redux film 775	20	10
FM47	20	9
AF31	16	14
Redux308A/NA	30	25
FM73	30	25
AF163-2	30	25
EA9330.1	12	6
SW9323B/A-150	12	16

Subsonic aircrafts are designed to perform within a service temperature range of +80 −55°C and the properties of the adhesives at these temperature have to be considered by designers. Typically the lap shear strength of the adhesives at these extremes of operating temperature are presented [12] in Table VII. Faced with these figures it is tempting to conclude that the epoxy systems are superior to the phenolic systems. However, structural engineers considering adhesive bonding for primary structures need also to concern themselves with the durability of the bonded joints in service, the effects of fluids contacted in service (i.e., water, fuel, oil, Skaydrol, de-icing fluids, etc.) as well as the effects of high humidity.

10.3. Process design and optimisation on the basis of effects of humid/hot environments

In recent years there have been much efforts to find suitable adhesives on their long term durability and performance of rubber to metal bonding. The manufacturers of of rubber to metal bonded components consume large quantities of volatile organic solvent-based materials to degrease the metal parts and bond rubber to metal [230]. This may cause considerable hazards to health such as risk of fire, explosion and harmful vapors and inevitably pollutes the working environment [49]. Therefore, there has been urgent need to promote a wider use of commercially important water-based cleaning materials and bonding agents. There are numerous aqueous bonding systems in the market at the present time. A more extensive use of these products has been hampered by lack of sufficient data on their long term durability and performance. Bond [231] studied the characteristics and performance of some waterborne adhesives and highlighted some of their advantages over the organic solvent-ones which are still being used for bonding metal to rubber adherends. Advantages of the water-based adhesives can be summarized on the basis of Bond's work [231]: (a) adherends for aqueous adhesives can be cleaned with warm water or soap solution, therefore eliminating the need for additional solvent usage. (b) comparatively lowering the costs of waste disposal, ventilation, and heated air. (c) In laboratory testing, waterborne adhesives achieve good results in bonding a variety of elastomers, including natural

rubber, to various substrates during the curing process. A recent work by Ansarifar *et al.* [49] also showed that using aqueous cleaning materials and bonding agents in rubber to nylon 6,6 bonding offers excellent bonding properties as well as a cleaner and safer working environment. Furthermore, costs can be reduced by eliminating the primer and using water-based covercoat. Nylon 6,6 is a suitable replacement for steel in rubber to metal bonding applications.

Balkova *et al.* [64] have investigated the effects of atmospheric condition and cool water at different temperatures (i.e., room temperature and 60°C) to select the most suitable epoxy-based adhesive for bonding glas fiber/polymer composites material systems. Lap shear specimens were tested within 1 year. In this study, three types of two-part epoxy-based adhesives (i.e., EPOXY 371, LETOXITE LX 012, LEPOX UNIVERSAL 11) were used for bonding fiber-reinforced plastic pultrusions. Selected adhesives are representatives of moisture-curable adhesives. Glass fiber/polyester composites, produced by pultrusion technique, were used as adherends. The rough area of the composite adherend was covered by thin film of fluid adhesive in order to wet the surface completely and leave no voids. Quality of adhesive bond was tested on single- and double-overlap shear specimens prepared according to ASTM standards D-1002 (single-lap), and D-3528 (double-lap). Four overlap lengths (10, 20, 30, and 40 mm) were tested to determine the optimal length of the lap [109, 232, 233]. Primer in EPOXY 371 was changed for another one "P11" on the basis of assumption that shear properties could improve.

It was observed [64] that the shear strength of double-lap shear specimens was always lower that of the single-lap ones. This was predominantly made by fracture of one weaker adhesive joint. Therefore, it was concluded that the results from single-lap shear specimens are more representative. It was also observed that application of adhesive on both bonded adherends improved the shear strength. From the variation of the overlap length, the optimal overlap length was determined to be as 10 mm using the dependence of stress at fracture on length of single-lap, as seen in Fig. 64. Balkova *et al.* [64] have tested the the glass-fiber/polyester composites joints in various environments (i.e., exposed to air at room temperature and 60°C, and cool water). LETOXIT LX 012 exhibited large strengthening during 1 year stored at room temperature. After that time the strength reached a value of about 13 MPa. Producers say [64] that adhesives should attain 90% of final strength within 5 days. This is valid for all adhesives except LETOXIT LX 012, which reached only about 70% of the strength at that time. The strength rose as curing process continued. The strength of joints immersed in water decreased after 10 days of storage except EPOXY 371. LEPOX UNIVERSAL 11 recorded the greatest deterioration of the shear strength, from 8 to 3 MPa. EPOXY 371, also with other type of primer (P11), exhibited good water-resistance. Composite materials may be applied at elevated temperature. They have chosen 60°C for testing shear properties (tested adhesives are applicable up to 80°C). They showed that the shear strength of all adhesive joints improved rapidly after 1 day in the oven against the same time at room temperature. LEPOX UNIVERSAL 11 stored at 60°C showed better shear properties compared to room temperature. Balkova *et al.* concluded that the most commonly used adhesive EPOXY 371 has maintained the shear properties without great change in all environments tested, also with other type of primer (P11), and exhibited the best shear strength in cool water. It was therefore recommended for universal usage. The elongation at break was also evaluated for all adhesive joints stored in water within 1 year. Elongation reached values from 1.3 to 2.5% in water, from 1 to 2.5% at 60°C, and from 1.3 to 3.0% at room temperature.

Kohli [6] studied the effect of prebond humidity by exposing the adhesive film (i.e., FM 300-2K) and the metal substrates (i.e., aluminum adherends) to two weeks at 80% relative humidity at 24°C. Whereas for postbond humidity studies, individually cut coupons were exposed to 71°C and 100% relative humidity for 30 days. The effects of these humidity on the durability of the bonded structures were evaluated using the various mechanical test methods [i.e., the lap shear (i.e., ASTM D1002); floating roller peel (i.e., ASTM D3167), (c) Honetcomb Sandwich Peel (i.e., ASTM D1781); flatwise Tensile (i.e., ASTM C297)]. The floating roller peel strength data is shown in Table VIII. The FM® 300-2 adhesive shows excellent retention of its strength up to 121°C after prebond and postbond humidity exposures.The outstanding moisture resistance of this adhesive is also demonstrated by its ability to

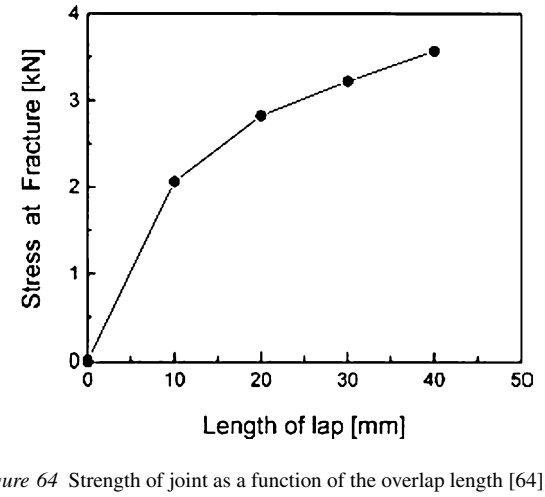

Figure 64 Strength of joint as a function of the overlap length [64].

TABLE VIII Effect of prebond and postbond humidity exposures on peel strength FM 300-2 K adhesive film BR 127 adhesive primer [6]

Prebond film exposure	Bonded coupon exposure	Floating roller peel (kN/m) 24°C	121°C
None	None	6.3	6.3
	30 days at 71°C/100% RH	6.2	6.9
15 days at 80% RH at 24°C	None	7.0	6.5
	30 days at 71°C/100% RH	5.6	6.3

TABLE IX Wet Nomex bonding with FM 300-2 K adhesive film [6]

Nomex core exposure	Bonded coupon (i.e., postbond) exposure	Flatwise tensile (MPa) 24°C	82°C	120°C
	None	5.4 (core)	5.3 (core)	4.3 (core)
3 weeks at 65% RH at 24°C	30 days at 71°C 100% RH	4.8 (core)	3.9 (core)	
Immersed in water for 24 h at 60°C then bonded within 2 h	None	5.0 (core)	5.1 (core)	4.2 (core)
	30 days at 71°C 100% RH	5.0 (core)	3.7 (core)	– (core)

Note: Failure mode: 100% core. Adhesive weight: 392 gm/cm^2.

bond to wet Nomex and maintain its strength up to 121°C even after humidity exposures. The wet Nomex honeycomb bonding data is shown in Table IX.

Kohli [6] has also studied the effect of humidity on the composite substrate (i.e., carbon-carbon substrates) using the same adhesive as mentioned previously. The bonded specimens were tested before and after humidity exposures. The wet conditioning of the bonded specimens involved exposure to 71°C/100% RH for 30 days for the Ciba 6376 precured substrates. The lap-shear strength data indicate that the performance of this adhesive system is not significantly affected by the exposure to moisture.This is a remarkable result and indicates that there is no need to dry the composite laminates prior to bonding with the FM 300-2 adhesive film.The post-bond humidity exposures data (82°C/wet) shows that in the case of precured laminates exposed to the dry or ambient conditions prior to bonding there is no degradation in performance. However, when the precured laminates were exposed to the hot/wet conditions prior to bonding, there was some degradation in properties after the post-bond humidity exposures. This shift in properties is attributed to the lowering of the stiffness of the composite and does not indicate a problem related to the adhesive system [6]. The failure mode in most cases was thin cohesive within the adhesive layer [6].

Xu *et al.* [111] have investigated the durability performance of galvanized steel to laminated glass-fiber PP/thermoplastic adhesive joints using two aging methods: (a) the Cataplasma aging tests, and (b) cyclic moisture/temperature tests. For the Cataplasma aging test, lap shear specimens were aged in an oven at 70°C for 5 weeks. The aged lap shear specimens were then tested. The cyclic moisture/temperature aging test was done by hanging the lap-shear samples in the different environmental conditions listed (i.e., 50°C, 100% humidity; 22°C; 50% humidity; −20°C). The complete cycle took one week, and the specimen was cycled for five weeks. For lap-shear joints made with HDPE-based thermoplastic adhesive, Cataplasma exposure and cyclic moisture/temperature exposure, were performed to study the joint durability. When the galvanized steel surface was treated with primer, the lap shear joints made with HDPE-based adhesive retained only in 11% of their initial strength after five weeks of Cataplasma aging (see

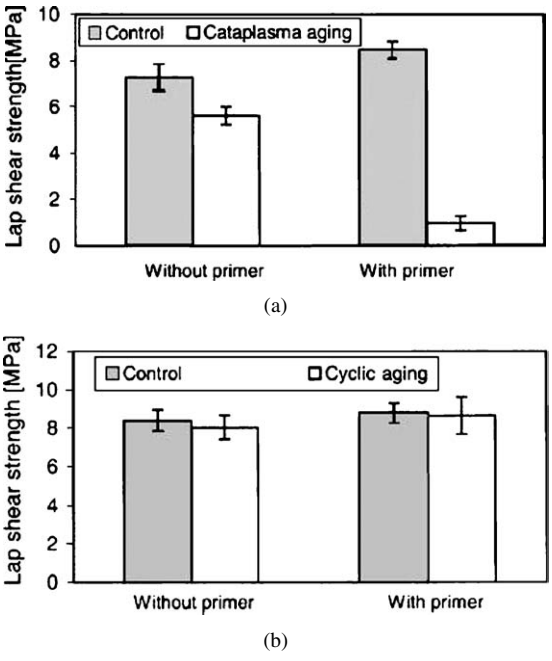

Figure 65 Strength retantion of the lap joints after Cataplasma and cyclic agings [111]: (a) Cataplasma aging and (b) Cyclic aging.

Fig. 65a). Without primer, the lap-shear joints made with HDPE-based adhesive retained about 77% of their initial strength after five weeks of Cataplasma aging (see Fig. 65a). The poor strength retention of adhesive joints with primer showed that the primer coating could not stand the severe Cataplasma aging conditions. However, the five weeks of cyclic moisture/temperature did not have any significant negative influence on the joint strength (see Fig. 65b) and failure mode of adhesive joints.

When new adhesive systems are being assessed the static properties are not the main criteria. For aircraft structure, durability is of greater importance and warm, wet, testing by soaking in water at 35°C for long periods or high humidity testing (at 95% RH and 70°C) is used to determine this [12]. Usually the testing is carried out back to back with a proven existing adhesive for comparison. Higgins [12] has recently studied the durability aspects of the adhesive bonding of aircraft structures using the main adhesives applied in aircraft industry. As Higgins pointed out, both epoxy and phenolic adhesive bonded joints have good resistance to fluid immersion tests but the phenolics perform better in high temperature/high humidity or warm (35°C) wet aging testing and this is born out by performance in service. Long-term warm, wet, aging studies [234] for up to two years immersion has shown that Redux Film 775 bonding has the best performance followed by AF 163-2 adhesive bonds. FM73 was slightly worse than AF 163-2 while Redux 308A was significantly worse than these. The two-part cold cure epoxy adhesive are least able to withstand warm, wet, aging. A past study [235] concluded that "Results from accelerated environmental tests on CAA (chromic acid anodised) aluminum adherends with Redux 775 (as well as AF 163-2) has shown that in the absence of primary bond line corrosion, that good stability of the interface between oxide and adhesive in the presence

of water at 35°C is obtained for periods of up to, and probably more than 4 years". This confirms the various studies carried over the past 20 years.This experience has shown that Redux 775 was even more durable on aluminum surfaces that had been prepared by alumina blasting and chromic/sulphiric acid pickling (with no primer [12].The high durability of Redux 775 is legendary. This is shown by the successful disbond free performance of primary structure on aircraft that have been in service for over 25 years [12].

11. Concluding remarks: Mechanical and environmental durabilty

Adhesive bonding is being increasingly used in structural applications recent years. The characteristics of adhesive joints make them attractive in industries such as aeronautics, automotive and civil engineering. When compared to mechanically fastened joints, adhesive joints have the advantages of having less sources of stress concentrations, more uniform distribution of load, and better fatigue properties [92]. One of the major advantages of adhesive bonding is its ability to join dissimilar materials [212, 236]. Adhesive bonding provides a more synergistic use of dissimilar materials in design. The potential of fast, in situ processses makes the thermoplastic bonding an attractive option for future manufacturing. For example, laminated glass-fiber—reinforced polypropylene (PP) provides fast and clean processing and lower costs than most thermoplastic composite.

The increased application of adhesive joints was accompanied by the development of mathematical models to analyze the behavior of those joints. Both analytical and numerical models (i.e., finite element model) have been developed [92]. However, its use in truly structural applications is still often limited. This is mainly due to a lack of confidence in the performance of adhesive joints, since the mechanical performance of the joints may deteriorate upon being subjected to cyclic-fatigue loading, especially if the joints are also exposed to a moist environment [211]. As Gonçalves *et al.* [92] pointed out, the ability to quantitatively describe this reduction in performance and to predict the lifetime of bonded joints would be a powerful tool, enabling manufacturers to make wider and more efficient use of adhesive bonding. The 2- and 3-D FEA approaches have been extensively applied by many workers (see for example references [92, 116, 237–247] to analyse the adhesive joints considering the linear and geometric nonlinearities. The 2-D FEA models that incorporate nonlinearities were also developed. Cooper and Sawyer [237] considered geometric nonlinearities in their model. A similar analysis was performed by Tsai and Morton [238]. Harris and Adams [116] incorporated material and geometric nonlinearities in their analysis. They used triangular and quadrangular plane strain elements and modeled the spew fillet at the end of the adhesive layer. Several special elements to model the behavior of adhesive layer were developed. Barker and Hatt [239] published one of the earlier works in this area. They developed a four-node element for 2-D analysis that behaves like a spring with normal and shear stiffnesses, which are dependent on the thickness of the adhesive layer. Carpenter [240] developed a simple element that considered the adhesive with no thickness. Later, the same author [241] developed another element that considers the adhesive thickness and a linear variation of the displacement field across it. Carpenter and Barsoum [242] developed two specific elements that incorporate some assumptions used in several analytical studies. These elements can be used with 2-D plane stress or plane strain elements, as well as with shell or beam elements. Rao *et al.* [243] developed a six-node isoparametric element similar to the one presented in [239]. Yadigari *et al.* [244] modified that element to include longitudinal normal stresses and viscoelastic analyses. Lin and Lin [245] introduced an element that represents both the adhesive layer and the adherends and that is based on Timoshenko's beam theory. Reddy and Roy [246, 247] developed a special element for geometric and material nonlinear analyses.

All the finite element analyses referred to above are two-dimensional . However, even for a simple adhesive joint such as the single-lap joint, stresses are of 3-D nature ([i.e., 91, 179, 248, 249]). This was investigated by Tsai and Morton [179] who performed 3-D linear elastic FEA of a single-lap joint in which boundary conditions account for the geometric nonlinear effects.These authors showed that 3-D regions exist in the specimen. They showed that the adherend and adhesive stress distributions in the overlap, near the free surface, are quite different from those occurring in the interior. Pandey and Narasimhan [248] also contributed to the identification of the 3-D nature of stresses in adhesively bonded single-lap joints by performing 3-D viscoelastic analysis considering material and geometric nonlinearities. Special elements that model the adhesive layer were also developed for 3-D analysis. Edlund and Klarbring [249] developed an element for geometric nonlinear analysis. They assumed that the adhesive layer is of negligible thickness and has linear elastic behavior. Andruet *et al.* [91] developed a model for 3-D analysis of adhesive joints based on shell and solid elements. The shell elements are used to model the adherends and the adhesive layer is modeled as a solid element with offset nodes in the mid-planes of the adherends.The element formulation includes geometric nonlinearities, and thermal and moisture effects.

In addition to considering the 3-D nature of adhesive joints, the calculation of accurate stresses at the adherend-adhesive interfaces is of primary concern. The failure of adhesive joints usually occurs in the adhesive (cohesive failure) or at the adherend-adhesive interfaces (adhesive failure). Moreover, cohesive failure usually occurs near the adherend-adhesive interface. However, conventional finite elements based on displacements do not satisfy the continuity of the stress vector at the interfaces. Cheikh *et al.* [250] proposed a technique, based on the finite element method formulated in terms of displacements that enables stress conditions to be imposed. They used 2-D FEA and applied their technique in the study of the stress distributions at the adherend-adhesive interfaces.

11.1. Effect of adherend surface pretreatment on the durability performance of joints

Many research works have been carried out in order to evaluate the effects of various surface pretreatment methods on the durability performance of adhesive joints (see for example, references [10, 33, 39, 213, 251]. It took almost a decade to acknowledge the criticality of surface pretreatment for metal-bonded structures. As pointed out by Kinloch *et al.* [251] the fracture mechanics approach provides an excellent method for evaluating the effects of the different surface pretreatments on the durability of the adhesively bonded joints. In Particular, the combination loading such cyclic-fatigue and the presence of an aqueous environment leads to an assessment of the environmental resistance of the bonded joint within a matter of weeks, as opposed to the more typical accelerated aging tests which involve exposing the joint, unstressed, in water for many months [251]. Also, in unstressed tests, the water temperature is often relatively high, well above any likely service temperature, in order to try to produce a large accelerated–aging factor. This frequently leads to unrepresentative failure mechanisms being observed in these tests, and very misleading results being obtained.

Knox and Cowling [33] have demonstrated that a surface pretreatment of adherends prior to bonding increased the durability performance using standard accelerated environmental testing techniques. For example, to ensure, initially, reasonably, strong joints, in the case of mild steel, it is generally sufficient to remove surface contamination and weak oxides [118] which may act as weak boundary layers. However, to produce durable joints, it is necessary to form stable oxides which are receptive to the adhesive/primer and to establish strong, stable, intrinsic forces at the adhesive or the primer and oxide surface.

While other experimental techniques may be used to quantify the effects of various surface pretreatments on durability performance they will generally not be as simple or give results as quickly. The Boeing wedge test is another technique which has been employed [33], as described in Section 4.1.2. As Knox and Cowling [33] claimed the results from this type of test are only qualitative in nature and it is not possible to distinguish quantitatively between different grades of interface stability [32]. Knox and Cowling [33] have developed a novel test method (i.e., scrap test) to rapidly discriminate amongst the durability performance of adherend surface conditions. This scrap test was applied to determine the effect of a silane primer on the durability performance of a steel adherend shot-blast surface. The Boeing wedge test would generally require a longer test duration than the scrap test experiments. It was pointed out [33] that the results are obtained so rapidly from the new scrape test as the test area, i.e., the bulk adhesive and the adhesive/adherend interface become very quickly saturated with water, due to the test geometry providing a larger surface area for water ingress. Whereas, in standard test specimens, e.g., lap shear joints, only a relatively small surface bond area is exposed to the environment, i.e., the bondline thickness. This limits the water penetration, by physically reducing the water flux to the interface and to the center of the joint. The most critical aspect of environmental durability testing is the assessment of the test results and the extrapolation of those results to predicted service life. The new test (i.e., scrap test) described in Section 4.2 was suggested to be ideal for rapidly discriminating amongst the improved structural adhesives and surface treatments, if not for predicting service life. The only major drawback seen for this new test method is that it can only be used on relatively smooth adherends [33].

It was demonstrated [33] that the use of silane primers increased the durability performance of mild steel adherend/epoxy adhesive joints. Wheras the use of silane leads to improving the durability of butt and lap joint types [28]. Lap joints without silane showed a strength loss during the first three weeks aging, then a strength recovery in the next 3–6 weeks, before a further strength loss [28]. Moisture degraded butt joints are faster than lap joints [28].

Molitor and Young [213] have investigated the effects of various surface pretreatments including Excimer laser cleaning and SHA (sodium hydroxide anodisation) on the adhesive bonding of a titanium alloy to a glass-fiber reinforced composite material in a hot/wet environment(i.e., in hot water at 70°C for 30 days) using the 90° peel tests. Based upon the 90° peel test results, SHA and surface cleaning by Excimer laser were selected. Both thermosetting and thermoplastic composites were evaluated using two aerospace industry standard film adhesives. An investigation of the durability of a titanium/glass fiber composite lap joints in a hot/wet environment using a single lap shear testing has shown that surface treatment by Excimer laser resulted in a five-fold increase in peel strength (dry), but the environmental durability was shown to be poor. In comparison, the surface preparation of the titanium adherend by SHA method resulted in relatively high peel strength and provided a durable composite/metal bond. It is important to understand how water has affected the titanium/adhesive interface. Two of the most important parameters governing the durability of titanium adherends are providing a surface with significant microroughness and providing a stable oxide layer [252]. The significant drop-off in shear strength following environmental aging indicates a requirement to protect the titanium oxide, possibly by a primer.

11.2. Environmental durability of adhesively bonded joints

Environmental resistance is fundamental to the durability of a bonded joint or repair. Most in-service failures are caused by environmental degradation of the interface between the bonding surface and the adhesive. These failures are characterized by adhesion failures at the interface. The environmental resistance of an adhesive bond is determined by the chemical bonds formed during cure of the adhesive and the resistance of the chemical bonds to environmental degradation. As discussed in the previous section, surface preparation is the most significant factor in determining the

environmental performance of a bonded joint, and the only method for producing a durable bond is to ensure that the surface is prepared using a process which has been correctly validated. There is no design technique to manage bond environmental degradation and bond strength will eventually decay to zero, if component failure does not occur first. It is well known that the most common and most important factors influencing the long-term behavior of unprotected adhesively bonded metal joints is the presence of high humidity or liquid water [32]. This has been a subject of concern for many years. Whereas the initial strength of a structural adhesive is fairly high and can be predicted from the vast amount of data available, subsequent time-dependent deterioration, particularly in humid conditions, may be observed. This type of failure is less predictable due to limited real-time, real-environment test data [253] and the relatively short time that synthetic structural adhesives have been in common use.

There are several physical mechanisms, which are responsible for the degradation in metallic adhesively bonded joints due to water uptake. These include [32]: (a) rupture of secondary bonds at the interface, which causes displacement of adhesive by water, (b) mechanical weakening due to the change in the oxide structure of adherend and (c) hydrolisis in the boundary of the adhesive layer. As pointed out by Abdel Wahab *et al.* [28], regardless which of these mechanisms is dominant, the strength of a joint is governed by other parameters, such as diffusion rate, change in mechanical properties due to moisture and swelling. The effect of change in elastic modulus and swelling on joint strength was discussed in Ref. [254]. The reduction in modulus due to moisture can reduce the stress concentration at the joint edges, which leads to beneficial effect on the joint strength. Swelling in the adhesive layer due to water uptake has an effect on the stress in the joint and in turn on the joint strength. Joint failure after aging appears to be intimately related to plasticisation of the polymer by water and weakening of the steel substrate adhesive interfacial zone [255].

Water is the substance that causes the greatest durability problems in the environmental stability of adhesive joints [32, 213]. There are two fundamental problems with water, its abundance and the fact that the polar groups (which is therefore readily attracted to pre-treated surfaces) that confer adhesive properties on a substance are inherently hydrophilic [29, 32]. Water may affect the adhesive properties by plasticisation and cracking. It may affect the adhesive/adherend interface by displacing the adhesive or by hydrating the metal or metal oxide surface of the adherend. For example, water has a weakening effect on epoxide, which is used, in the matrix of a large number of fibrous composites [213]. In a marine application the majority of bonded structural components will be exposed to moist air and if the relative humidity is high then over a period of time the strength of the joint will usually decline. Previous studies in the literature have demonstrated this by exposing adhesive joints to high humidity, natural climates or laboratory environments (see for example references [32, 218]). Water may enter and affect adhesively bonded joints by one or a combination of the following processes [32, 255]: (a) diffusion through the adhesive [256], (b) transport along the interface, and (c) capillary action through cracks and crazes in the adhesive and/or diffusion through the adherend, if it is permeable. Water entry may cause weakening by one or a combination of the following actions [32, 213, 255]: (a) altering the adhesive properties in a reversible manner, such as by platicisation; (b) altering the adhesive properties in an irreversible manner either by causing it to hydrolyse, crack, or craze; (c) attacking the interface, either by displacing the adhesive or hydrating the metal or metal oxide.

Zanni-Deffarges and Shanahan [257] proposed that the phenomenon of capillary diffusion excarbates water ingress. Surface tension effects near the metal oxide/polymer interfacial regions increase the effective driving force of water penetration. Such mechanism has been reported in the degradation of composite materials [258] where water enters along the interface between the matrix and fiber. Interfacial transportation can not be excluded as a possible mechanism of water entry into the joint. It was shown [259] that a full depth spew fillet has a distinct influence on stress distribution within the joint and joint strength. The benefits through leaving the spew fillet intact may be due to a number of contributing factors [29]: (a) Firstly, due to simple geometric considerations, a spew fillet will increase the total path length that the water must travel. However, as seen in Fig. 66 the water can penetrate a joint with all fillets removed to a depth of 5 mm in 12 weeks. This demonstrates that a specimen with a fillet can be affected by water in the test time span, as a typical fillet is approximately 3 mm in length. Therefore, there is a sufficient length of time for water to penetrate into the critical load-bearing zone. (b) Secondly, removal of the spew fillet after cure modifies the exposed adhesive surface. When the spew fillet removed, the surface texture of the exposed adhesive is rougher and of a matt finish, exposing any voids or cracks in the adhesive layer, which may act as entry sites for the water into the adhesive [32]. Therefore, water diffuses into the bulk adhesive causing aging of the adhesive itself. The diffusion process into critical areas is slowed down by leaving the spew fillet intact due to increased diffusion path length, reduced interfacial stress and surface conditions of the exposed adhesive.

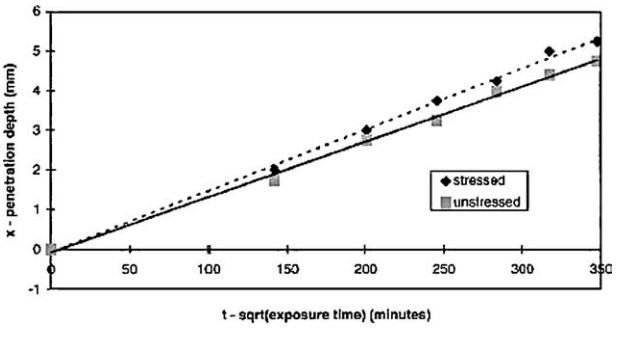

Figure 66 Water penetration into and AV119-bonded steel lap shear joint during accelerating aging (30°C, 100 Relative humidity) [29].

11.3. Effects of joint shapes (i.e., fillet, spew, chamfer, recessing) on the joint durability performance

There are many processing variables (geometrical and materials variables) in designing a durable adhesive joint. These include (a) fillet, (b) spew, (c) chamfer, (d) recessing, (e) bond length, (f) adhesive thickness, (g) adherend thickness, (h) choosing suitable materials for adhesives and adherends .

Knox and Cowling [29] have studied the effect of a spew fillet and preload on the durability performance of AV119-bonded steel lap joints (see Fig. 60). Considering first the results relating to unstressed samples, it can be seen that the initial drop in strength (of approximately 21%) in the first two week period is followed by a much slower decline in joint strength over the next 10 weeks. Other workers have found similar trend in results [76, 211]. It was suggested [29] that if a line is fitted through the results after the initial strength reduction, using regression analysis, the rate of decline in the samples with fillets is less than that of the samples with fillets removed and thus this indicates that a fillet is beneficial to durability performance. Using a numerical analysis Crocombe [260] also came to a similar conclusion. He reported that the effect of fillet of adhesive at the end of an overlap region on the kinetics of moisture diffusion is significant over considerable time scales. The general trend for the stressed samples is similar to the unstressed sample, showing first a large reduction in strength followed by a much slower decline in joint strength [29]. However, the difference between stressed samples with and without fillets is less distinctive and there is also a larger amount of scatter in the results. It may therefore be concluded that a stressed sample has a poorer durability performance than an unstressed sample (Fig. 60), and that the fillet has little influence on stressed sample performance.

As pointed out by Knox and Cowling [29], the benefits through leaving the spew fillet intact may be due to a number of contributing factors, none of which are dominant: (a) Firstly, due to simple geometric considerations, a spew fillet will increase the total path length that the water must travel. However, as this study showed water can penetrate a joint with all fillets removed to a depth of 5 mm in 12 weeks (see Fig. 66). This demonstrates that a specimen with a fillet can be affected by water in the test time span, as a typical fillet is approximately 3 mm in length. Therefore there is a sufficient length of time for water to penetrate into the critical load-bearing zone. (b) Secondly, removal of the spew fillet after cure modifies the exposed adhesive surface. Initially, after cure, the adhesive surface has a "glossy" appearence. When the spew fillet is removed, the surface texture of the exposed adhesive is rougher and of a matt finish, exposing any voids or cracks in the adhesive layer, which may act as entry sites for the water into the adhesive [32]. (c) Finally, by leaving the fillet intact, the stresses at the interface are reduced and peak stresses occur at approximately 45° to the surface of the adherend near th corner [260]. It may be assumed that a stress is the required driving force for water entry into a joint at the interface [29]. But if stress alone was the driving force then the unstressed samples with all fillets removed should not be affected by water. This is not the case (see Fig. 60). As stress does influence joint performance (Fig. 60), a reduction in stress at the interface must be of added benefit. It may be suggested that the spew fillet acts as a "seal" on the joint edge and reduces water penetration into the joint at the interface due to the contributory factors discussed above.

Using the finite element analysis method, Belingardi *et al.* [61] have investigated the effect of spew (exploring a wide range of spew angles, from 90° (i.e., square edge to 15°) and chamfer size on the stresses (i.e., shear and peel) in metal/plastics adhesive joints. It was shown [61] that the stress reduction can be achieved not only if the spew type adhesive extremity is adopted but, by varying properly the geometry of spews, an optimal solution can be devised. Further improvement can be obtained by adopting the spew and chamfer-type adhesive extremity. The magnitude of the stress peaks (for both shear and peeling components) decrease in entity with the decrease of the spew angle, although the most of the advantage is obtained within 45° solution. The stress distribution in the adhesive, in the cases of spew solution, shows the presence of a secondary peak whose entity can exceed the primary peak magnitude when the spew angle is large but tends to disappear as the spew angle decreases. They pointed out, hovever, that yet for angles of 45° the peak stress reduction is adequate and of the order of five times for the peel component (which is usually the most harmful for the adhesive) and of two times for the shear component with respect to the basic solution.The stress distribution in the adhesive, in the cases of both spew and chamfer solution, shows again the presence of a secondary peak whose magnitue can exceed that of the primary peak when the spew angle is large, but tends to disappear as the spew angle decreases. Their study has, also indicated that yet for angles of 45° the peak stress reduction is adequate and of the order of two times for the peel component (which is usually the most harmful for the adhesive) and of two times for the shear component with respect to the previous spew solution. Belingardi *et al.* [61] concluded that adopting the spew and chamfer solution, an advantage of one order of magnitued for the peel stress component and of one half order of magnitude for the shear stress component can be gained in the maximum stress values in the adhesive layer. With respect to other solutions presented in the literature, those considered here are feasible and geometrically simple. Obviously, the obtained result concerns the elastic behavior, thus it can not be directly inferred that the ultimate strength of the joint increases as much as the peak stress is reduced.

Li and Lee-Sullivan [46] investigated the filleted single-lap balanced joints in tension using the finite element analysis and experimental techniques. They concluded that there is minimal difference between plane strain and plane stress conditions in FEM predictions of the bending moment factor, k, and the adhesive stress distributions. The influence of rotation/no-rotation boundary conditions on the bending moment k is fairly large at low tensile loads but becomes increasingly smaller as the tensile loads are increased. The

predicted k values using the analytical solution proposed by Oplinger are similar to FEM simulations for rotation boundary conditions within the tensile force range studied.

Steven and Xie [261, 262] have developed a simple evolutionary structural optimization (EVOLVE) procedure (i.e., a FEA method) for the optimisation of adhesively bonded joints by shaping the adherend profiles to reduce peak stresses at the end of the overlaps. The EVOLVE method consists basically of removing the low stressed part of the material progressively from the structure [3]. Typically, the selection of an adequate joint requires a number of design and analysis cycles which rely heavily on the trial-and-error method. The EVOLVE method relies on an iterative FEA and progressive removal of elements which takes the guess work out of the design loop. Firstly, in this procedure a FEA of the desired structure is performed and the stress distribution found. A plate stress file is then set-up and using some criterion for rejection, here called a rejection criterion (RC) [3], such as the Von Mises stress, the low stressed material is removed. For example, elements which have a Von Misses stress in the structure are deleted. The FEA and rejection cycle are then repeated until a steady state (s.s.) is reached. This process is repeated until the desired optimum is reached, for example, till all stress levels are 20% of the maximum in the whole structure. Therefore, the objective is to minimise the maximum stresses in the joints. The EVOLVE code was found to be effective in reducing the maximum principal stress in the adhesive for all models studied [3]. Rispler *et al.* [3] have proposed another method called a stepped optimisation process in order to achieve accurate solutions both in terms of stress magnitudes and optimum shape of fillets.This method effectively reduces computation time in reaching an optimum design.

Rispler *et al.* [3] have recently employed the EVOLVE method to optimize the shape of adhesive fillets found in the tabs of tensile test speciments in which the adherends were titanium and T800 unidirectional tape bonded with a generic paste adhesive. In this study, the reduction in maximum principal stress achieved with respect to the baseline model (CFRP upper and middle adherends with $E_{\text{adhesive}} = 3.8$ GPa) ranged between 48 and 64%. The peak peel stresses in the central CFRP adherend and in the adhesive were reduced by up to 66%. All double lap joint models had a CFRP middle adherend. The minimum principal stress in the adhesive was achieved by optimising the configuration with a titanium upper adherend and adhesive with a Young's modulus of 2.6 Pa. The minimum peel stresses in the adhesive and the central CFRP adherend were obtained with the configuration having titanium as an upper adherend and an adhesive a Young's modulus of 5.0 GPa.The maximum tension allowable of the epoxy adhesive is 40 MPa [3]. Rispler *et al.* [3] concluded by comparing the maximum principal stress values obtained from the optimised models, that the only optimised structure that come close to the maximum tension allowable is the configuration with titanium as upper adherend and an adhesive with a Young's modulus of 2.6 GPa. Thus, a further reduction of approximately 8% would be needed to ensure a margin of safety equal to one.

With increasing use of adhesive bonding joints in industry, the analysis and design of the joints are becoming more and more important. Cost and weight are design criteria that are becoming increasingly important, especially in the automotive and aerospace industries [63]. Therefore, it is important to find a suitable design criteria for adhesive bonding that may provide some means of reducing cost and weight. For example, one method of doing so is recessing the adhesive layer by removing portions of the adhesive within the overlap [62]. This technique is termed as RECESSED BONDING. A recess joint is shown in Fig. 12g. Analysis of recessed bonded joints is limited in the literature, as most researchers concentrate on continuous single-lap joints (see for example, Refs. [72, 237, 263, 264]) or on single-lap joints that have the substrate profile altered to reduce peak stresses [265, 266]. Olia and Rosettos [267] performed an analytical study on the effects of gaps (i.e., recess) in single-lap adhesive joints subjected to combined axial and bending loads. They viewed the gap as a defect, such as debond or a void, that may reduce the joint strength rather than as a possible means of reducing cost and weight. Their results showed that the presence of a gap creates high peel stresses at the free edges created by the gap. However, if the gap is centrally located, the peel stresses at the outside edges increase only slightly as compared to the case without the gap. The shear stresses remain essentially uneffected at distances far from the gap. In two earlier papers [268, 269], Rosettos and his co-workers have shown that the shear stresses are hardly affected by a central void size of up to 70% of the overlap length. If the void is very close to the overlap ends, differences of the order of 20% in maximum shear stresses may occur. Mazumdar and Mallick [196] have experimentally investigated the effects of recessing on the failure load of single-lap joints. By conducting static tensile tests on single-lap joints with varied degrees of recessing, and comparing the results to a continuous joint, they showed that the average failure load did not increase with increased recessing. However, the lap shear values (i.e., peak load divided by the net bonded area) nearly doubled by recessing the joint, which indicates that the average strength of the bond increases with recessing.

Let us now summarize the above-mentioned results. Recessing a single-lap joint does not cause a significant increase in the maximum stresses near the adhesive spew terminus. Since stress conditions do not change significantly with recessing, it appears that recessed joints should be considered a viable alternative for structural applications where weight and cost savings are highly desirable. A joint with small effective lap length would be similar to a spot-welded joint, since the adhesive is used only near the ends of the overlap [62]. From the standpoint of fatigue failure, small effective lap length may not be desirable; however, it is possible to combine spot adhesive layers with other types of fasteners to create a fatigue resistant joint. It should be noted that large amounts of recessing creates

localized stress peaks at the recess ends [62]. At the interface, on the loaded side of the joint, σ_{xx} and σ_{yy} become compressive at the recess ends, which may help prevent crack propagation in that area of the joint. At the unloaded side, large tensile stresses occur, which need to be accounted for.

References

1. F. L. MATHEWS, "Handbook of Polymer Composites for Engineeres" (Woodhead Publishing Limited, Cambridge, UK, 1999).
2. M. DAVIS and D. BOND, *Int. J. Adhesion Adhesives* **19** (1999) 91.
3. A. R. RISPLER, L. TONG, G. P. STEVEN and M. R. WINSOM, *ibid.* **20** (2000) 221.
4. L. J. HART-SMITH, in "Joining Fiber Reinforced Plastics," edited by F. L. Mathews (Elsevier, London, 1987).
5. J. F. P. OWENS and P. LEE-SULLIVAN, *Int. J. Adhesion Adhesives* **20** (2000) 39.
6. D. H. KOHLI, *ibid.* **19** (1999) 231.
7. R. E. POLITI, SAMPE International Technical Conference (1987) Vol. 19, p. 36.
8. MEL M. SCHWARTZ, "Composite Materials Handbook," 2nd ed. (McGraw-Hill, 1992) p. 6.39.
9. A. B. CARTER, *SAMPE J.* **25**(4) (1989) 21.
10. L. J. HART-SMITH, *Int. J. Adhesion Adhesives* **19** (1999) 181.
11. E. PAUL DE GARMO, J. T. BLACK and R. A. KOHSER, "Materials and Processes in Manufacturing," 8th ed. (Prentice-Hall, 1997) Chap. 8, p. 1051.
12. A. HIGGINS, *Int. J. Adhesion Adhesives* **20** (2000) 367.
13. J. K. JETHWA and A. J. KINLOCH, *J. Adhesion* **61** (1997) 71.
14. C. H. WANG and P. CHALKLEY, *Int. J. Adhesion Adhesives* **20** (2000) 155.
15. R. N. HAWARD, "The Physics of Glassy Polymers" (Applied Science Publishers, London, 1973).
16. P. B. BOWDEN and J. A. JUKES, *J. Mater. Sci.* **7** (1972) 52.
17. M. Y. M. CHIANG and H. CHAI, *Int. J. Solids Struct.* **31** (1994) 2477.
18. C. H. WANG and L. F. R. ROSE, *Int. J. Adhesion Adhesives* **17** (1997) 17.
19. J. D. FERRY, "Viscoelastic Properties of Polymers" (Wiley, New York, 1980).
20. P. MOLITOR, V. BARRON and T. YOUNG, *Int. J. Adhesion Adhesives* **21** (2001) 129.
21. L. J. HART-SMITH, Adhesive-Bonded Single Lap Joints, NASA CR 112236, January 1973.
22. M. KALNINS and J. OZOLINS, *Int. J. Adhesion Adhesives* **22** (2002) 179.
23. M. KALNINS, "Adhesive Interaction of Polyethyelene with Steel" (Riga. Latvia, Zinatne, 1990) p. 143.
24. M. KALNINS, *J. Adhesion* **35** (1991) 173.
25. M. KALNINS and J. MALERS, *ibid.* **50** (1995) 83.
26. M. R. BOWDITCH, *Int. J. Adhesion Adhesives* **16** (1996) 73.
27. W. BROCKMAN, The Environmental Resistance of Metal Bonds in New Industries and Applications for Advanced Materials Technology, 19th SAMPE Symp., Exhibition, Azuza, CA, 1974.
28. M. M. ABDEL WAHAB, A. D. CROCOMBE, A. BEEVERS and K. EBTEHAJ, *Int. J. Adhesion Adhesives* **22** (2002) 61.
29. E. M. KNOX and M. J. COWLING, *ibid.* **20** (2000) 323.
30. S. SMILTNIEKS and G. M. SPINKS, in Proc. of Structural Adhesives in Engineering (V. Bristol, UK, Inst. of Materials, 1998), p. 47, ISBN 1-86125-066-5.
31. D. G. LEE, J. W. KWON and D. H. CHO, *J. Adhesion Sci. Technol.* **12** (1998) 1253.
32. A. J. KINLOCH, in "Durability, of Structural Adhesives," edited by A. J. Kinloch (Elsevier, Amsterdam, Applied Science, 1983).
33. E. M. KNOX and M. J. COWLING, *Int. J. Adhesion Adhesives* **20** (2000) 201.
34. D. J. ARROWSMITH and A. MADDISON, *ibid.* **7** (1987) 15.
35. CONSTANTINO. CRETON, "Materials Science of Pressure Sensitive Adhesives, Materials Science and Technology; Processing of Materials," edited by R. W. Cahn, P. Haasen and E. J. Kramer (Wiley-VCH, Weinheim, Germany, 1997) Vol. 18, p. 724.
36. A. GUIU and M. E. R. SHANAHAN, *Int. J. Adhesion Adhesives* **22** (2002) 415.
37. K. CHO, H. R. BROWN and D. C. MILLER, *J. Polym. Sci. Polym. Phys.* **28** (1990) 1699.
38. E. BOUCHER, J. P. FOLKERS, M. HERVET and C. CRETON, *Macromolecules* **29** (1996) 774.
39. A. BALDAN, *J. Materials Sci.* **39** (2004) 4729.
40. H. H. KAUSCH and M. TIRRELL, *Annu. Rev. Mater. Sci.* **19** (1989) 341.
41. R. P. WOOL, B. L. YUAN and O. MCGAREL, *J. Polym. Eng. Sci.* **29** (1989) 1340.
42. A. N. GENT and A. AHAGON, *J. Polym. Sci. Phys.* **13** (1975) 1285.
43. A. N. GENT and R. P. PETRICH, *Proc. R. Soc. London* A **310** (1969) 433.
44. M. SHANAHAN and C. BOUNGOS-MONNIER, *Int. J. Adhesion Adhesives* **16** (1996) 129.
45. A. N. GENT and G. R. HAMED, *Polym. Eng. Sci.* **17** (1977) 462.
46. G. LI and P. LEE-SULLIVAN, *Int. J. Adhesion Adhesives* **21** (2001) 211.
47. P. B. LINDLEY, *J. Inst. Rubber Ind.* **5** (1971) 243.
48. M. A. ANSARIFAR, J. ZHANG, J. BAKER, A. BELL and R. J. ELLIS, *Int. J. Adhesion Adhesives* **21** (2001) 369.
49. M. A. ANSARIFAR, J. ZHANG, A. BELL and R. J. ELLIS, *ibid.* **22** (2002) 245.
50. D. W. AUBREY, G. N. WELDING and T. WONG, *J. Appl. Polym. Sci.* **13** (1969) 2193.
51. C. DRAIL, A. ALLAL, G. MARTIN and P. TORDJEMAN, *J. Adhesion* **61** (1997) 123.
52. C. G'SELL and J. J. JONES, *J. Mater. Sci.* **14** (1977) 583.
53. *Idem.*, *ibid.* **16** (1981) 1956.
54. D. W. VANKREVELEN, "Properties of Polymers: Their Correlation with Chemical Structure" (Elsevier, Amsterdam, 1990).
55. J. VERDU, Materiaux Polymers, Relations, Structure-Propriétés. Lectures ENSAM, Paris, 1992.
56. F. H. HAMMOD, *ASTM Spec. Tech. Publ.* **360** (1964) 123.
57. D. KALELBLE, *Trans. Soc. Rheol.* **4** (1960) 45.
58. J. JOHNSON, *Adhesive Age* **11** (1968) 20.
59. T. IGARASHI, *J. Polym. Sci. Polym. Phys. Ed.* **13** (1975) 2129.
60. B. D. AGARWAL and L. J. BROUTMAN, "Analysis and Performance of Fiber Composites," 2nd ed. (John Wiley and Sons, Inc., 1990) p. 277.
61. G. BELINGARDI, L. GOGLIO and A. TARDITI, *Int. J. Adhesion Adhesives* **22** (2002) 273.
62. T. P. LANG and P. K. MALLICK, *ibid.* **19** (1999) 257.
63. C. SATO and K. IKEGAMI, *ibid.* **20** (2000) 17.
64. R. BALKOVA, S. HOLONEROVA and V. CECH, *ibid.* **22** (2002) 291.
65. M. R. MAHERI and R. D. ADAMS, *ibid.* **22** (2002) 119.
66. C. H. WANG and L. R. F. ROSE, *ibid.* **20** (2000) 145.
67. A. R. RISPLER and L. TONG, *ibid.* **20** (2000) 221.
68. J. COTTON, J. W. GRANT, M. K. JENSEN and B. J. LOVE, *ibid.* **21** (2001) 65.
69. G. LI and P. LEE-SULLIVAN, *ibid.* **21** (2001) 211.
70. R. D. ADAMS, J. COMYN and W. C. WAKE, "Structural Adhesive Joints in Engineering" (Kluwer Academic Publishers, London, 1997).
71. O. VOLKERSEN, *Luftfahrtforschung* **15** (1938) 41.
72. M. GOLAND and E. REISSNER, *J. Appl. Mech.* **11A** (1944) 17.
73. W. LI, L. BLUNT and K. J. STOUT, *Int. J. Adhesion Adhesives* **19** (1999) 315.
74. L. F. M. DA SILVA and R. D. ADAMS, *ibid.* **22** (2002) 311.
75. L. D. R. GRANT, The Characterisation of Adhesive Joints Found Typical in the Automotive Industry, Ph.D. Dissertation, University of Bristol, 1994.
76. R. A. SHENOI and F. L. M. VIOLETTE, *J. Compos. Mater.* **34** (1990) 644.
77. R. A. BARTHOLOMEUSZ, A. SEARL, A. A. BAKER and R. J. CHESTER, Bonded Composite Reinforcement of the

F/A-18 Y470.5 Bulkhead, Applications with Through Thickness Stresses. International Aerospace Congress, Sydney, 24–27 Feb. 1997.
78. C. H. WANG and L. R. F. ROSE, *Int. J. Adhesion Adhesives* **17** (1997) 17.
79. M. Y. M. CHIANG and H. CHAI, *Int. J. Solids Struct.* **31** (1994) 2477.
80. R. B. HESLEHURST, *Int. J. Adhesion Adhesives* **19** (1999) 133.
81. W. K. LOH, A. D. CROCOMBE, M. M. ABDEL WAHAB and I. A. ASHCROFT, *Eng. Fracture Mechanics* **69** (2002) 2113.
82. A. J. KINLOCH, *J. Adhesion* **10** (1979) 193.
83. J. W. WYLDE and J. K. SPELT, *Int. J. Adhesion Adhesives* **18** (1998) 237.
84. I. A. ASHCROFT, M. M. ABDEL WAHAB, A. D. CROCOMBE, D. J. HUGHES and S. J. SHAW, *Composites*, Part A **32** (2001) 45.
85. M. M. ABDEL WAHAB, I. A. ASHCROFT, A. D. CROCOMBE, D. J. HUGHES and S. J. SHAW, *ibid.* **32** (2001) 59.
86. D. BREWIS, J. COMYN and J. TEGG, *Int. J. Adhesion Adhesives* **1** (1980) 35.
87. J. CRANK and G. PARK (eds), "Diffusion in Polymers" (New York, Academic Press, 1968).
88. D. R. LEFEBURE, D. A. DILLARD and T. C. WARD, *J. Adhesion* **27** (1989) 1.
89. A. KAUL, N. SUNG, I. CHIN and C. SUNG, *Polym. Eng. Sci.* **24** (1984) 493.
90. B. R. K. BLACKMAN, J. P. DEAR, A. J. KINLOCH, H. MACGILLIVRAY, Y. WANG, J. G. WILLIAMS and P. YAYLA, *J. Mater. Sci.* **30** (1995) 5885.
91. R. H. ANDRUET, D. A. DILLARD and S. M. HOLZER, *Int. J. Adhesion Adhesives* **21** (2000) 17.
92. J. P. M. GONÇALVES, M. F. S. DE MOURA and P. M. S. T. DE CASTRO, *ibid.* **22** (2002) 357.
93. O. VOLKERSEN, *Constr. Met.* **4** (1965) 3.
94. L. J. SEGERLIND, *J. Appl. Mech.* **35** (1968) 177.
95. W. J. RENTON and J. R. VINSON, *ibid.* **44** (1977) 101.
96. I. U. OJALVO and H. L. EIDINOFF, *AIAA J.* **16** (1978) 204.
97. D. A. BIGWOOD and A. D. CROCOMBE, *Int. J. Adhesion Adhesives* **9** (1989) 229.
98. G. R. WOOLEY and D. R. CARVER, *J. Aircraft* **8** (1971) 817.
99. T. R. GUESS, R. E. ALLREDA and F. P. GERSTLE, *J. Test. Eval.* **5** (1977) 84.
100. N. I. HARRISON and W. J. HARRISON, *J. Adhesion* **3** (1972) 195.
101. R. D. ADAMS and N. A. PEPPIATT, *J. Strain Anal.* **9** (1974) 185.
102. D. W. OPLINGER, *Int. J. Solids Struct.* **31** (1994) 2565.
103. L. J. HART-SMITH, "Adhesive Bonded Single Lap Joints," NASA Contractor Report 112236, 1973.
104. D. W. OPLINGER, A Layered Beam Theory For Single Lap Joints. Army Materials Technology Laboratory Report MTL TR 91-23, 1991.
105. M. V. TSAI and J. MORTON, *Int. J. Solids Struct.* **31** (1994) 2537.
106. A. TOWSE, K. D. POTTER, M. R. WINSOM and R. D. ADAMS, *Int. J. Adhesion Adhesives* **19** (1999) 71.
107. R. B. HESLEHURST, Repair of Composite and Bonded Aircraft Structures, Course Notes. Australia Defence Force Academy.
108. R. B. HESLEHURST, J. P. BAIRD, H. M. WILLIAMSON and R. K. CLARK, Can Aging Adhesively Bonded Joints be Found? in Proc. 41st SAMPE Int. Symp. And Exhibition, Anaheim, CA, 1996, p. 925.
109. Locitite Corporation. In: Locitite Worlwide Design Handbook, Edition 1996/1997.
110. M. A. ANSARIFAR and G. J. LAKE, *J. Adhesion* **53** (1995) 183.
111. C. XU, K. RAMANI and G. KUMAR, *Int. J. Adhesion Adhesives* **22** (2002) 187.
112. W. FUNKE, *J. Coat. Technol.* **55** (1985) 31.
113. A. H. LANDROCK, "Adhesive Technology Handbook" (Noyes Publication, Park Ridge, NJ, 1985).
114. I. KULESHOV, S. KAIBIN and M. KALNINS, *Vysokomol Soedin* B **25** (1983) 366.
115. J. BIKERMAN, *J. Adhesion* **3** (1972) 333.
116. J. A. HARRIS and R. D. ADAMS, *Int. J. Adhesion Adhesives* **4** (1984) 65.
117. A. J. KINLOCH, *J. Mater. Sci.* **17** (1980) 617.
118. W. BROCKMAN, "Durability of Structural Adhesives," edited by A. J. Kinloch (Amsterdam, Elsevier Applied Science Publishers, 1983), p. 306, Chap. 7.
119. S. A. HASHIM and M. J. COWLING, in Proceedings of the Structural Adhesives in Engineering IV (Bristol, UK, Inst. of Materials, 1995) p. 245.
120. W. ALTHOF, Verfahren zur Ermittlung von Schubspannungs Gleitungs Diagrammen von Konstruktions Klebstoffen in dünnen Klebschichten, DFVLR IB 152-74/18, 1974.
121. R. B. KRIEGER, "Stiffness Characteristics of Structural Adhesives for Stress Analysis in Hostile Environment" (American Cyanamid Co., Havre de Grace, MD, 1975).
122. R. D. ADAMS and J. OPPENDALE, *J. Mech. Eng. Sci.* **18** (1976) 149.
123. J. D. BARDIS and K. T. KEDWARD, Department of Mechanical and Environmental Engineering University of California, Santa Barbara, CA 93106.
124. JEANS-YVES SENER, T. FERRACIN, L. CAUSSIN and F. DELANNAY, *Int. J. Adhesion Adhesives* **22** (2002) 129.
125. P. B. CROSLEY and E. J. RIPLING, *J. Test. Eval.* **19** (1991) 24.
126. D. J. CHANG, R. MUKI and A. WESTMANN, *Int. J. Solids and Structures* **12** (1976) 13.
127. F. E. PENADO, *J. Comp. Mater.* **27** (1993) 383.
128. A. K. EL-SENUSSI and J. P. H. WABBER, *J. Appl. Phys.* **56** (1984) 885.
129. J. COGNARD, *J. Adhesion* **57** (1996) 31.
130. S. J. BENNISON, G. A. ANDREJACK and L. A. SILVERMAN, in Proc. Euradh'96 (Cambridge University Press, 1996) p. 439.
131. E. J. RIPLING, S. MOSTOVOY and R. L. PATRICK, *Mater. Res. Standards (ASTM Bulletin)* **4**(3) (1964) 129.
132. S. MOSTOVOY, P. B. CROSLEY and E. J. RIPLING, *J. Mater.* **2** (1967) 661.
133. ASTM, ASTM D3433, in Annual Book of ASTM Standards: Adhesion Section 15, Philadalphia, 1990.
134. B. R. K. BLACKMAN, H. HADAVINIA, A. J. KINLOCH, M. PARASCHI and J. G. WILLIAMS, *Eng. Fracture Mech.* **70** (2003) 233.
135. J. COGNARD, *J. Adhesion* **22** (1987) 97.
136. *Idem.*, *ibid.* **20** (1986) 1.
137. E. J. RIPLING, S. MOSTOVOY and C. BERSCH, *ibid.* **3** (1971) 145.
138. F. SLOAN, *J. Comp. Mater.* **27** (1993) 1606.
139. W. S. JOHNSON and L. M. BUTKUS, *Fatigue and Fract. Engng. Mater. Struct.* **21** (1988) 465.
140. JONG-KYO KIM and YIU-WING MAI, "Interfaces in Composites," Materials Science and Technology, edited by R. W. Cahn, P. Haasen and E. J. Kramer, Structure and Properties of Composites (VCH, Weinheim, 1993) Vol. 13, p. 241.
141. M. A. ANSARIFAR and G. J. LAKE, Failure of Rubber-to-Metal Bonded Units, Adhesion 93, The Fifth Int. Conference of the Adhesives, Section of the Polymer Industry Divisionn of the Institute of Materials, York, UK, 1993.
142. T. SCHÜLLER and B. LAUKE, *Int. J. Adhesion Adhesives* **22** (2002) 169.
143. British Standard, BS 903, Part A21, 1989.
144. ASTM: D429-81. Annual Book of ASTM Standards, vol. 09.01, 1993.
145. ASTM: D429-64, Method B and ASTM: D429-64, Method C.
146. T. SCHÜLLER, W. BECKERT, B. LAUKE and K. FRIEDRICH, *Comp. Sci. Technol.* **60** (2000) 2077.
147. B. R. K. BLACKMAN, A. J. KINLOCH, A. C. TAYLOR and Y. WANG, *J. Mater. Sci.* **35** (2000) 1867.
148. P. A. FAY, R. E. DAVIS and G. D. SUTHURST, in Proc. of Impact and Fatigue Testing of Adhesives (Plastics and Rubber Institute, London, 1990).

149. R. A. DICKIE and S. M. WARD, in "Mittal Festschrift," edited by W. J. van Ooij and H. R. Anderson (VSP, Zeist, 1997) p. 1.
150. International Standard Organisations, ISO 11343 (ISO, Geneva, 1993).
151. L. TONG and G. P. STEVENS, "Analysis and Design of Structural Bonded Joints" (Kluwer, Dortrecht, 1999.
152. A. D. CROCOMBE and R. D. ADAMS, *J. Adhesion* **13** (1981) 141.
153. R. D. ADAMS, R. W. ATKINS, J. A. HARRIS and A. J. KINLOCH, *ibid.* **20** (1986) 29.
154. H. L. GROTH, *Int. J. Adhesion Adhesives* **11** (1991) 204.
155. R. D. ADAMS and N. A. PEPPIATT, *J. Strain Anal.* **9** (1974) 185.
156. L. DORN and L. WEIPING, *Int. J. Adhesion Adhesives* **13** (1993) 21.
157. M. HILDEBRAND, *ibid.* **14** (1994) 261.
158. T. P. LANG and P. K. MALLICK, *ibid.* **18** (1998) 167.
159. *Idem.*, *ibid.* **19** (1999) 257.
160. R. D. ADAMS and J. A. HARRIS, *ibid.* **16** (1996) 61.
161. J. A. HARRIS and R. D. ADAMS, An Assessment of the Impact Performance of Bonded Joints for Use in High Energy Absorbing Structures, in *Proc. Inst. Mech. Engrs.* **199** (1985) 121.
162. A. J. KINLOCH and G. A. KODOKIAN, *J. Adhesion* **24** (1987) 109.
163. J. L. LATAILADE and C. KEISLER, Charobonnet, ph. Effect of the Substrate on the Adhesion in Adhesive Bonds Loading at High Strain Rate, Preprint EURADH 92 (1992) 585.
164. F. CAYSSIALS and J. L. LATAILLADE, *J. Adhesion* **58** (1996) 584.
165. T. YOKOYAMA, "A New Test Technique for Determining the Impact Shear Strength of Adhesive Joints," in Proceedings of the ATEM' 97, 1997, p. 221.
166. A. A. BEZEMER, C.B. GUYT and A. VOLT, *Int. J. Adhesion Adhesives* **18** (1998) 255.
167. L. W. ZACHARY and C. P. BURGER, *Exp. Mech.* **20** (1980) 162.
168. K. R. BERG, "Problems in the Design of Joints and Attachments," edited by F. W. Wendt, H. L. Liebowitz and N. Perrone (Mechanics of Composite Materials, Pergamon, New York, 1970).
169. J. HART-SMITH, Adhesive-Bonded Double Lap Joints, NASA Contractual Report, NASA CR-112235, January 1973.
170. R. B. HESLEHURST, Ph.D. Dissertation, School of Aerospace and Mechanical Engineering, University College, UNSW, ADFA, Canberra, 1998.
171. D. A. BIGWOOD and A. D. CROCOMBE, *Int. J. Adhesion Adhesives* **10** (1990) 31.
172. G. RICHARDSON, A. D. CROCOMBE and P. A. SMITH, *ibid.* **13** (1993) 193.
173. M. V. TSAI, *J. Morton, Mech. Mater.* **20** (1995) 183.
174. M. V. TSAI, *J. Morton, Comp. Struct.* **32** (1995) 123.
175. M. Y. TSAI and J. MORTON, *J. Comp. Mater.* **29** (1995) 1163.
176. M. Y. TSAI, D. W. OPLINGER and J. MORTON, *Int. J. Solids Struct.* **35** (1998) 1163.
177. W. C. CARPENTER, *J. Adhesion* **35** (1991) 55.
178. W. K. CHIU and R. JONES, *Int. J. Adhesion Adhesives* **12** (1992) 219.
179. M. Y. TSAI and J. MORTON, *J. Strain Anal.* **29** (1994) 137.
180. C. H. WANG and L. R. F. ROSE, *J. Adhesion Adhesives* **17** (1997) 17.
181. G. LI, P. LEE-SULLIVAN and R. W. THRIG, *Comp. Struct.* **46** (1999) 395.
182. F. P. BEER and R. JOHNSON, "Mechanics of Materials," Matric. ed. (McGraw-Hill, England, 1992).
183. S. YADIGARI, C. PAPI REDDY and T. SANJEEVA REDDY, *Comp. Struct.* **27** (1987) 445.
184. W. C. CARPENTER and R. BARSOUM, *J. Adhesion* **30** (1989) 25.
185. S. AMIJIMA and T. FUJII, *Int. J. Adhesion Adhesives* **7** (1987) 199.
186. M. V. TAYLOR, M.Sc. Degree, Engineering Mechanics Department of Virgina Polytechnic Institute and State University, Blacksburg, VA, 1996.
187. S. NABOULSI and S. MALL, *Theoret. Appl. Fracture Mech.* **26** (1997) 1.
188. J. N. REDDY, "An Introduction to the Finite Element Method," 2nd ed. (McGraw-Hill, New York, 1993).
189. K. J. BATHE, "Finite Element Procedures" (Prentice-Hall, Englewood Cliffs, NJ, 1996).
190. H. L. GROWTH, *Int. J. Adhesion Adhesives* **8** (1988) 107.
191. A. D. CROCOMBE, D. A. BIGWOOD and G. RICHARD, *ibid.* **12** (1990) 167.
192. R. D. ADAMS, *J. Adhesion* **30** (1989) 219.
193. T. SCHÜLLER, W. BECKERT, B. LAUKE, C. AGEORGES and K. FRIEDRICH, *Composites* A **31** (2001) 661.
194. ABAQUS, General-Purpose Finite Element System, Hibbit, Karlson and Sorensen, Inc., 100 Medway Street, Providence, RI, 1997.
195. S. K. MAZUMDER and P. K. MALLICK, *Polym. Comp.* **19** (1997) 139.
196. *Idem.*, in Proc. 12th Annual Tech. Conf., American Society for Composites, October 1997, "Static and Fatigue Properties of Adhesive Joints in SRIM-SRIM Composites."
197. R. D. ADAMS and V. MALLICK, *J. Adhesion* **38** (1992) 199.
198. L. DORN and L. WEIPING, *Int. J. Adhesion Adhesives* **13** (1993) 21.
199. M. F. S. F. DE MOURA, J. P. M. GONÇALVES, A. T. MARQUES and P. M. S. T. DE CASTRO, *J. Compos. Mater.* **31** (1997) 1462.
200. J. P. M. GONÇALVES, M. F. S. F. DE MOURA, P. M. S. T. DE CASTRO and A. T. MARQUES, *Eng. Comput.: Int. J. Comput-Aided Eng. Software* **17** (2000) 28.
201. R. S. RAGHAVA, R. M. CADELL and G. S. YEH, *J. Mater. Sci.* **8** (1973) 225.
202. W. R. BROUGHTON, Shear Properties of Unidirectional Carbon Fiber Composites. Ph.D. Thesis, Darwin College, Cambridge.
203. G. W. WYCHERLEY, S. A. MESTAN and I. GRABOVAC, *J. Test. Eval.* **18** (1990) 203.
204. A. GUIU and M. E. R. SHANAHAN, *J. Polym. Sci. Polym. Phys.* **39** (2001) 2843.
205. E. M. KNOX, Marin Applications for Structural Adhesives, Ph.D. Thesis, Glasgow, University, Glasgow, UK, 1996.
206. P. T. REYNOLDS, *J. Mater. Sci. Lett.* **4** (1985) 1194.
207. D. MAVGIS and M. BARQUINS, "Adhesion," edited by K. W. Allen (Elsevier, London, 1988) Vol. 12, p. 205.
208. C. DRAIL, A. ALLAT, G. MARTIN and P. TORDJEMAN, *J. Adhesion* **68** (1998) 203.
209. F. X. GIBERT, A. ALLAT, G. MARIN and C. DRAIL, *J. Adhesion Sci. Technol.* **13** (1999) 1029.
210. R. J. ROARK, "Roark's Formulas for Stress and Strain," 6th ed. (McGraw-Hill, New York, London, 1989).
211. A. J. KINLOCH, "Adhesion and Adhesives" (Chapman and Hall, London, Glasgow, 1994).
212. A. J. KINLOCH, *Proc. Int. Mech. Eng.* **211** (Part G) (1997) 307.
213. P. MOLITOR and T. YOUNG, *Int. J. Adhesion Adhesives* **22** (2002) 101.
214. S. BISTAC, M. F. VALLAT and J. SCHULTZ, *ibid.* **18** (1998) 365.
215. D. M. BREWIS, G. W. CRITLOW and C. A. CURTIS, *ibid.* **19** (1999) 253.
216. A. N. RIDER and D. R. ARNOTT, *ibid.* **20** (2000) 209.
217. S. U. NING, R. I. MACKIE and W. J. HARVEY, *ibid.* **12** (1992) 85.
218. M. P. ZANNI-DEFFARGES and M. E. R. SHANAHAN, *ibid.* **13** (1993) 41.
219. R. E. DAVIS and P. A. FAY, in Proc. of the Adhesion'90, Cambridge, UK, The Plastics and Rubber Institute, 1990, p. 27/1-27/6; ISBN 1 871571 219.
220. R. A. GLEDHILL and A. J. KINLOCH, *J. Adhesion* **6** (1974) 315.
221. E. M. KNOX, Ph.D. Thesis, Glasgow University, Glasgow, UK, 1996.
222. P. A. FAY and A. MADDISON, in Procs. of Structural Adhesives in Enginerring II (Butterworths Scientific, Bristol, UK, 1989) p. 112.
223. M. GETTINS and A. J. KINLOCH, *J. Mater. Sci.* **12** (1977) 2511.
224. D. A. TOD, R. W. ATKINS and S. J. SHAW, *Int. J. Adhesion Adhesives* **12** (1992) 159.

225. S. P. BHUNIYE and S. MAITI, *Europ. Polym. J.* **38** (2002) 195.
226. A. J. KINLOCH, *J. Mater. Sci.* **12** (1980) 2141.
227. M. BABIC, *Int. J. Adhesion Adhesives* **21** (2001) 11.
228. D. K. KOHLI, in *Proc. of 10th Int. Eurepean Chapter Conference of the SAMPE* **55** (1989) 239.
229. D. K. KOHLI, 39th International SAMPE Symposium, 11–14 April 1994.
230. International Standard: ISO 813-1986 (E).
231. K. BOND, *Adhesive Age* **33**(Part 2) (1996) 22.
232. L. KOVAVIC, Lepenie Kovov a Plastov, Praha, SNTL, 1980.
233. I. SKEIST (ed), "Handbook of Adhesives" (Chapman and Hall, New York, 1990).
234. Various Bae Internal Studies of Long Term Warm/Wet Test Pieces of Hexcel Redux 775, Hexcel Redux 308 A, Cytec FM 73 and 3M Co, AF 163-2 Adhesives.
235. D. DIXON, Prediction of Lap Shear and Peel Strength of Adhesive Bonds, and Update on Results of Accelerated Environmental Testing, Bae Sowerby Research Centre, Report No. 3S 13729, May 1997, p. 3.
236. J. COMYN, "Adhesion Science" (The Royal Society of Chemistry, UK, 1997).
237. P. A. COOPER and J. W. SAWYER, Report No. TP-1507, NASA, 1979.
238. M. Y. TSAI and J. MORTON, *Int. J. Solids Struct.* **31** (1994) 2537.
239. R. M. BARKER and F. HATT, *AIAA* **11** (1973) 1650.
240. W. C. CARPENTER, *Int. J. Numer. Methods Eng.* **6** (1973) 430.
241. *Idem.*, *ibid.* **15** (1980) 1659.
242. W. C. CARPENTER and R. BARSOUM, *J. Adhesion* **30** (1989) 25.
243. B. N. RAO, Y. K. RAO and S. YADIGARI, *Fibre Sci. Technol.* **17** (1982) 77.
244. S. YADIGARI, C. P. REDDY and T. S. REDDY, *Comput. Struct.* **27** (1987) 445.
245. C. C. LIN and Y. S. LIN, *Int. J. Solids Struct.* **30** (1993) 1679.
246. J. N. REDDY and S. ROY, *Int. J. Non-Linear Mech.* **23** (1988) 97.
247. S. ROY and J. N. REDDY, *Int. J. Numer. Methods Eng.* **26** (1988) 2531.
248. P. C. PANDEY and S. NARASIMHAN, *Comput. Struct.* **79** (2001) 769.
249. U. EDLUND and A. KLARBRING, *Comput. Methods Appl. Mech. Eng.* **96** (1992) 329.
250. M. CHEIKH, P. COOREVITSA and A. LOREDO, *Int. J. Adhesion Adhesives* **21** (2001) 249.
251. A. J. KINLOCH, M. S. G. LITTLE and J. F. WATTS, *Acta Mater.* **48** (2000) 4543.
252. A. MAHOON, "Titanium Adherends in Durability of Structural Adhesives," edited by A. J. Kinloch (1983) p. 259.
253. A. MADDISON, in *Proc. of the Structural Adhesives in Engineering V* (Inst. of Materials, Bristol, UK, 1998) p. 68.
254. Y. WEITSMAN, *J. Comp. Mater.* **11** (1977) 378.
255. M. R. BOWDITCH, *Int. J. Adhesion Adhesives* **16** (1996) 73.
256. R. A. GLEDHILL and A. J. KINLOCH, *J. Adhesion* **6** (1974) 315.
257. M. P. ZANNI-DEFFARGES and M. E. R. SHANAHAN, *Int. J. Adhesion Adhesives* **15** (1995) 1520.
258. C. S. SMITH, "Design of Marine Structures in Composite Materials" (Applied Science, Amsterdam, Elsevier, 1990) Chap. 3, p. 99.
259. R. D. ADAMS, "Structural Adhesives in Engineering," C180/86, (I. Mech. E., London, 1986), p. 17.
260. A. D. CROCOMBE, *Int. J. Adhesion Adhesives* **17** (1997) 229.
261. Y. M. XIE and G. P. STEVEN, *Comput. Struct.* **49** (1994) 885.
262. *Idem.*, *Eng. Comput.* **11** (1994) 295.
263. I. U. OJALVO and H. L. EIDONOFF, *AIAA J.* **16** (1978) 204.
264. W. J. RENTON and J. R. VINSON, *J. Adhesion* **7** (1975) 175.
265. F. ERDOGAN and M. RATWANI, *J. Comp. Mater.* **5** (1971) 378.
266. R. C. GIVLER and R. B. PIPES, "Analysis of the 'Joggle-Lap' Joint for Automotive Applications," edited by K. T. Kedward (Joining of Composite Materials, Vol. ASTM STP 749, ASTM, 1985), p. 61.
267. M. OLIA and J. N. ROSSETTOS, *Int. J. Solids Struct.* **33** (1996) 2681.
268. J. N. ROSSETTOS, P. LIN and H. NAYEB-HASHEMI, *J. Engng. Mater. Technol.* **116** (1994) 533.
269. J. N. ROSSETTOS and E. ZANG, *J. Appl. Mech.* **60** (1993) 559.

Received 10 September 2003
and accepted 1 April 2004